UNCLASSIFIED

AD 401 131

Reproduced by the

DEFENSE DOCUMENTATION CENTER

FOR

SCIENTIFIC AND TECHNICAL INFORMATION

CAMERON STATION ALEXANDRIA, VIRGINIA

UNCLASSIFIED

NOTICE: When government or other drawings, specifications or other data are used for any purpose other than in connection with a definitely related government procurement operation, the U. S. Government thereby incurs no responsibility, nor any obligation whatsoever; and the fact that the Government may have formulated, furnished, or in any way supplied the said drawings, specifications, or other data is not to be regarded by implication or otherwise as in any manner licensing the holder or any other person or corporation, or conveying any rights or permission to manufacture, use or sell any patented invention that may in any way be related thereto.

10

CATALOGED BY ASTIA
AS AD No. 401131

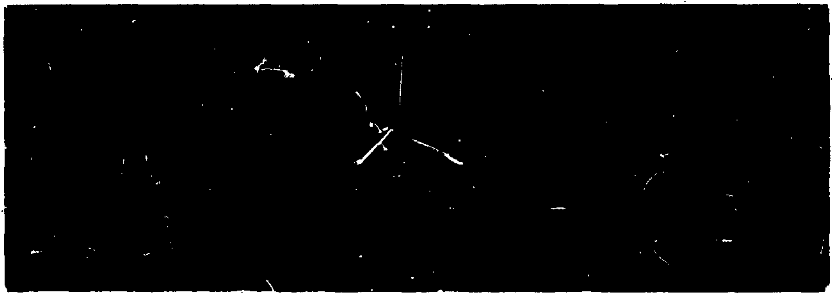

Ford Motor Company
AERONUTRONIC DIVISION

401 131

16600

(5) Ford Motor Company
AERONUTRONIC DIVISION

(11) Publication No. U-2059

(12)

(13) [illegible]

(7) FINAL TECHNICAL ~~REPORT~~.

(6) STUDY OF DETONATION BEHAVIOR OF SOLID PROPELLANTS

Prepared for: Department of the Navy
Bureau of Weapons
Washington 25, D. C.

(12) Under Contract NOw 62-0503-c, ~~Task 1~~

(8) Prepared by: M. H. Boyer,
D. A. Schermerhorn, and
H. Uyehara,

(9) 30 March 1963

(10) 115 p [illegible] Tables, 34 refs.

ASTIA
RECEIVED
APR 15 1963
TISIA D

CONTENTS

SECTION PAGE

1 INTRODUCTION 1

2 THE PHYSICAL MODEL

2.1 General Considerations 4
2.2 The Conservation Equations 4
2.3 Equation of State 5
2.4 The Chemical Rate Equations 12

3 MATHEMATICAL PROCEDURES

3.1 General Principles 23
3.2 The Flow Scheme - One Dimensional Program 30

4 INPUT DATA

4.1 Equations of State - Gas Phase 43
4.2 Equation of State - Solid Phase 43
4.3 The Reaction Rate Equations 44

5 CALCULATIONS AND DISCUSSION

5.1 Introduction 48
5.2 General Characteristics of Computed Waves 49
5.3 Effect of Grain Surface Burning Versus Point Burning of Wave Behavior 58
5.4 Calculations of Minimum Pressure for Initiation. . 67
5.5 Calculation of Steady State Characteristics . . . 74

6 TWO DIMENSIONAL TREATMENT 79

7 EXPERIMENTAL INVESTIGATION OF EQUATION STATE 82

NOMENCLATURE 107

REFERENCES 108

DISTRIBUTIONS 111

ILLUSTRATIONS

FIGURE		PAGE
1	Compression of Solid by Combustion Product Gases	19
2	Wave Profiles With and Without Von Neuman Q	26
3	Hugoniot Diagram for Detonation Process	27
4	Effect of Parameter b on Wave Trajectory	50
5	Reaction and Pressure Profiles Through Computed Detonation Wave in TNT	52
6	Solid-Phase Energy Density and Solid and Gas Specific Volumes Through a Detonation Wave in TNT	53
7	Propagation of a Detonation in Propellant Material	55
8	Reaction Zone Profiles for Detonation Wave in Propellant Material	56
9	Reaction Profiles for Binder and Oxidizer and Pressure Profile Through a Detonation Wave in Composite Double-Base Propellant	57
10	Propagation of Computed Detonation Wave in TNT	59
11	Initial Trajectory of Detonation Wave in TNT	60
12	Reaction and Pressure Profiles Through Computed Detonation Wave in TNT	61
13	Reaction Zone Profile Through Detonation Wave in TNT	62
14	Propagation of Computed Detonation Wave in TNT	64
15	Propagation of Computed Detonation Wave in TNT	65
16	Profiles Through Computed Detonation Waves in TNT for Point and Surface Ignition, Z = 0.035 CM	66

ILLUSTRATIONS

FIGURE PAGE

17 Position and Magnitude of Peak Pressure in Fading 68

18 Position and Magnitude of Peak Pressure in Fading Wave in TNT ($A_1/R = 4715^{\circ}K - A_2/R = 9430^{\circ}K$) 70

19 Trajectory and Peak Pressures of Detonation Wave in Composite Double-Base Propellant 72

20 Trajectory and Peak Pressure of Fading Detonation Wave in TNT 73

21 Wave Trajectories Showing Effect of Programmed Reaction Delay 77

22 Trajectory of Computed Wave in TNT with Delayed Ignition and Fine Zoning 78

23 High Pressure Piston-Cylinder Press 83

24 High-Pressure Plate 84

25 Typical Form of Pressure - Displacement Curve 85

26 Detail of Press Set-Up 87

27 Pressure-Volume Curves for Sodium Chloride at 24°C . . . 90

28 Pressure-Volume Curves for Sodium Chloride at N100°C . . 91

29 Pressure-Volume Curve for Polyurethane at 23°C 92

30 Pressure-Volume Curve for Polyurethane at 99.5-101°C . . 93

31 Pressure-Volume Curves for Ammonium Perchlorate at 21.5°-220°C 94

32 Pressure-Volume Curve for Ammonium Perchlorate at 100°-102°C 95

ILLUSTRATIONS (Continued)

FIGURE PAGE

33 Pressure-Volume Curves for Sodium Chloride-Polyurethane Mixture (40-60% by wt.) at 22-23°C 96

34 Pressure-Volume Curves for Sodium Chloride-Polyurethane Mixture (40-60% by wt.) at 91-94°C 97

35 Pressure-Volume Curves for Sodium Chloride-Polyurethane Mixture (70-30% by wt.) at 23°C 98

36 Pressure Volume Curves For Sodium Chloride-Polyurethane Mixture (70-30% by wt.) at 99-102°C 99

37 Pressure-Volume Curves for Sodium Chloride-Ammonium Perchlorate (50-50% by wt.) at 21°C 100

38 Pressure-Volume Curves for Sodium Chloride-Ammonium Perchlorate (50-50% by wt.) at 99-101°C 101

39 Pressure-Volume Curves for Aluminized Solid Propellant (B.F. Goodrich Designation E107M) at 23°C 102

40 Pressure-Volume Curve for Aluminized Solid Propellant (B.F. Goodrich Designation E107M) at 100°C 103

NOMENCLATURE

t = time
p = pressure
q = von Neumann "q"
v = volume
u = material velocity
e = specific energy
h = Planck's constant
k = Boltzman constant
τ = ignition delay
w = empirical pressure constant
β = equation of state constant
γ = equation of state constant
ϵ = equation of state constant
T = temperature
$R\begin{cases} = \text{gas constant} \\ = \text{Eulerian Coordinate} \end{cases}$
ν = vibration frequency
ϕ = potential function
f = fraction of material unreacted
F = fraction of material in zone
$A\begin{cases} = \text{activation energy} \\ = \text{area of revolution} \end{cases}$
B = pre-exponential constant
m = reaction order

Q = heat of reaction
Q' = effective heat of reaction used in grain burning equation
E = chemical energy released
ξ = zero point energy
C_v = specific heat
$L\begin{cases} = \text{charge length} \\ = \text{2D Lagrange coordinate} \end{cases}$
$z\begin{cases} = \text{grain radius} \\ = \text{Eulerian coordinate} \end{cases}$
= density
a = molecular diameter
P = applied surface pressure
U = wave velocity
N = Avogadro's number
D = diffusion coefficient
K = 2D Lagrange coordinate
χ = Courant number
c = sound speed
θ, λ = constants in q calculation
η = geometry factor
b = constant in   calculation
ψ = integration control constant
Γ = integration control constant

Subscripts

o	ambient condition
1	ignition process
2	oxidizer process
3	binder process
4	diffusion process
g	gas phase
s	solid reaction phase
r	inert phase
G	Gruneisen constant
a	initial conditions
z	final conditions
i	index
c	hydrodynamic coordinate mesh interval
n	time mesh coordinate
j	space mesh coordinate
ℓ	local space variable
b,c,f	space coordinates

Superscripts

o	ignition point
s	high pressure term
bar	average value

SECTION 1

INTRODUCTION

The Aeronutronic program on the detonation behavior of propellants is directed to the development of mathematical techniques by which such behavior can be determined solely from basic hydrodynamic principles and properties of the material. Particular interest is in the prediction of: (1) initiation behavior, and (2) energy yield and the stability of detonation, as a function of type of initiation, material parameters and geometry.

The approach which has been adopted involves representation of the detonation process in terms of a set of basic equations consisting of the Navier-Stokes conservation equations, the appropriate equations of state, and the rate equations which describe the release of chemical energy. This system of equations is integrated numerically in time and space making use of electronic computer techniques to obtain the history of any defined initial disturbance. Computation of such histories for various configurations and initial conditions will define detonation behavior.

The prosecution of the program has been in several phases worked on more or less concurrently: (1) development of the proper form of the basic equations, (2) development of suitable mathematical techniques for solution of the basic equations, (3) development of the necessary input data on pertinent propellant materials, (4) performance of calculations on explosive charges of experimentally known behavior, and comparison of computed and experimental results, and (5) calculation of the behavior of propellant grain configurations of particular interest to the propulsion field to determine dependence of behavior upon grain design parameters.

Phases 1 and 2 of this program have been completed, and some work has been carried out on phases 3 and 4. The basic equations have been written in a form which now appears to correctly incorporate at least those parameters and material characteristics which are of greatest significance to the detonation process. Mathematical techniques and associated computer programs have been written and checked out for solving the basic equations in one or two space dimensions and for pressure initiation. The problem of thermally initiated detonation has been extensively studied with the conclusion that it is beyond the capability of the present generation of computers. Experimental data have been obtained on the equation of state parameters for the unreacted solid phase. Similar data for the reacted gaseous products have been obtained from the detonation literature.

As of the present time, considerable success has been achieved in demonstrating, on the part of theoretically computed detonations, general agreement with experimentally observed behavior. This has served to verify the validity of the theoretical methods, and in doing so, it has contributed substantially to our understanding of the detonation process since the factors responsible for the various aspects of detonation behavior are readily seen from the basic equations. For example, the initiation of a detonation wave is found to be dependent upon the equation of state of the unreacted material, the kinetics of the chemical reactions and the heat of reaction. The concept of the ignition zone which developed from this work and its relation to the hot spot theory of initiation as advanced by Bowden and Yoffe have made clear the details of such dependence. Wave growth following initiation has been shown to be in accord with the classical grain burning model of Eyring and coworkers; however, in some respects a point ignition internal burning model appears to be more realistic. Finally, the phenomena of low order detonation which heretofore was not capable of clear theoretical explanation, has been shown to be a normal consequence of certain combinations of the above processes.

In addition to its success in demonstrating and explaining the general aspects of detonation behavior, the theoretical method has also been used to compute the quantitative initiation behavior of real materials. Such efforts are severely handicapped by a lack of the material data needed for input to the problem. However, in the case of two propellants for which such data were available, calculation of minimum pressures for initiation showed excellent agreement with experiment.

Remaining work to be done involves (1) the procurement of needed additional data on the various equations of state and on the parameters appearing in the equations which describe the rate of release of chemical energy, (2) carrying out additional calculations on the detonation behavior of propellants and high explosives which can be compared with experimental observations for the purpose of further definition of the validity of the mathematical methods, and (3) performance of calculations which are of application to the development and practical evaluation of new propellant systems.

SECTION 2

THE PHYSICAL MODEL

2.1 General Considerations

A detonation is represented as a hydrodynamic shock in which chemical reaction takes place in the expansion zone behind the shock front. The expansion converts part of the heat of reaction into work and the combination of this added work with that lost in the shock by dissipation effects corresponding to the entropy increase, radiation, thermal conduction, lateral expansion, etc. is the condition which determines the wave history. When the work loss exceeds the work added by reaction the wave fades; when the work added by reaction exceeds the loss, the wave grows, when the two are the same, the wave is at steady state.

A process such as that described can be represented mathematically by a set of basic equations consisting of (1) the equations of conservation of mass, momentum and energy, (2) the equations describing the rate of release of chemical energy, and (3) the equations of state of the various material phases taking part in the process. Three requirements exist: first, the equations must be stated in a form capable of representing the model in a fashion sufficiently detailed for the requirements of the treatment; second, the parameters which appear in the equations representing the chemical and physical properties of this material must be known, and third, techniques for obtaining solutions to the system of expiration must be available.

2.2 The Conservation Equations

The numerical techniques (to be discussed later) used in the treatment of detonation problems are most conveniently applied when the conservation equations are expressed in Lagrange form. If the medium is a fluid, only pressure and viscous forces need be considered, otherwise additional forces due to mechanical rigidity are present. Since pressures of interest to detonation phenomena generally exceed the mechanical strength of materials by a wide margin, the assumption will be made that all materials act as fluids. Viscous forces affect detonation behavior only in terms of the work dissipation effects occurring at the shock front. It is convenient to include such forces in an artificial viscosity term, "q", original devised by von Newman and Richtmeyer[1] which is designed not only to provide the correct work dissipation in a shock, but also to convert the mathematical form of the shock from a discontinuity, which it assumes in a nonviscous medium to a continuous function in which rates of change are small enough to permit numerical integration. This greatly simplified treatment of the problem in the shock region.

With these considerations, the conservation expirations are the following:

$$\text{Mass} \quad \left(\frac{\partial}{\partial t} + \vec{\mu} \cdot \nabla\right) \rho = - \rho \nabla \cdot \bar{\mu} \tag{1}$$

$$\text{Momentum} \quad \rho\left(\frac{\partial}{\partial t} + \vec{\mu} \cdot \nabla\right) \vec{\mu} = - \nabla \left(\rho + q\right) \tag{2}$$

$$\text{Energy} \quad \rho\left(\frac{\partial}{\partial t} + \vec{\mu} \, \nabla\right) e = - \left(\rho + q\right) \nabla \cdot \bar{\mu} \tag{3}$$

$$\text{where } q = \begin{cases} \rho\left[\theta^2\left(\frac{\partial u}{\partial x}\right)^2 - c\lambda \left(\frac{\partial u}{\partial x}\right)\right] & \text{if } \partial u/\partial x < 0 \\ 0 & \text{if } \partial u/\partial x \geqslant 0 \end{cases} \tag{4}$$

θ^2, and λ are an arbitrary constants which define the width of the region of space over which the shock zone is spread and the rate of change of the variables in this region.

2.3 Equation of State

Reaction in the detonation of a condensed explosive involves the transformation solid (or liquid) ⟶ gas. As previously mentioned, it is assumed that under detonation conditions, both solids and liquids behave a condensed fluids, so that only two phases need to be considered which are empirically designated as solid and gas. The detonation process therefore is postulated to initiate in a solid phase, and terminate in a gaseous phase. The situation in between is dependent upon the nature of the reaction process. This is discussed in the following section where it will be shown that the most reasonable concept of the reaction process, due to Eyring and co-workers[2] is consistent with the concept of the partially reacted material as a physical mixture of the solid and gaseous phases.

If these phases are physically different the difference will appear as a difference in their respective equations of state. In accordance with the conception of the solid phase as a fluid, any such distinction should become small and the two equations of state should tend to become identical at high pressure. At low pressure, on the other hand, they should reduce to the conventional gas law, and a solid equation of state which properly describes the important aspects of the behavior of solids at ambient conditions. It is desirable to consider the form of equations which possess these characteristics.

a. Equation of State-Gas Phase

The equation of state of the gaseous products of a detonation process appears in the steady state theory of detonation, and comparison of the ideal detonation velocity predicted by steady state theory with experimental value provides some insight into the nature of this equation. The general form seems to be that of the perfect gas law with one arbitrary variable parameter. Specifically the co-volume equation of state with co-volume term as a function of volume:[3]

$$p\left(v - \alpha(v)\right) = RT \tag{5}$$

the form with a pressure dependent parameter[4]

$$pv = nRT + \alpha(p) \tag{6}$$

the Kistiakowsky-Wilson equation[5]

$$pv = \frac{nRT}{M}\left[1 + xe^{\sigma x}\right] \tag{7}$$

with

$$x = \sum(N_i\ k_i/T^{\phi}vM \tag{8}$$

and the Boltzman equation of state[4] (in various modifications)

$$\frac{pv}{nRT} = 1 - \frac{b_o}{v} + 0.625\frac{b_o{}^2}{v^2} + 0.2869\frac{b_o{}^3}{v^3} \tag{9}$$

have all been used with some success in computing various aspects of steady state behavior which agree well with experiment. In none of these cases has it been possible to determine the variable parameter from independent data, a fact which makes difficult any independent choice between them.

Some work which is believed to have an important bearing on this problem concerns studies on the equation of state of solids and liquids at detonation pressures.[6,7] It suggests that they are well represented by a simple perfect gas equation of state in the form:

$$pv = (\gamma - 1)\, e \tag{10}$$

if a value $\gamma = 3$ is used. In accord with the principle, cited above, that solids and gases should possess similar equations of state at high pressure, it is deduced that the perfect gas equation of state is also valid for gases at high pressure provided an appropriate value of is used. These concepts suggest an equation of state of the form of (10) for the gas phase in which γ is the variable parameter having values in the range of 1.3 for perfect gases at 1 atmosphere to $\gamma \simeq 3$ at very high pressures.

Such an equation of state has been examined by calculating the range of values needed to be assumed by γ in order for equation (1), when used in conjunction with steady state theory, to provide detonation velocities in accord with experiment. Writing 5 in a form analagous to (10), i.e.

$$\begin{aligned} p\left(v_g - \alpha(v_g)\right) &= (\gamma_o - 1) e_g \\ pv_g &= \left[\left(\gamma_o - 1\right) + \frac{p\alpha}{e_g}\right] e_g, \end{aligned} \tag{11}$$

one obtains:

$$\left(\gamma_g - 1\right) = \left(\gamma_o - 1\right) + \frac{p\alpha}{e_g}$$

$$\gamma_g = \gamma_o + \frac{\alpha(\gamma_o - 1)}{\left(v_g - \alpha\right)} \tag{12}$$

By means of studies on a series of explosives, M.A. Cook[3] experimentally determined the function α (v). By comparison of (5) with the virial equation of state, it is found that α can be satisfactorily represented by the expression

$$\alpha = v\left(1 - \frac{v^2}{v^2 + bv + b^2}\right), \tag{13}$$

in which the first three terms of the virial expansion are used.

Combination of (12) and (13) leads to:

$$\gamma_g = \gamma_o + \frac{b}{v_g}\left(1 + \frac{b}{v_g}\right)(\gamma_o - 1). \tag{14}$$

The validity of expression (14) is shown in Table I, where experimental values of α as obtained by Cook are to be compared with values computed from (14) at a series of values of v_g. The agreement shown is surprisingly good, in view of the fact that application of (14) is extended to the condition where $\frac{b}{v} > 1$ and the virial equation of state no longer converges.

Some interpretation as to the meaning of the parameter γ is desirable. As it is used in equation 5, it can be shown to be defined by:

$$\gamma = \left(\frac{\partial \ln p}{\partial \ln \rho}\right)_S - \frac{1}{p}\left(\frac{\partial p\,\alpha}{\partial v}\right)_S \tag{15}$$

For a perfect gas ($\alpha = o$) this reduces to:

$$\gamma = \left(\frac{\partial \ln p}{\partial \ln \rho}\right)_S \tag{16}$$

which can be shown to be equivalent to the familiar relation:

$$\gamma = \frac{C_p}{C_v} \tag{17}$$

Any departure of the observed γ from (17) can be interpreted as the appearance of a significant contribution by the term

$$1/p\left(\frac{\partial p\alpha}{\partial v}\right)_S$$

Analagous lines of reasoning can be followed for the other equations of state, 6, 7, and 9.

b. Equation of State - Solid Phase

The body of work which has become available on the equation of state of condensed materials in recent years is much too extensive to be discussed comprehensively here. The most pertinent information appears to derive from studies on shock propagation[6,7] and these lead to observations that at pressure in the detonation range, a simple, perfect gas

TABLE I

CALCULATION OF α FROM EQUATION (13) and γ FROM EQUATION (14) COMPARISON WITH EXPERIMENTAL DATA

$v(cm^3)$	α(exp)	α(calc.)*	γ*
1.25	0.75	0.751	1.75
1.0	0.68	0.676	1.93
0.837	0.62	0.611	2.12
0.714	0.56	0.555	2.36
0.625	0.51	0.507	2.61
0.555	0.47	0.466	2.89
0.50	0.43	0.431	3.19
0.455	0.39	0.400	3.52
0.19	0.17	0.185	11.7

* $b = 1.03$, $\gamma_o = 1.3$

equation of state

$$pv = (\gamma - 1)e$$

where γ has a value of about 3, is applicable within experimental uncertainty. At lower pressures, this expression is clearly not applicable since it does not provide for a finite volume at zero pressure. This suggests the addition of additional parameters β and ϵ to give an equation of the following form:

$$(p + \beta)\, v = (\gamma_s - 1)e - \epsilon \qquad (18)$$

Equation (18) is of the form of an equation of state deduced for solids by Grüneisen, based upon the Einstein concept of the solid phase as a collection of harmonic oscillators. If the possible frequencies are ν_i, the equation obtained from such a model is the following:[8]

$$\left[p + \frac{\partial \phi}{\partial v}\right] v = \sum \gamma_i \frac{h\nu_i}{\left[\exp\frac{h\nu_i}{RT} - 1\right]} \qquad (19)$$

where

$$\gamma_i = -\left[\frac{\partial \ell n \nu_i}{\partial \ell n\, v}\right]_T \qquad (20)$$

Here the summed terms represent the internal thermal energy of the material and ϕ is a potential function such that the internal potential energy is given by

$$e_\phi = \int_\infty^v \frac{\partial \phi}{\partial v}\, dv \qquad (21)$$

For present purposes, internal thermal energy is meant to include the kinetic and potential energy associated with atomic and molecular vibration, and internal potential energy represents that energy due to atomic and molecular distortion.

At high temperature the summation in equation (19) reduces to

$$RT \sum \gamma_i - \xi \qquad (22)$$

where ξ is the zero point energy. If all of the γ_i are equal, substitution of (22) in (19) gives:

$$\left(p + \frac{\partial\phi}{\partial v}\right) v = \gamma_G \left(3NkT - \xi\right) \qquad (23)$$

The oscillator model upon which equation (23) is based is closely approximated only by a perfect single crystal. However, the form of the equation is a consequence of the condition that the potential and thermal forms of internal energy are respectively dependent upon the volume only and upon the temperature only, and aretherefore separable into different terms. If it is assumed that however poorly the simple oscillator model may represent reality in other respects, this separation of thermal and potential energy is valid for real materials, then the equation is of general application, provided only that the functions $\frac{\partial\phi}{\partial v}$ and γ_G, which now must be regarded as somewhat empirical in nature, are known.

In treating detonation behavior, it is more convenient to express the equation of state in terms of total energy, since the conservation equations refer to total energy. Adding equation (21) to both sides of (23), one has ultimately

$$\left[p + \frac{\partial\phi}{\partial v} + \frac{\gamma_G}{v}\int_{v_o}^{v} \frac{\partial\phi}{\partial v}\, dv\right] v = \gamma_G e + \gamma_G \left[3\ nkT_o + \xi\right] \qquad (24)$$

This is now the form of the solid equation of state presently in use where

$$\beta' = \left[\frac{\partial\phi}{\partial v} + \frac{\gamma_G}{v}\int_{v_o}^{v} \frac{\phi}{v}\, dv\right] \qquad (25)$$

$$\epsilon' = \gamma_G \left[3Nkt_o + \xi\right] \qquad (26)$$

The quantities β' and ϵ' can be expressed in terms of their values β and ϵ at ambient conditions as follows:

$$\beta' = \beta + f_\beta\left(\frac{\partial\phi}{\partial v}, \gamma_G, v\right) \qquad (27)$$

$$\epsilon' = \epsilon + f_\epsilon\,(\gamma_G) \qquad (28)$$

where $f_\beta = f_\epsilon = o$

at ambient conditions.

One obtains

$$p = \frac{(\gamma_g-1)\left[\bar{e} - (f_s\beta v_s + f_s\epsilon)/(\gamma_s-1)\right]}{\left[\left(\frac{\gamma_g - \gamma_s}{\gamma_s-1}\right) f_s v_s + \bar{v}\right]} \qquad (34)$$

An equation for pressure during the ignition phase is obtained through use of expression (18). Upon differentiation we obtain

$$(p + \beta)\, dv + v dp = (\gamma - 1)\, de + e d\gamma$$

combination with

$$de = -(p + q)\, dv$$

and

$$q = \frac{\theta^2}{v}\left(\frac{\partial u}{\partial x}\right)^2 + c\Lambda\frac{\partial u}{\partial x}$$

gives, finally, to a good approximation:

$$(p + B/\gamma + q)\ v^{\gamma}(\gamma-1)^{-\left[\frac{p + \beta - \epsilon/v}{p + \beta/\gamma + \frac{\gamma-1}{\gamma}q}\right]} = \text{constant} \qquad (34a)$$

2.4 The Chemical Rate Equations

a. General Model

Reaction in a detonation wave is divided into two distinct phases; an ignition phase in which follows an Arrhenius rate law, and a subsequent burning phase based upon the Eyring grain burning model.[2] These two phases occur in succession, and involve separate portions of the charge material. The fraction of the charge included in each is one of the parameters of the material and must be supplied as input to a given problem.

b. Ignition Phase

The portion of the charge which takes part in the ignition phase is based upon the concept, somewhat analagous to the hot spot theory of initiation, that only certain discrete portions of the charge are caused to react by the event which initiates detonation. This is

Substituting and transposing

$$(p + \beta)\ v = \gamma_G e + \epsilon + f_\epsilon - v\ f_\beta$$

$$= \left[\gamma_G + \frac{f_\epsilon - v f_\beta}{e}\right] e + \epsilon \tag{29}$$

Setting

$$\gamma - 1 = \left[\gamma_G + \frac{f_\epsilon - v f_\beta}{e}\right] \tag{30}$$

One has finally the previously deduced expression

$$(p + \beta)\ v + (\gamma - 1)e + \epsilon \tag{18}$$

When β and ϵ are constants obtainable from the properties of the material at ambient conditions and $(\gamma-1)$ is a complicated function of $\frac{\partial \phi}{\partial v}$, γ_G, v and e, equal to γ_G at ambient conditions. Equation 18 was used as the solid equation of state throughout the present work, with $(\gamma_s - 1)$ taken as an experimentally determined variable parameter.

Although only fragmentary data are available from which to determine the value of $\gamma - 1$ for solids at high pressure, it is a logical deduction that gaseous and condensed phases are essentially indistinguishable at detonation pressures. Accordingly the assumption was made that the information discussed in the previous section on the value of γ_g for the reaction products of detonation could be applied directly to define γ_s for the solid phase. Accordingly, γ_s was computed by an expression analagous to 14, namely

$$\gamma_s = \gamma_o + \frac{b}{v_s}\left(1 + \frac{b}{v_s}\right)\left(\gamma_o - 1\right) \tag{31}$$

Equations (18) and (31) were the ones used throughout the program to represent the solid phase.

In regions where the charge consists of a half reacted mixture of solid reactant and gaseous products, it is necessary to have an equation giving the pressure in terms of the relative proportions of solid and gas, and the energy density. This is found by eliminting e_s, e_g and v_g between equations 10 and 18 and

$$\bar{v} = \gamma_s\ v_s + (1 - \gamma_s)\ v_g \tag{32}$$

$$\bar{e} = \gamma_s\ e_s + (1 - \gamma_s)\ e_g \tag{33}$$

presumed to be a consequence of an effect, either of such areas being raised by the initiation event to a higher temperature than their surroundings (hot spot theory) or of being more reactive. Reaction in these regions is assumed to be represented by an Arrhenim function of the form

$$\frac{df}{dt} = (1-f)\ \exp\left(\frac{C_v A}{Re}\right) \qquad (35)$$

As discussed in the previous section on equation of state, expression is in terms of total energy density, e, rather than temperature. If reaction is dependent only upon thermal energy density, then the form of 35 involves the tacit assumption that all energy changes are thermal. This is likely to be erroneous to some degree at detonation pressures.

Two physical conceptions of the ignition region of the charge are possible which have significant implications in terms of the following reaction process to be discussed in the following section. The first is based upon a grain structure for the detonable material and conceives the ignition region to be a thin skin of material on the grain surface. Material in this skin is assumed to be more reactive than that in the middle of the grain, and to react uniformly throughout its volume the latter being required in order for it to exhibit a reaction rate according to 35. This assumption can be justified on the basis of arguments that reaction at the interior of a lattice structure involves creation of a discontinuity, a highly endothermic process. Furthermore, reactive solids are normally observed to react at interfaces or discontinuities.

The second concept requires no formal grain structure, but visualizes the ignition region to consist of a large number of more or less regularly spaced regions of finite volume located throughout an otherwise continuous material. These regions are postulated to be different from contiguous material such that when an initating event occurs, the material in these regions reacts first and according to the rate law (35).

They correspond to the hot spot concept of Bowden and Yoffee,[9,10] explained by those authors as due to such mechanisms as contact between grit particles, compression of small voids and the like. It is of interest to consider one of these in some detail, namely, ignition regions due to the pressure of small voids or gas bubbles.

A number of investigators have considered the possibility that the sensitizing effect of a porous structure upon explosives was due to the presence of gas in the pores, which, when adiabatically compressed by a transient pressure, would be heated to temperature above the ignition point of the surrounding material. There is no question but that occluded presumed to be a consequence of an effect, either of such areas being raised by the initiation event to a higher temperature than their surroundings (hot spot theory) or of being more reactive. Reaction in these regions is assumed to be represented by an Arrhenim function of the form

$$\frac{df}{dt} = (1-f)\ \exp\left(\frac{C_v A}{Re}\right) \qquad (35)$$

As discussed in the previous section on equation of state, expression is in terms of total energy density, e, rather than temperature. If reaction is dependent only upon thermal energy density, then the form of 35 involves the tacit assumption that all energy changes are thermal. This is likely to be erroneous to some degree at detonation pressures.

Two physical conceptions of the ignition region of the charge are possible which have significant implications in terms of the following reaction process to be discussed in the following section. The first is based upon a grain structure for the detonable material and conceives the ignition region to be a thin skin of material on the grain surface. Material in this skin is assumed to be more reactive than that in the middle of the grain, and to react uniformly throughout its volume the latter being required in order for it to exhibit a reaction rate according to 35. This assumption can be justified on the basis of arguments that reaction at the interior of a lattice structure involves creation of a discontinuity, a highly endothermic process. Furthermore, reactive solids are normally observed to react at interfaces or discontinuities.

The second concept requires no formal grain structure, but visualizes the ignition region to consist of a large number of more or less regularly spaced regions of finite volume located throughout an otherwise continuous material. These regions are postulated to be different from contiguous material such that when an initating event occurs, the material in these regions reacts first and according to the rate law (35).

They correspond to the hot spot concept of Bowden and Yoffee,[9,10] explained by those authors as due to such mechanisms as contact between grit particles, compression of small voids and the like. It is of interest to consider one of these in some detail, namely, ignition regions due to the pressure of small voids or gas bubbles.

A number of investigators have considered the possibility that the sensitizing effect of a porous structure upon explosives was due to the presence of gas in the pores, which, when adiabatically compressed by a transient pressure, would be heated to temperature above the ignition point of the surrounding material. There is no question but that occluded gas could be heated to a very high temperature by such a mechanism. However, analysis of this system by Johansson[11] has raised some doubts as to whether the quantity of heat generated in this way would be sufficient to cause ignition. He found it necessary to postulate the presence in the pores of a vapor capable of exothermic decomposition so that additional heat could be accounted for.

An alternative mechanism exists, however, by which additional heat can be derived from pore collapse. Two factors are of importance in defining this mechanism.

First, increased porosity is accompanied by an increase in the effective specific volume and compressibility. This results in an increase in the energy deposited in the material by a shock or pressure transient. Second, this extra energy is not deposited uniformly throughout the material. It appears primarily as a consequence of high-speed viscous flow and other dissipative effects which accompany collapse of the voids as well as of the adiabatic or shock heating of occluded gases retained by the voids. The excess energy is therefore concentrated in regions of the material contiguous to the voids, which become the so-called hot spots.

The present mathematical methods are not capable of representing the charge material with sufficient resolution to permit treatment of the formation of such hot spots. However, the effect can be simulated by adjusting the value of the activation energy used in the ignition zone.

It can be shown that for material which obeys an equation of state 18, the energy deposited by a heavy shock ($p \gg p_o$) is the following:

$$e_s = 1/2 \left[pv_o - \frac{p^2 v_o(\gamma_s - 1) + p\epsilon}{p(\gamma_s + 1) + 2\beta} \right] \tag{36}$$

Neglecting ϵ as small compared to e, one has

$$e_s \cong kv_o ,$$

where

$$k = 1/2 \left[p - \frac{p^2(\gamma_s - 1)}{p(\gamma_s + 1) + 2\beta} \right]. \tag{37}$$

The increase in energy Δe_s deposited for a given increase in initial volume, Δv, then becomes

$$\Delta e_s = k\Delta v$$

If all of this increase is deposited in a region containing a fraction, F_1, of the material, the increase in energy of this region becomes

$$\Delta e_s = \left[k/F_1\right]\Delta v_o. \tag{38}$$

If one now assumes that energy generated because of the collapse of a void is deposited in a volume of material approximately equal to the void volume, then one has

$$\Delta e_s = (k/F_1)F_1\, v_o = kv_o\ . \tag{39}$$

Thus the energy density in a hot spot created by the collapse of a void will always be approximately twice the energy of the bulk material. Simulation of a "hot spot" ignition region arising from voids in the material then becomes possible by use of an activation energy one-half that of the grain-burning reaction for the ignition process. It also follows that the term F_1, previously used to represent the fraction of material in the ignition zone, becomes equal to the fraction of the specific volume which consists of voids.

c. Burning Phase - Homogeneous Materials

When material in the ignition region has reacted completely, further reaction is postulated to take place via a surface regressive process according to the Eyring grain-burning concept. It was shown by Eyring[2] that this led to a rate expression of the form

$$\frac{df}{dt} = (1-f)^{2/3}\ \frac{a\,B}{Z}\ \exp\left[\frac{C_v A}{Re_z}\right] \tag{40}$$

where e_z/C_v was taken to be the explosion temperature. For the present application two modifications are made in the equation.

The first is based upon the argument that at low pressures, equation 40 should approach conventional expressions for the burning rate of a solid combustible material which means that it should become proportional to some power of the pressure. Since potential applications of the present treatment include low pressure processes, a term was added to make 40 conform to such behavior.

The second modification is based upon the fact that energy density at the regressing grain surface is, in reality, equal to the energy in the solid prior to reaction, plus the heat of reaction, less any work done in expansion during reaction. It is assumed that the surface regressive reaction is analagous to a deflagration, i.e., a constant pressure process. It is therefore obtained that

$$e_z = e_s + \frac{Q}{\gamma_g}$$

With these two changes, the form of grain-burning equation used in this work is the following

$$\frac{df}{dt} = (1-f)^{2/3} \frac{aB}{Z} \frac{p}{p/W + 1} \exp\left[\frac{C_v A}{R(e_s + \frac{Q}{\gamma_g})}\right] \qquad (41)$$

In cases where the ignition region is taken to be a point rather than a grain surface an analagous expression is obtained by setting

$$(1-f) = f$$

and defining Z as one half the distance between centers. The corresponding equation becomes

$$-\frac{df}{dt} = f^{2/3} \frac{aB}{Z} \frac{p}{\frac{p}{W} + 1} \exp\left[\frac{C_v A}{R(e_s + \frac{Q}{\gamma_g})}\right] \qquad (42)$$

Integration of equations 41 and 42 requires knowledge of e_s and γ_g, terms which are variable throughout the problem. γ_g is obtained as a function of volume from equation 14. Development of a suitable procedure for determining e_s represents a problem of significantly greater complexity.

It was shown by Eyring and co-workers that the high regression rates of grain surfaces during the grain-burning process effectively prevents conduction of heat into the unburned solid. Accordingly only two processes exist by which the energy of the solid can change; first by overall compressions or expansions due to hydrodynamic motion, and second, by an effect analagous to the burning of a solid material in a completely filled bomb. The latter is shown by the diagram of figure 1. The top diagram (a) shows the filled bomb before any material has burned. The cross-hatched area at the left represents material which is about to react, i.e. the reaction zone. The second diagram (b) represents the situation after this material has reacted. The reacted material now occupies a greater volume because it obeys a different equation of state and because of the released energy of reaction which it contains. The remaining solid has been compressed and is at a higher energy density because of the compressive work performed upon it. This process amounts to a transfer of energy from the gas to the solid as pv work.

The mixture of solid and gaseous materials which comprises the partially reacted material is assumed to be represented by a collection of units similar to that shown on figure 1, the walls of the bomb, in each case consisting of surrounding neighbors. These units move as entities in response to hydrodynamic forces, with the effects discussed above superimposed. Treatment of the overall process is therefore approached in the following way.

Changes in volume of the gaseous phase, dv_g, are taken as the sum of three effects: Hydrodynamics expansions or contraction, transfer of material from the solid to the gaseous phase and addition of heat to the gaseous phase. Considering the first and second of these together, one has:

First,

$$de_s = - pdv_s \tag{43}$$

From the solid equation of state:

$$(p + \beta) v_s = (\gamma_s - 1) e_s + \epsilon \tag{18}$$

$$(p + \beta) dv_s + v_s \, dp = (\gamma_s - 1) de_s + e_s d\gamma_s = -(\gamma_s - 1) pdv_s$$

Then:

$$\left[- \frac{e_s \, d\gamma_s}{p \, dv_s} + \frac{\beta}{p} + \gamma_s \right] pdv_s = - v_s \, dp$$

$$\frac{d\ln p}{d\ln v_s} = - \left[\frac{\beta}{p} + \gamma_s - \frac{e_s}{p} \frac{d\gamma_s}{dv_s} \right] \tag{44}$$

And for the gas ($\beta = 0$)

$$\frac{d\ln p}{d\ln v_g} = - \left[\gamma_g - \frac{e_g}{p} \frac{d\gamma_g}{dv} \right] \tag{45}$$

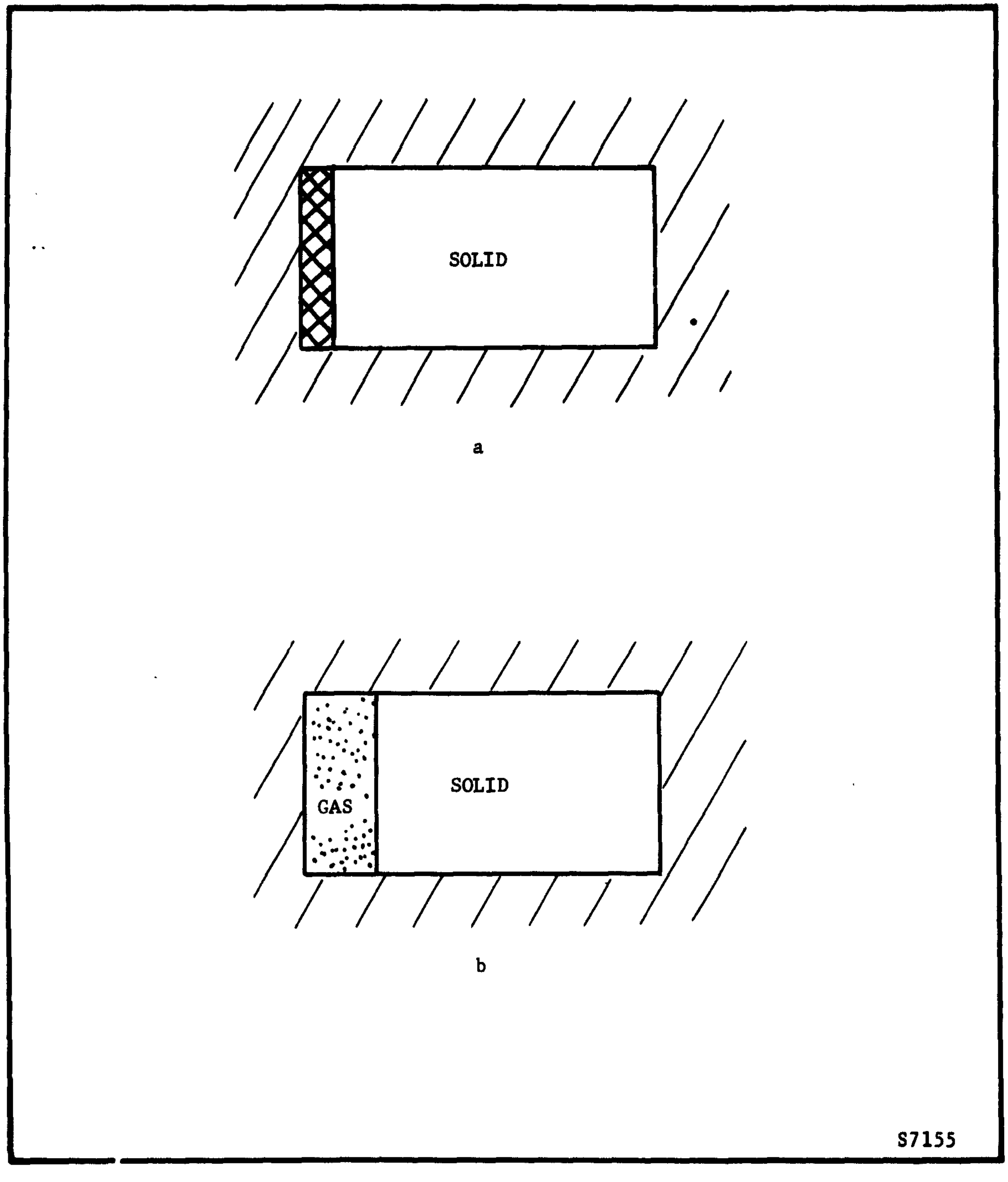
SOLID
a
SOLID
GAS
b
S7155

FIGURE 1. COMPRESSION OF SOLID BY COMBUSTION PRODUCT GASES

Also:

$$(1 - f_s)\, v_g + f_s v_s = \bar{v}$$

$$(1 - f_s)\, dv_g - v_g df_s + f_s dv_s + v_s df_s = d\bar{v}$$

From (44) and (45)

$$\frac{dv_g}{dv_s} = \frac{v_g}{v_s} \frac{\left(\gamma_s + \beta/p - \frac{e_s}{p}\frac{d\gamma_s}{dv_s}\right)}{\left(\gamma_g - \frac{e_g}{p}\frac{d\gamma_g}{dv_g}\right)} \qquad (46)$$

Combining and solving for dv_g:

$$dv'_g = \frac{d\bar{v}\ (v_s - v_g)\ df_s}{1 - f_s \left[1 - \frac{v_s \left(\gamma_g - \frac{e_g}{p} \frac{d\gamma_g}{dv_g}\right)}{v_g \left(\gamma_s + \beta/p - \frac{e_s}{p} \frac{d\gamma_s}{dv_s}\right)} \right]}$$

Treatment of the third effect causing change in vg involves the assumption that all heat due to chemical reaction remains in the gas phase. One then has:

$$f_g de_g = dE - f_g p dv_g \qquad (48)$$

$$f_s de_s = p f_s dv_s \qquad (49)$$

From the equations of state:

$$de_s = \frac{1}{\gamma_s - 1}\left[(p + \beta)\ dv_s + v_s\ dp\right] \qquad (50)$$

$$de_g = \frac{1}{\gamma_g - 1}\left[p dv_g + v_g dp\right] \qquad (51)$$

Also:

$$dv_s = - \frac{1 - f_s}{f_s} dv_g \qquad (52)$$

Elimination of dp, de_s, de_g and dv_s between equations 48-52 gives

$$dv_g'' = \frac{(\gamma_g - 1)\ dE}{(1 - f_s)\ p\ \gamma_g + (p\gamma_s + \beta)\ \frac{v_g}{v_s}\ \frac{(1 - f_s)^2}{f_s}} \tag{53}$$

One then has

$$dv_g = dv_g' + dv_g'' \tag{54}$$

By similar methods, the expression for dv_s is found to be:

$$dv_s = \frac{d\bar{v} - (v_s - v_g)\ df_s}{f_s + (1 - f_s)\ \frac{v_g}{v_s} \left[\frac{\gamma_s + \beta/p - \frac{e_s}{p}\ \frac{d\gamma_s}{dv_s}}{\gamma_g - \frac{e_g}{p}\ \frac{d\gamma_g}{dv_g}} \right]} \tag{55}$$

and finally:

$$de_s = -p dv_s$$

Equations 54, 55 and 56 are integrated through the problem and provide knowledge of e_s at every point for use in equations 41 and 42.

c. Burning Phase - Composite Materials

The necessity of a capability for treating composite or multiphase detonable materials requires some extension of the grain-burning concept of reaction. The material is conceived as an assemblage of units, each consisting of a spherical grain of one phase, normally the oxidizer, surrounded by the second phase, i.e. binder. The ignition region is taken to occur at the interface between the two.

If both phases are self-reactive, then the reaction of the spherical grain is described by an expression of the form of (38) and reaction of the binder phase by an equation such as (39) modified to provide for initiation at some finite radius. This capability is available in the present numerical program. However, in all problems of this type which were treated, it was deemed satisfactory to describe the reaction of both phases by identical expressions, either 38 or 39, simply using appropriately different values of the rate parameters. No distinction is made in the physical properties of the various solid phases so that a single solid equation of state is used and a single value of e_s is computed in the integration.

In multiphase systems, the possibility also exists that the products of reaction in one phase can react with other phases upon mixing. It is presumed that the mixing takes place more slowly than the solid surfaces recede as a consequence of the grain burning or vaporization reactions, the diffusional reaction then being regarded as something analagous to a diffusion flame located approximately at the original interface region. It follows that the rate of the process is approximately that of the diffusion of material from a sphere with the surface concentration always zero. From diffusion theory[12] the following approximate expression is obtained for the fractional completion of such a diffusion process

$$f_4 = 1 - \left[0.8 \exp\left(- \frac{D\pi^2 (t-\tau)}{z^2}\right) + 0.2 \exp\left(- \frac{4D\pi^2(t-\tau)}{z^2}\right)\right] \quad (57)$$

This process is particularly applicable to the case of composite propellants where the binder phase is nonself-reactive. However, it contributes to the effective heat release in the material only when oxidizer particle sizes are in the range of one micron.

The diffusion coefficient D and the grain radius Z, both change with hydrodynamic expansion in the region of the detonation wave behind the shock front. If expansion is significant through the reaction zones of either the diffusion or grain burning reactions, representation of this change is necessary. It is much more likely to be required with the diffusion reaction since when the initial value of z is greater than one micron, as is normally the case the diffusion reaction is very slow. These two quantities are calculated by means of the following expressions:

$$D = D_s + Do/p \quad (57a)$$

$$Z = Zo \frac{Vg}{Vo} \quad (57b)$$

D_s is taken as the diffusion coefficient in liquids, and D_o that in gases, at ambient pressure. Z_o and V_o are the initial grain radius and specific volume of the explosive material.

SECTION 3

MATHEMATICAL PROCEDURES

3.1 GENERAL PRINCIPLES

Finite difference methods for solving systems of equations such as those discussed in the previous section are described by Richtmeyer.[13] The concepts and nomenclature used by this author are relatively straightforward and have been used in this work. Many ways of differencing are possible, depending primarily upon the order in which the various needed quantities are computed, i.e., upon the path through the computational scheme. Not all of these produce satisfactory results. The most convenient method of evaluating a given procedure is by trial; while the methods presented here appear to be satisfactory, their present form is the result of continuous modification and development throughout the course of the program, and it is likely that further improvement is possible. A few specific points merit special attention.

In the ignition calculation, it is assumed that no chemical energy is released until the material ignites, at which point all the energy from the ignition process is added, and is taken to be uniformly distributed through the charge. This procedure is based upon the precept that during the initial stages of ignition, when reaction is relatively slow, there will be time for conduction out of the ignition region. In the latter stages, an exponential increase in rate occurs so that most of the heat release occurs in a very short period of time. The procedure used is thus a reasonable approximation to the behavior which is to be expected. It has the consequence that ignition behavior is defined primarily by hydrodynamic heating and is relatively independent of the chemical energy release.

The differencing of Equations 49 and 50 which appear in the grain burning phase, involves evaluation of the contribution of chemical reaction to the energy density in the gas phase, dE. This was done as follows.

Burning is a process by which heat and mass are added to the gas phase. If this is conceived as occurring in discrete steps in which the mass is added first, and the energy second, one can write

$$dE = \left(e_g^{n+1} - e_g^{n}\right) f_g^{n+1} \tag{58}$$

However the overall process is:

$$\begin{aligned} f_g^{n+1} e_g^{n+1} - f_g^{n} e_g^{n} = {} & Q_2F_2\left(f_2^{n} - f_2^{n+1}\right) + Q_3F_3\left(f_3^{n} - f_3^{n+1}\right) \\ & + Q_4F_4\left(f_4^{n} - f_4^{n+1}\right) + e_s^{n}\left(f_s^{n} - f_s^{n+1}\right) \end{aligned} \tag{59}$$

Transposing and subtracting $e_g^{n} f_g^{n+1}$ from both sides:

$$\begin{aligned} dE = \left(e_g^{n+1} - e_g^{n}\right) f_g^{n+1} = {} & \left(e_s^{n} - e_g^{n}\right)\left(f_s^{n} - f_s^{n+1}\right) + Q_2F_2\left(f_2^{n} - f_2^{n+1}\right) \\ & + Q_3F_3\left(f_3^{n} - f_3^{n+1}\right) + Q_4F_4\left(f_4^{n} - f_4^{n+1}\right) \end{aligned} \tag{60}$$

Considerable difficulty has been encountered in computing the correct ultimate velocities and Chapman-Jouguet characteristics for detonation waves, as predicted by steady state theory and reported from experimental observation. Many explanations for this are conceivable; however, the one which is now believed to be correct is related to the use of the von Neuman-Richtmeyer "q." This term was originally used in numerical procedures for integrating through shocks in unreactive media. The basic equations in such problems, consist of the conservation equation and an equation of state, which together define shock behavior. It was shown that although use of the "q" term causes distortion in the shock region, it has no effect on quantities such as energy, pressure, and particle velocity at some distance on either side of the shock region, and provides correct treatment of propagation velocity. However, for detonations, definition of wave behavior requires an additional relation generally known as the Chapman-Jouguet condition. It now appears that under some circumstances use of the von Neuman "q" can lead to an incorrect Chapman-Jouguet condition. This point can be understood by means of the following arguments.

Figure 2a shows an actual pressure profile through a detonation wave as envisioned in terms of the hydrodynamic theory. The wave is initiated as a shock in which the pressure rises discontinuously from p_o to p_2. Reactions start at pressure p_2 and continue until completion at the Chapman-Jouguet point, p_1.

Figure 2b shows the same wave computed using equations which include the von Neuman "q". Here the wave initiates with a gradually rising continuous pressure front which has a rounded off peak pressure, p_2. In between there is a region of steeply rising pressure. The "q" used in the calculation is computed continuously through the rising pressure region as proportional to the square of the rate of compression, and provides for the same total energy deposition at the peak of the wave, p_2, as in a shock process. In both cases the propagation velocity is given by

$$U = \frac{1}{\rho_o} \sqrt{-\frac{p_1 - p_o}{v_1 - v_o}} \qquad (61)$$

With the situation represented as in Figure 2b, it is evident that if chemical reaction in the charge is readily initiated, such initiation may take place during the initial part of the pressure rise and reaction may be largely complete by the time the material has passed through the front and reached the point, p_2. Thus, in contrast to the situation represented in Figure 2a, a major part of the chemical reaction and the corresponding heat release occurs, in effect, as part of the shock process. This has been observed to occur in typical examples of computed waves.

The consequences of such behavior in terms of wave velocity can be appreciated by consideration of a typical Hugoniot diagram as shown on Figure 3. According to the conventional interpretation,[14,15] Figure 2a is represented on such a diagram as a process in which an increment of material starts at 0 as undisturbed material, jumps to 2 on passing through the lead shock and then moves down the line 21 while undergoing reaction, to 1, the Chapman-Jouguet point. At point 2, energy deposited by the shock in unreacted material is given by area 042. In the subsequent expansion to point 1, work represented by area 4216 is performed and the reaction energy, Q, is released. Thus, at point 1, energy remaining in the system is given by area 061 + Q.

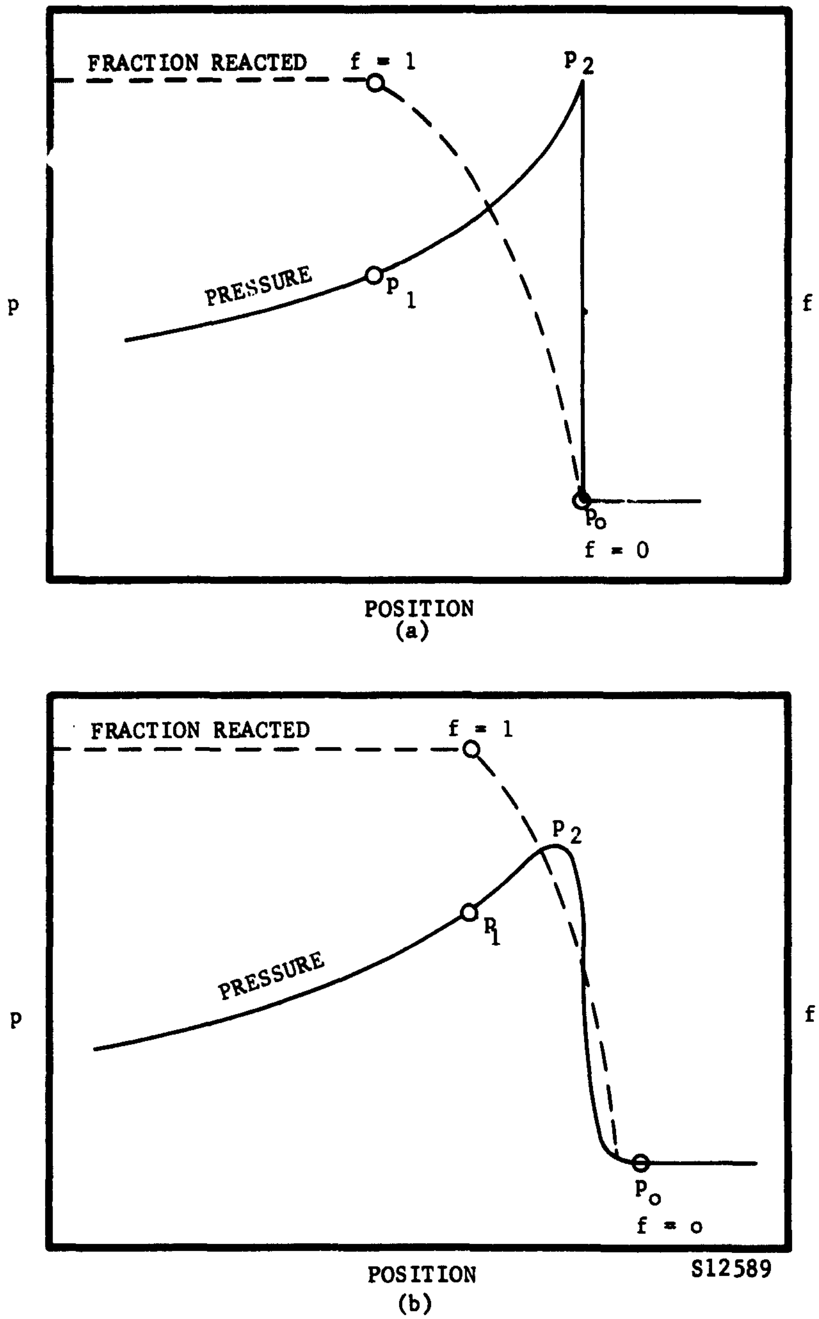
FRACTION REACTED
f = 1
P 2
PRESSURE
P 1
p
f
P o
f = 0
POSITION
(a)
FRACTION REACTED
f = 1
P 2
P 1
PRESSURE
p
f
P o
f = o
POSITION
S12589
(b)

FIGURE 2. WAVE PROFILES WITH AND WITHOUT VON NEUMAN Q

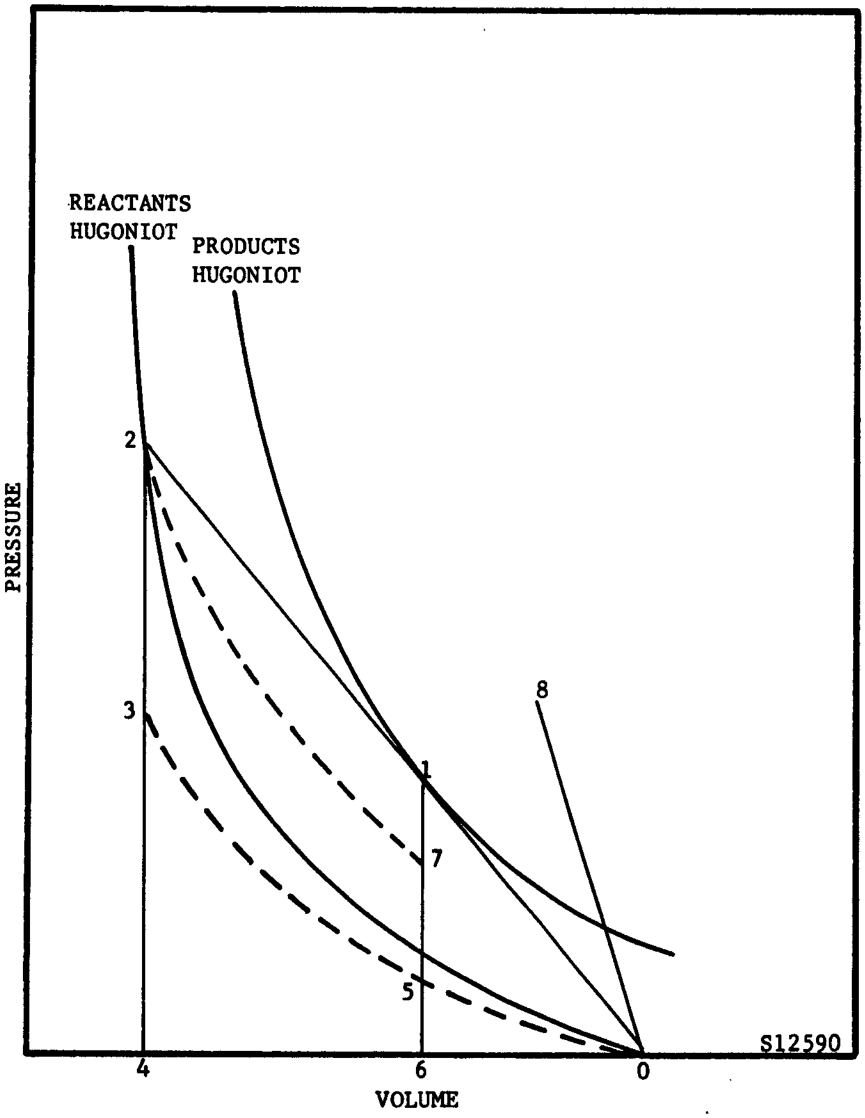
REACTANTS HUGONIOT
PRODUCTS HUGONIOT
PRESSURE
VOLUME
2
3
1
7
8
5
4
6
0
S12590

FIGURE 3. HUGONIOT DIAGRAM FOR DETONATION PROCESS

In the representation of the process shown in Figure 2b on a Hugoniot diagram, it is convenient to consider the extreme case in which reaction has gone to completion by the time point 2 is reached. In this circumstance, points 1 and 2 coincide and on Figure 2 the system goes directly from point 0 to point 1. Since this is treated as a shock transition, energy equivalent to area 061 is deposited in the process. The system energy at point 1, therefore, is equivalent to area 061 + Q, exactly as before.

The first process can be considered as an isentropic compression along the adiabat 053, followed by heating (via shock dissipation) along 32 with a corresponding increase in entropy given by $\int_3^2 TdS$ = area 032, thence isentropic expansion along the adiabat 27, followed by heating due to reaction along 71, the latter involving a further entropy increase given by $\int_7^1 TdS = Q$ (the heat of reaction). The second process is made up of compression along the adiabat 05, and heating along 51 (due to chemical reaction and shock dissipation) with entropy increase corresponding to $\int_5^1 TdS$ = area 051. Considering that temperatures are highest at the Chapman-Jouguet point, it is apparent from these relations that the entropy increase in the second process is smaller than the first. Since the final energy content is the same in both cases, it must be concluded that the second process results in a higher pressure at the Chapman-Jouguet point than does the first. Therefore, the second process cannot terminate at point 1, but must instead arrive at some point at a higher pressure, such as 8. From equation (1), the relative propagation velocities in the two cases will be given by ratio of the square root of the slopes of the lines 01 and 08. It thus becomes evident that the situation represented by Figure 2b will correspond to a higher velocity than the value deduced from the steady state treatment.

In present procedures, the foregoing effect is avoided by arbitrarily holding up all reactions until the zone in question has passed completely through the shock, as determined by the condition $q = 0$. This is believed to be in accordance with the hydrodynamic concept of a shock as a discontinuity, which implies an instantaneous transition from ambient pressure to peak shock pressure, so that reaction is initiated at the point of peak pressure.

For reasons similar to the above, it is also probable that small consistant errors in computing pressure in the region of the shock will tend to produce erroneous ultimate steady state behavior. For example, a consistent overshoot in peak pressure amounts to an effective addition of energy to the wave. Avoidance of such effects requires accurate treatment in the shock zone which in turn implies a requirement of very fine zoning in this region. To meet this requirement without having to accept excessive computing times, a procedure was developed to impose an ultra-fine space mesh onto the main space mesh.

The fine zone routine is designed to automatically insert a fine zone mesh in front of the oncoming shock and to merge the fine zones back into their original zones whenever the reaction rates fall below certain specified values.

At the beginning of every problem, two counters are set which control the insertion and deletions of the fine zone mesh. These two counters, j_b, which define the lower boundary of the fine zone mesh, and j_c, which defines the upper boundary of the fine zone mesh, are initialized to j_{max}, where j_{max} is the total number of points in the problem at the beginning. The insertion of the first fine zone occurs at the end of the first microcycle, before point j_{max} is accelerated. At this time, a Δx is subtracted from $x_{j_{max}}$ to define the boundary of the new fine zone (x_f). A check is made to insure that x_f is $\geq x_{j_{max-1}} + \Delta x/3$. When x_f passes this test, j_{max} and j_c are increased by one and the mesh is moved one slot upward in memory from j_b to j_{max}. x_f is then inserted in the slot formerly occupied by x_{j_b} and indeed is the new x_{j_b}. The mass associated with the previous x_{j_b} is distributed between the old and the new zone. The time associated with the new point is the minimum of the time associated with the point $x_{j_{b-1}}$ and the old x_{j_b}. The program then returns to the main loop and does point j_b to j_{max}.

The general scheme for inserting a fine zone is much the same as for the first one, except for determining where and when it should be inserted. The criteria for the insertion of a fine zone, in the general case, are:

(1) $U_j = 0$

(2) $\Gamma_{j+1} < 0$

(3) $j = j_b$

(or) $j+1 = j_b$

One other significant factor to be accounted for is the case when $x_f < x_{j_{b-1}} + \Delta x/3$. When this occurs, no fine zone is inserted; one is subtracted from j_b and the problem is allowed to continue.

At the end of every macrocycle, the fine zone mesh is checked to evaluate whether any of the fine zones pass the qualifications to be re-merged into their original zones. The qualification for a fine zone to be re-merged requires that the reaction rate of f_1 must fall below a preset value. In addition, it is required that re mergence must be continuous and contigious from the ignition end.

An additional procedure for conserving computing time was developed in the form of a so-called "variable time step" (Aeronutronic Hop Program). In effect, it involves calculation of a separate time interval for each space zone, based upon the rate at which the variables are changing in the zone. Calculations of the variables are carried out only in those regions for which this t is less than the macrocycle time Δt_c, an arbitrary time interval by which the main time frame is advanced. When all zones arrive at the time of the main frame, the latter is advanced by Δt_c, new variables are computed for the inactive points, and the process is repeated.

Application of the Hop and fine zoning techniques to the treatment of detonation behavior is believed to represent the best combination of accuracy and economy of computing time that is presently available.

3.2 THE FLOW SCHEME - ONE DIMENSIONAL PROGRAM

The difference equations used in the one dimensional case are given here in the form of a flow scheme of the computer program. The fine zoning routine is not included. All variables are referred to the space coordinate j-1/2 unless otherwise indicated.

3.2.1 HYDRODYNAMIC EQUATIONS INCLUDING DISSIPATIVE q FACTOR

$$\Delta t_j^{n+1/2} = \min \left(\Delta t_{j-1/2}^{n+1/2} , \Delta t_{j+1/2}^{n+1/2} \right) \tag{62}$$

$$t_j^n + \Delta t_j^{n+1/2} \quad : \quad t_c^{n+1} \tag{63}$$

(a) if $<$, go to 64

(b) if $\geq$, $\Delta t_j^{n+1/2} = t_c^{n+1} - t_j^n$

$$u_j^{n+1/2} = \frac{\Delta t^{n+1/2} + \Delta t^{n-1/2}}{(\rho\Delta x)^n_{j+1/2} + (\rho\Delta x)^n_{j-1/2}} \left(p^n_{j-1/2} + q^{n-1/2}_{j-1/2} - p^n_{j+1/2} - q^{n-1/2}_{j+1/2}\right) + u_j^{n-1/2} \tag{64}$$

$$\rho^n_{j-1/2}\left[\left(x_j^n\right)^\eta - \left(x_{j-1}^n\right)^\eta\right] = \rho^{n+1}\left[\left(x_j^{n+1}\right)^\eta - \left(x_{j-1}^{n+1}\right)^\eta\right] \tag{65}$$

where $\eta = 1, 2, 3$ for slab, cylindrical, or spherical geometry

$$x_j^{n+1} = x_j^n + u_j^{n+1/2}\, \Delta t^{n+1/2} \tag{66}$$

In equation 64 the q term is the von Neuman-Richtmeyer artificial viscosity and is given by:

$$q^{n-1/2}_{j-1/2} = \rho^n \left[\theta^2 \left(u_j^{n-1/2} - u_{j-1}^{n-1/2}\right) - \lambda c_j^n\right]\left(u_j^{n-1/2} - u_{j-1}^{n-1/2}\right) \tag{67}$$

when $\left(u_j^{n-1/2} - u_{j-1}^{n-1/2}\right) \geq 0$

$$q^{n-1/2}_{j-1/2} \equiv 0$$

The mass behind the j^{th} coordinate is defined by:

$$m_{j-1/2} = \left(\rho_a\right)_{j-1/2}\left[\left(x_a\right)_j^\eta - \left(x_{j-1}\right)^\eta\right]$$

$$v^{n}_{j-1/2} = 1/\rho^{n}_{j-1/2}$$

$$\rho^{n+1}_{j-1/2} = \frac{m_{j-1/2}}{\left(x^{n+1}_{j}\right)^{\eta} - \left(x^{n+1}_{j-1}\right)^{\eta}}$$

$$\tau_{j} \; : \; 0 \tag{68}$$

(a) If $\overline{<}$, go to ignition routine

(b) If $>$, go to burn routine

3.2.2 IGNITION PHASE

$$\gamma^{n+1}_{s} = \gamma_{o} + \left[\frac{b}{\bar{v}^{n+1}} + \left(\frac{b}{\bar{v}^{n+1}}\right)^{2}\right]\left(\gamma_{o} - 1\right)$$

$$p^{n+1} = \left(p^{n} + \frac{\beta}{\gamma^{n}_{s}} + q^{n+1/2}\right)\left(\frac{\rho^{n+1}}{\rho^{n}}\right)^{\gamma^{n+1}_{s}}$$

$$\cdot \left[\frac{\gamma^{n}_{s} - 1}{\gamma^{n+1}_{s} - 1}\right]\left(\frac{p^{n} + \beta - \epsilon/\bar{v}^{n}}{p^{n} + \beta/\gamma^{n}_{s} + \frac{\gamma^{n}_{s} - 1}{\gamma^{n}_{s}} \, q^{n+1/2}}\right)$$

$$- \frac{\beta}{\gamma^{n+1}_{s}} - q^{n+1/2} \tag{69}$$

$$e^{n+1} = \left[\left(p^{n+1} + \beta\right)\bar{v}^{\,n+1} - \epsilon\right] \Big/ \left(\gamma_s^{n+1} - 1\right) \qquad (70)$$

When a shock is passing through an unignited zone, the ignition reaction calculations are by passed until the zone begins to expand.

For contracting material

$$c_j^{n+1} = \left(\frac{\gamma_s^{n+1} \quad \rho^{n+1} + \beta}{e^{n+1}}\right)^{1/2} \qquad (71)$$

$$\Delta t_j^{n+1} = \frac{\chi\left(x_j^{n+1} - x_{j-1}^{n+1}\right)}{c_j^{n+1} - 4\theta^{2}\,\Delta u_j^{n+1/2} + \lambda\, c_j^{n+1/2}} \qquad (72)$$

Return to Main Hydro (73)

For expanding material:

Define: $\Delta t_o = t_j^n - (t_\ell)_j^n$ i.e, Δt_o is the difference between main coordinate time and zone local time $(t_\ell)_j^n$ before any hydro calculations have been made (74)

Set: $\Delta t = \Delta t_o$

$$y = A_1 \Big/ \left[\left(e^n + e^{n+1}\right) \Big/ 2 - Q_1\left(1 - f_1\right)\right] \qquad (75)$$

$$G = B_1\, c^{-y} \qquad (76)$$

$$G : o \qquad (77)$$

(a) if $=$, $f_1^n \rightarrow f_1^{n+1}$, go to 71

(b) if $\neq$, continue

Set $\delta t = \dfrac{\psi}{f_1^n \, G}$ (78)

$\delta t \; : \; \Delta t$ (79)

(a) if $>$, go to 80

(b) if $<$, go to 82

$f_1^{n+1} = f_1^n \, e^{-G \delta t}$ (80)

$f_{1_{j-1/2}}^{n+1} \; : \; \Gamma$

(a) If $>$; $\Delta t - \delta t \rightarrow \Delta t$ (81)
go to 75

(b) If $\leq$, $1 \rightarrow f_1^{n+1}$
go to 84

$f_1^{n+1} = e^{-G \, \Delta t}$ (82)

$f_{1_{j-1/2}}^{n+1} \; : \; \Gamma$ (83)

(a) If $>$, go to 71

(b) If $\leq$, $1 \rightarrow f_1^{n+1}$

continue

$$\tau_j = t_j^n + \Delta t_o - \Delta t \qquad (83)$$

go to 71

3.2.3 BURNING PHASE

The variables are initialized as follows upon first entry into the Burn Routine.

Grain Surface Burning

$$\gamma_g^n = \gamma_s^n \qquad (85)$$

$$e_s^n = e^n \qquad (86)$$

$$e_g^n = e^n \qquad (87)$$

$$f_4^n = 1.0 \qquad (88)$$

$$\left(f_3^{1/3}\right)^n = 1.0 \qquad (89)$$

$$\left(f_2^{1/3}\right)^n = 1.0 \qquad (90)$$

$$v_s^n = v_{j-1/2}^n \tag{91}$$

$$v_g^n = v_{j-1/2}^n \tag{92}$$

$$\left(\Delta\gamma_{g/\Delta v_g}\right)^n = 0 \tag{93}$$

$$\left(\Delta\gamma_{s/\Delta v_s}\right)^n = 0 \tag{94}$$

$$f_1^n = F_2 + F_3 + F_r \tag{95}$$

$$\left(f_2^{1/3}\right)^{n+1} = \left(1 - F_1\right)^{1/3} \tag{96}$$

$$\left(f_3^{1/3}\right)^{n+1} = \left(1 - F_1\right)^{1/3} \tag{97}$$

Internal Grain Burning

Same as above with the following exceptions:

$$\left(f_2^{1/3}\right)^n = 0 \tag{98}$$

$$\left(f_3^{1/3}\right)^n = 0 \tag{99}$$

$$\left(f_2^{1/3}\right)^n = F_1^{1/3} \tag{100}$$

$$\left(f_3^{1/3}\right)^n = F_1^{1/3} \qquad (101)$$

$$\begin{aligned} B_2 &= -B_2 \\ B_3 &= -B_3 \\ Q_2 &= -Q_2 \\ Q_3 &= -Q_3 \end{aligned} \qquad (102)$$

The burning phase equations are the following:

$$z^n = z^o \left(\frac{v_g^n}{v_s^n} \right)^{1/3} \qquad (103)$$

$$D^{n+1} = \frac{\pi^2 \left[D_s + D_o \big/ \rho^n \right] \left(t_j^n - \tau_j \right)}{\left(z^2 \right)^n} \qquad (104)$$

$$f_4^{n+1} = 0.8 \exp\left(-D^{n+1}\right) + 0.2 \exp\left(-4D^{n+1}\right) \qquad (105)$$

$$f_4^{n+1} : F_1$$

(a) If $\leq$; $F_1 \rightarrow f_4^{n+1}$; go to 107

(b) If $>$; go to 107

$$\overline{e}^{\,n} : 0$$

(a) If < ; $\left(f_2^{1/3}\right)^n \rightarrow \left(f_2^{1/3}\right)^{n+1}$

$$\left(f_3^{1/3}\right)^n \rightarrow \left(f_3^{1/3}\right)^{n+1} \tag{107}$$

go to 110 or 111

(b) If $\geq$; go to 108

$$\left(f_2^{1/3}\right)^{n+1} = \left(f_2^{1/3}\right)^n \frac{a\,\beta_2\Delta t_i}{Z^n} \frac{p^m}{\frac{p^m}{w}+1} \exp\left(\frac{c_v A_2}{R\left[e_s^n + \frac{Q_2'}{\gamma_g^n}\right]}\right) \tag{108}$$

$$\left(f_3^{1/3}\right)^{n+1} = \left(f_3^{1/3}\right)^n \frac{a\beta_3\Delta t_i}{Z^n} \frac{p^m}{\frac{p^m}{w}+1} \exp\left(\frac{c_v A_3}{R\left[e_s^n + \frac{Q_3'}{\gamma_g^n}\right]}\right) \tag{109}$$

For Surface Burning:

$$f_s^{n+1} = F_2\, f_2^{n+1} + F_3\, f_3^{n+1} + f_r \tag{110}$$

For Internal Burning:

$$f_s^{n+1} = F_2 \left(1-f_2\right)^{n+1} + F_3 \left(1-f_3\right)^{n+1} + F_r \tag{111}$$

$$f_1^{n+1} \quad : \quad 0 \tag{112}$$

(a) If ≤ 0; go to 113

(b) If > 0; go to 120

$$v_s^n \rightarrow v_s^{n+1} \tag{113}$$

$$\bar{v}^{\,n+1} \rightarrow v_g^{n+1} \tag{114}$$

$$\gamma_g^{n+1} = \gamma_o + \left[\frac{b}{v_g^{n+1}} + \left(\frac{b}{v_g^{n+1}}\right)^2\right]\left(\gamma_o - 1\right) \tag{115}$$

$$p_{j-1/2}^{n+1} = \frac{\left(\gamma_g^n - 1\right)\left[e^n + J^{n+1} - \left(p^n + 2q^{n+1/2}\right)\left(\frac{\bar{v}^{\,n+1} - \bar{v}^{\,n}}{2}\right)\right]}{\bar{v}^{\,n+1} + \left(\gamma_g^{n+1} - 1\right)\left(\frac{\bar{v}^{\,n+1} - \bar{v}^{\,n}}{2}\right)} \tag{116}$$

where

$$J^{n+1} = F_2Q_2\left(f_2^n - f_2^{n+1}\right) + F_3Q_3\left(f_3^n - f_3^{n+1}\right) + Q_4\left(f_4^n - f_4^{n+1}\right) \tag{117}$$

$$e_{j-1/2}^{n+1} = e^n - \left(p^{n+1} + p^n + 2q^{n+1/2}\right)\left(\frac{\bar{v}^{\,n+1} - \bar{v}^{\,n}}{2}\right) + J^{n+1} \tag{118}$$

Go to 129 (119)

$$I^{n} = \frac{\gamma_{s}^{n} + \dfrac{\beta - e_{s}^{n}\left(\dfrac{\Delta\gamma_{s}}{\Delta v_{s}}\right)^{n}}{p^{n}}}{\gamma_{g}^{n} - \dfrac{e_{g}^{n}}{p^{n}}\left(\dfrac{\Delta\gamma_{g}}{\Delta v_{g}}\right)^{n}} \qquad (120)$$

$$I^{n} = I^{n}\left(\frac{v_{g}}{v_{s}}\right)^{n}$$

$$v_{s}^{n+1} = \frac{v_{s}^{n} + \left(\bar{v}^{\,n+1} - \bar{v}^{\,n}\right) - \left(v_{g}^{n} - v_{s}^{n}\right)\left(f_{s}^{n} - f_{s}^{n+1}\right)}{f_{1}^{n+1} + \left(1 - f_{s}^{n+1}\right) I^{n}} \qquad (121)$$

$$v_{g}^{n+1} = \frac{v_{g}^{n} + \left(\bar{v}^{\,n+1} - \bar{v}^{\,n}\right) - \left(v_{g}^{n} - v_{s}^{n}\right)\left(f_{s}^{n} - f_{s}^{n+1}\right)}{\left(1 - f_{s}^{n+1}\right)\left(1 - 1/_{I^{n}}\right)}$$

$$+ \frac{\left(\gamma_{g}^{n} - 1\right)\left[\left(e_{s}^{n} - e_{g}^{n}\right)\left(f_{s}^{n} - f_{s}^{n+1}\right) + J\right]}{\left(1 - f_{s}^{n+1}\right)\left[p^{n}\gamma_{g}^{n} + \left(p^{n}\gamma_{s}^{n} + \beta\right)\left(\dfrac{v_{g}}{v_{s}}\right)^{n}\left(\dfrac{1 - f_{s}^{n+1}}{f_{s}^{n+1}}\right)\right]} \qquad (122)$$

$$\gamma_{g}^{n+1} = \gamma_{o} + \left[\frac{b}{v_{g}^{n+1}} + \left(\frac{b}{v_{g}^{n+1}}\right)^{2}\right]\left(\gamma_{o} - 1\right) \qquad (123)$$

$$\gamma_s^{n+1} = \gamma_o + \left[\frac{b}{v_s^{n+1}} + \left(\frac{b}{v_g^{n+1}} \right)^2 \right] \left(\gamma_o - 1 \right) \tag{124}$$

$$p^{n+1} = \frac{\left(\gamma_g^n - 1\right) \quad \bar{e}^{\,n} - \frac{f_s^{n+1}}{\left(\gamma_s^{n+1} - 1\right)} \left(\beta\, v_s^{n+1} - \epsilon \right) + J - \left(p^n + 2q^{n+1/2} \right) \left(\frac{v^{n+1} - v^n}{2} \right)}{\bar{v}^{\,n} + \left[\frac{\gamma_g^{n+1} - \gamma_s^{n+1}}{\gamma_s^{n+1} - 1} \right] f_s^{n+1}\, v_s^{n+1} + \left(\gamma_g^{n+1} - 1 \right) \left(\frac{\bar{v}^{\,n+1} - \bar{v}^{\,n}}{2} \right)} \tag{125}$$

$$\bar{e}^{\,n+1} = \bar{e}^{\,n} - \left[\left(p^{n+1} + p^n + 2q^{n+1/2} \right) \left(\frac{\bar{v}^{\,n+1} - \bar{v}^{\,n}}{2} \right) - J \right] \tag{126}$$

$$e_g^{n+1} = \frac{p^{n+1}\, v_g^{n+1}}{\gamma_g^{n+1} - 1} \tag{127}$$

$$e_s^{n+1} = e_s^n + \left(\frac{v_s^n - v_s^{n+1}}{2} \right) \left(p^n + p^{n+1} + 2q^{n+1/2} \right) \tag{128}$$

$$c^{n+1} = \frac{1}{p^{n+1}} \left[\left(f_s^{n+1}\, \gamma_s^{n+1} + \left(1 - f_s^{n+1} \right) \gamma_g^{n+1} \right) p^{n+1} + \beta\, f_s^{n+1} \right] \tag{129}$$

$$\Delta t_j^{n+1/2} = \frac{x\, \Delta\, x_j^{n+1}}{c^{n+1} - 4\theta^2 \quad \Delta u_j^{n+1/2} + 2\, \lambda\, c^{n+1}} \tag{130}$$

Return to main hydro (131)

Definitions:

$$\left(\frac{\Delta\gamma_g}{\Delta v_y}\right)^{n+1} = \frac{\gamma_g^{n+1} - \gamma_g^{n}}{v_g^{n+1} - v_g^{n}} \tag{132}$$

$$\left(\frac{\Delta\gamma_s}{\Delta v_s}\right)^{n+1} = \frac{\gamma_s^{n+1} - \gamma_s^{n}}{v_s^{n+1} - v_s^{n}} \tag{133}$$

SECTION 4

INPUT DATA

4.1 EQUATIONS OF STATE - GAS PHASE

The only parameter appearing in the gas equation of state, equation 10, is the γ. This is taken to be a function of volume, defined by equation 14 of Section 2. As discussed in Section 2, the term b appearing in 14 is determined to have a value of 1.03 by fitting to experimental data obtained by M. A. Cook. The term γ_o refers to the specific heat ratio of a normal gas at ambient conditions and was assigned the value of 1.3

4.2 EQUATION OF STATE - SOLID PHASE

The required input for the equation of state of the solid phase, equation 18, are values or functions which define the parameters γ, β and ϵ. An experimental program for procurement of the necessary information is discussed in a later section. It has only recently been completed, however, and the data which it has provided have not become available in time to be used in the theoretical calculations on detonation behavior which are reported herein. For these calculations, preliminary estimates of the above parameters have been made in the following way.

As discussed in a previous section, a reasonable approximation is that at detonation pressures, the equations of state of solids and gases are similar. It was accordingly assumed that the γ for the solid could be calculated by means of an expression identical to that for the gaseous phase, equation 14, i.e.,

$$\gamma_s = \gamma_o + \left[\frac{b}{v_s} + \frac{b^2}{v_s^2}\right] (\gamma_o - 1) \qquad (14S)$$

The term γ_o in this equation is assigned a value appropriate to a harmonic oscillator solid, namely 1.3. b is determined from the data of M. A. Cook to be 1.03 as discussed in Section 2.

The quantity β was chosen to be consistent with the approximate isothermal compressibility shown by rubber-like materials at ambient pressure. This was regarded as reasonable since the compressibility of such materials decreases rapidly at increasing pressure, and a major part of the energy deposition during compression will occur at low pressures. Data given by Bridgeman,[16] and by Weir,[17] for the compressibility of rubbers from 0 to 1000 atmospheres are shown in Table 2. It indicates an average value of $\frac{1}{v}\frac{dv}{dp}$ in the range of 3×10^{-5}. From Equation 18 one has

$$\frac{1}{v}\frac{dv}{dp} = \frac{1}{p+\beta}$$

so that at zero pressure

$$\beta = 3 \times 10^4 \text{ bar}$$

It is normally to be expected that propellants will be somewhat harder than rubbers, so that the value actually used in the calculations was:

$$\beta = 5 \times 10^4 \text{ bar.}$$

The parameter ϵ appears in expression 18 primarily to permit a finite volume and pressure at $e_s = 0$. Its value is calculated from the material density at ambient conditions for any specific problem.

4.3 THE REACTION RATE EQUATIONS

The parameters appearing in the rate equations are of two types: those which differ only to a small extent among different materials, and those which differ among different materials to such a degree as to produce significant differences in rate. Included in the first group are a, Z, F, w, D_o, D_s. The second includes m, A_1, A_2, A_3, B_1, B_2, B_3, Q_1, Q_2, Q_3, Q_4.

Values were deduced for members of the first group in the following way. The term, a, was taken as the effective thickness of a molecular layer, and assigned the average value of 4×10^{-8}cm. D_o and

TABLE 2

COMPRESSIBILITY OF RUBBERS

Material	Average Compressibility (bar^{-1}) (0-1000 bar)
Hycar OR-25[17]	3.35×10^{-5}
Hycar OR-15[17]	3.35×10^{-5}
Neoprene[17]	2.8×10^{-5}
Thiokol ST[17]	2.73×10^{-5}
Gum Rubber[16]	2.6×10^{-5}

D_s were assigned average values observed for the diffusion coefficients of gaseous and liquid materials, i.e. 0.1 $\mathrm{cm}^2/\mathrm{sec}$ and $10^{-4}\mathrm{cm}^2/\mathrm{sec}$ respectively. These values were used for all materials and all problems.

The terms Z and F_1, are independent of the chemical nature of the materials but depend upon its physical structure. Values of Z used in different problems varied from 3×10^{-5}cm, where diffusion controlled processes take place at significant rates, to 0.14 cm, the largest values of grain size reported for TNT.[18] F_1 was more or less arbitrarily assigned values in the range of 0.001 to 0.10. Some information on propellants was obtained indicating that porosities, to which F_1 can be directly related as discussed previously, are generally in the range of 1%.

The parameter w which defines the way in which the grain burning reaction becomes insensitive to pressure was arbitrarily chosen to be 20 kilobars. Use of this number means that the grain burning reactions are only slightly affected by pressure above 100 kilobars.

Parameters of the second group relate to the chemical nature of the material. The order of the reaction, m, was taken as 1 in all cases. Heats of reaction as obtained from various literature sources were used. The six rate parameters A_1, A_2, A_3, B_1, B_2, B_3, are the most crucial in terms of the prediction of detonation behavior. They are also present the greatest difficulty in terms of evaluation by independent means since the conditions under which they are required to define reaction rate are attainable only by detonation or shock processes. In this program it has been necessary to make use of some rate data obtained under more accessible conditions.

Four types of experimental information have been utilized. These are:

1. Thermal decomposition data
2. Minimum initiation pressure data
3. Linear pyrolysis rate
4. Differential thermal analysis

The first type refers to data reported by M. A. Cook[19,18] and used by him to calculate reaction zone widths for detonation waves in TNT on the basis of the grain burning concept. The second refers to a method by which the rate constants for the ignition reaction are adjusted until computed values for the minimum pressure for initiation are in agreement with results reported from the experimental measurements of such pressure. Experimental data used for comparison were reported by Jaffee and others at the Naval Ordnance Laboratory.[20] The third type refers to data on ammonium perchlorate obtained by Charken, Anderson and others at the Aerojet-General Corporation from their hot plate experiments.[21] The fourth type of data, obtained by differential thermal analysis on double base propellants was obtained from the Allegany Ballistics Laboratory.[22]

A summary of the complete input used in calculations on various types of explosive or propellant material is given in Tables 4-7 inclusive. Examples of computed detonation behavior carried out with this input, and their comparison with experimental behavior are discussed in the following section.

SECTION 5

CALCULATIONS AND DISCUSSION

5.1 INTRODUCTION

The mathematical techniques discussed in the previous sections permit an examination of detonation phenomena in a detail not possible by experimental methods, through the medium of what may be called computed detonation waves. These are, in effect, mathematical representations of actual detonation processes, and in the course of their creation data on pressure, specific volume of reacted and unreacted material, energy density of reacted and unreacted material, particle velocity and propagation velocity are computed at all points in the wave as a function of time and propagation distance. Such information cannot presently be obtained from the observation of experimental detonations. Conversely, however, the information is useful only if there is confidence that it truly represents reality and this can arise only from extensive demonstration of conformity between the characteristics of the computed and experimental waves. It is axiomatic that such demonstrations will have to be in terms of those characteristics of experimental waves which are observable.

The discussion in this section will be concerned with the general characteristics of computed waves. It will not be attempted to present a detailed comparison between experimental and computed waves because, as discussed under Section 4, a great deal of uncertainty exists as to the input data which should be used in the calculations for specific materials. In fact when calculations are stated in the following "to be carried out for a specific material" this should be understood to mean only that the input data were selected to simulate that material as closely as possible. Nevertheless pertinent examples of conformity between computed and experimental behavior will be indicated.

Examples of the latter obtained during the early work on the program were presented in a recent publication[23] and will not be repeated here. It is to be noted that the mathematical techniques and computer routines which are used have been subjected to continuous modification and improvement throughout the course of this program. Consequently, the early calculations may differ in detail from some of those performed more recently. However, in no case do the later results requires significant alteration in the conclusions derived from the earlier work.

5.2 GENERAL CHARACTERISTICS OF COMPUTED WAVES

The calculations provide wave trajectories, a typical example of which is shown in Figure 4. Input for this case corresponded to TNT and was as given in Table 4 with the difference that $Z = 0.035$ It is noted that the final steady state velocity attained was 11.8 mm/μsec which substantially exceeds the theoretical value. This problem was discussed in Section 3 and will be considered further in the following.

Typical curves showing the reaction and pressure profiles through a wave in TNT with $Z = 0.14$ cm are shown in Figure 5, and profiles of v_g, v_s and e_s are shown in Figure 6. Input data for these latter two curves was as shown in Table 4.

Similar calculations have been carried out on composite materials and composite double base materials with input data taken as shown in Tables 3 and 5.

Figure 7 gives the velocity of a wave in a polyurethane -APC propellant initiated with a 100 kbar shock. An initial velocity of 4.2 mm/μsec is obtained which subsequently decays and finally the wave fades completely, after progressing a distance of about 10 centimeters into the charge. The explanation for this behavior is shown by the reaction-zone profile of Figure 8, in which the degree of completion of the three main reaction processes, f_1, f_2, f_4, is plotted as a function of position in the charge and at a time of 19.4μsec after initiation It is seen at once that at this point, only the ignition reaction, f_1, is proceeding to any appreciable extent. The energy derived therefrom is evidently not sufficient to maintain the wave, and decay ultimately ensues.

Similare profiles through a wave in a composite double base material are shown in Figure 9. This figure is of interest in that it shows only slight reaction of the ammonium perchlorate. The binder material, on the other hand reacted completely at first in

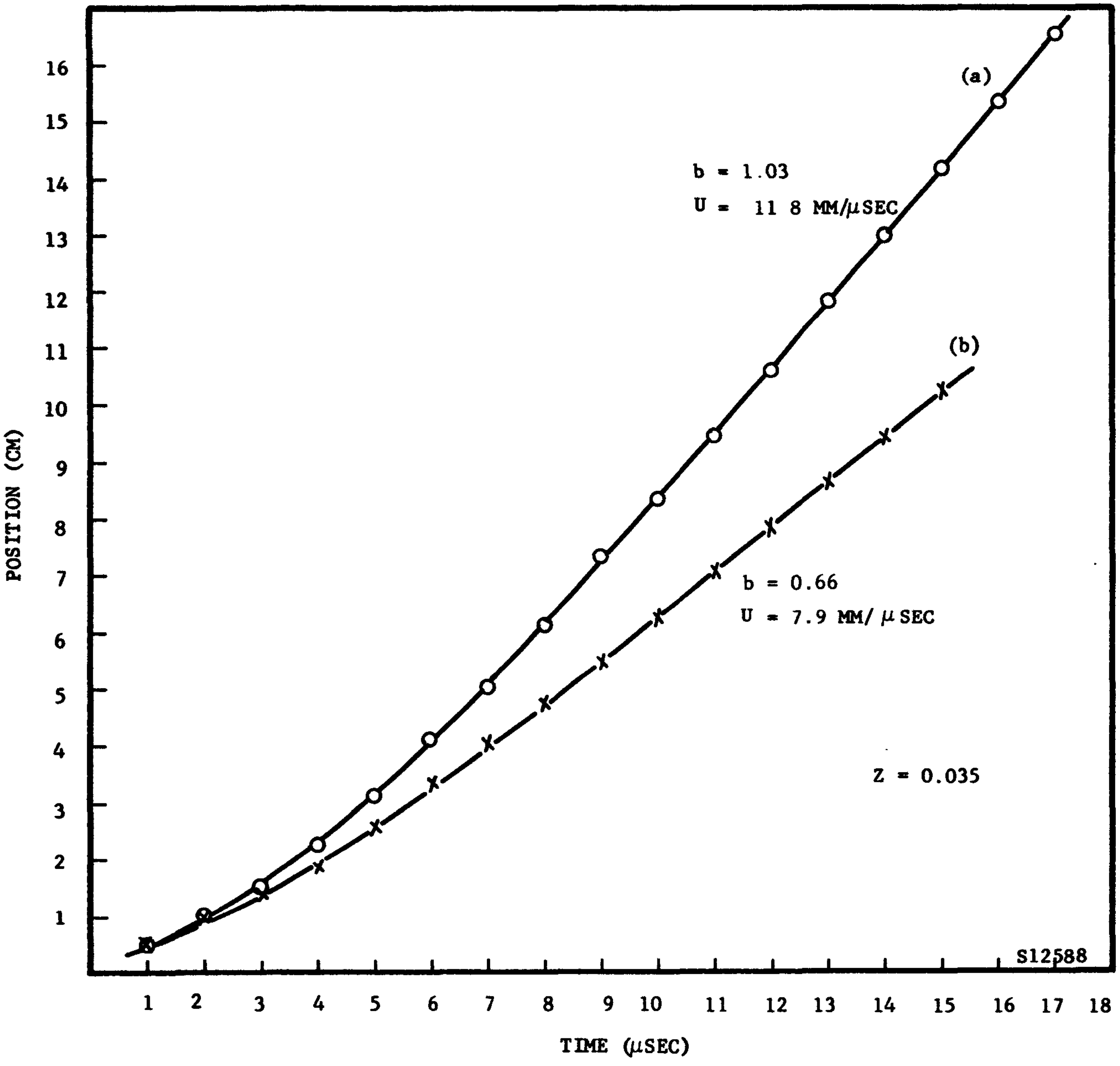

FIGURE 4. EFFECT OF PARAMETER b ON WAVE TRAJECTORY

TABLE 3

INPUT DATA FOR POLYURETHANE-APC PROPELLANT

$= 50$ kilobars

$= 466$ cal/gm

$B_1 = 1.6 \times 10^{12}$

$B_2 = 8.8 \times 10^{13}$

$B_3 = 0$

$A_1/R = 5500^{\circ}K$

A_2 $R = 11000^{\circ}K$

$A_3/R = 11000^{\circ}K$

$Z = 3 \times 10^{-3}$ cm

$m = 1$

$t_p = 3 \mu sec$

$_a = 1.6$

$F_1 = 0.10$

$F_2 = 0.75$

$F_3 = 0.15$

$F_i = 0$

$Q_1 = 1000$ cal/gm

$Q_2' = Q_2 = 380$ cal/gm

$Q_3 = -76$ cal/gm

$Q_4 = 696$ cal/gm

$R = 0.02$ cal/gm-deg

$P = 100$ kbar

TABLE 4

INPUT DATA FOR TNT

$= 795$ cal/gm

$= 50$ kbar

$Q_1 = 1130$ cal/gm

$Q_2' = Q_2 = 1130$ cal/gm

$Q_3' = Q_3 = 0$

$Q_4 = 0$

$A_1/R = 4715^{\circ}K$

$A_2/R = 9430^{\circ}K$

B_1 1.08×10^{13}

$B_2 = 1.08 \times 10^{1}$

$B_3 = 0$

$F_1 = 0.01$

$F_2 = 0.99$

$F_3 = 0$

$F_i = 0$

$Z = 0.14$ cm

$\rho a = 1.5$ gm/cm^3

$P = 100$ kbar

$t_p = 1.5 \mu sec$

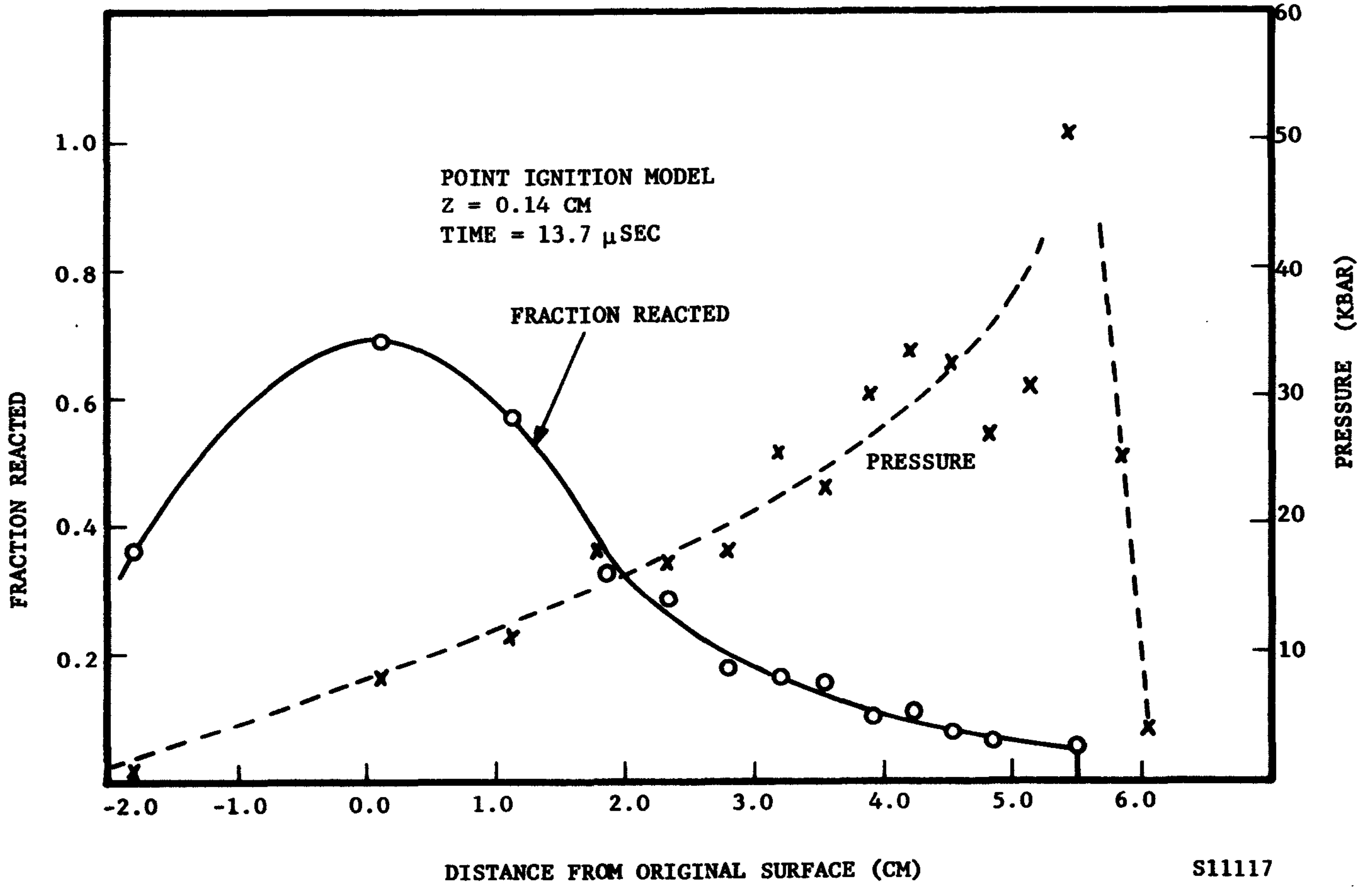

FIGURE 5. REACTION AND PRESSURE PROFILES THROUGH COMPUTED DETONATION WAVE IN TNT.

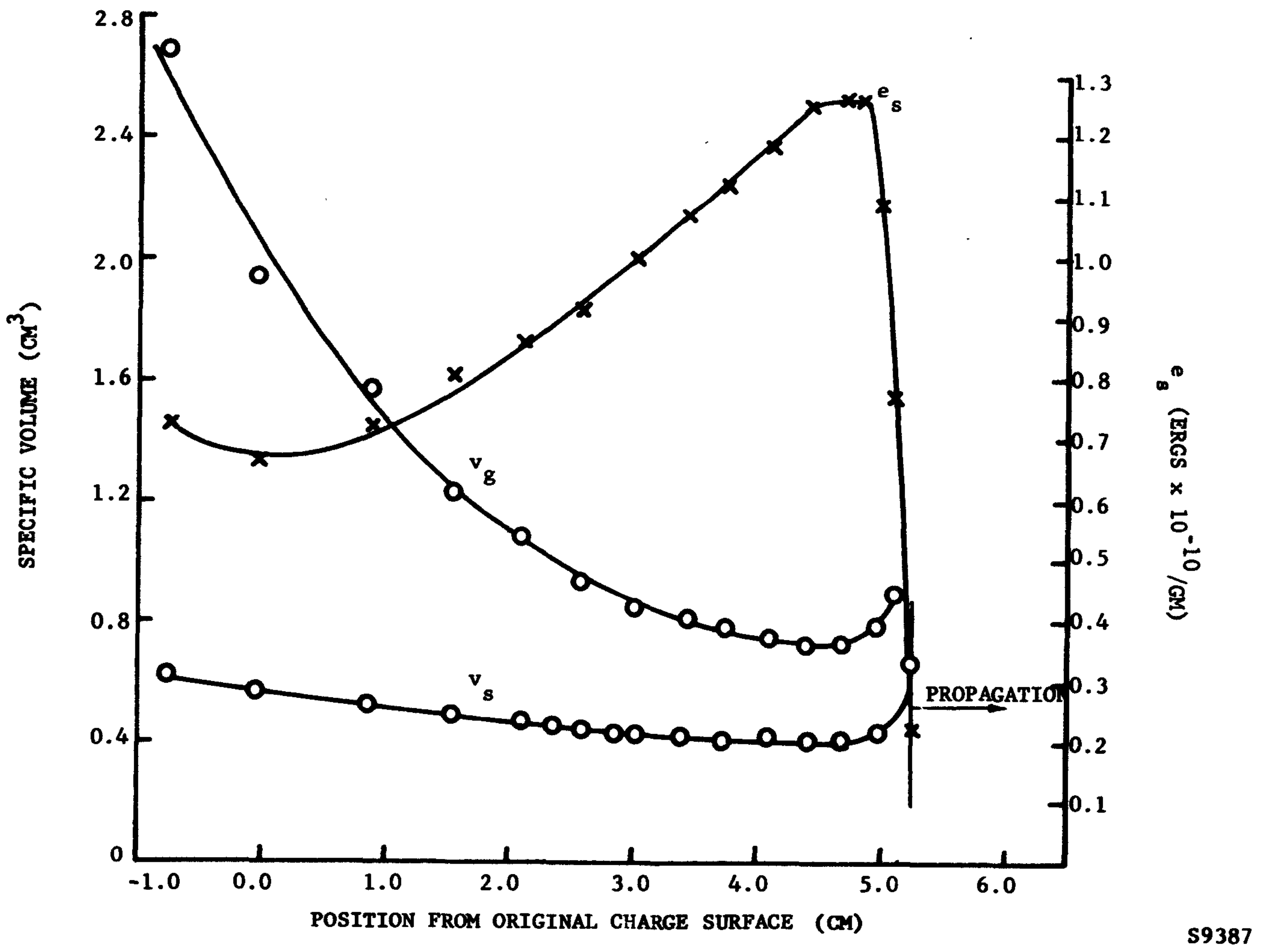

FIGURE 6. SOLID-PHASE ENERGY DENSITY AND SOLID AND GAS SPECIFIC VOLUMES THROUGH A DETONATION WAVE IN TNT

TABLE 5

INPUT DATA FOR COMPOSITE DOUBLE BASE PROPELLANT

ϵ = 664 cal/gm

β = 50 kbar

Q_1 = 622 cal/gm

$Q_2' = Q_2$ = 380 cal/gm

$Q_3' = Q_3$ = 864 cal/gm

$Q_4 = 0$

$A_1/4$ = 5500°K

$A_2/4$ = 11 000°K

$A_3/4$ = 19,400°K

$B_1 = 1.6 \times 10^{12}$

$B_2 = 1.6 \times 10^{12}$

$B_3 = 4.6 \times 10^{15}$

$F_1 = 0.01$

$F_2 = 0.205$

$F_3 = 0.470$

$F_i = 0.315$

$Z_2 = 2.5 \times 10^{-3}$ cm

$Z_3 = 12 \times 10^{-3}$ cm

ρ_a = 1.80 gm/cm^2

P = 100 kbar

t_p = 4 μsec

TABLE 6

INPUT DATA FOR DOUBLE-BASE PROPELLANT

ϵ = 664 cal/gm

β = 50 kbar

$B_1 = 4.6 \times 10^{15}$

$B_2 = 0$

$B_3 = 0$

A_1/R = 9700°K

A_2/R = 19400°K

A_3/R = 19400°K

Q_1 = 864 cal/gm

$Q_2' = Q_2$ = 864 cal/gm

$Q_3' = Q_3 = 0$

$Q_4 = 0$

$Z_1 = 2.5 \times 10^{-2}$

ρ_a = 1.80 gm/cm^3

$F_1 = 0.001$

$F_2 = 0.999$

$F_3 = 0$

$F_i = 0$

P = 100 kilobars

t_p = 3.0 μsec

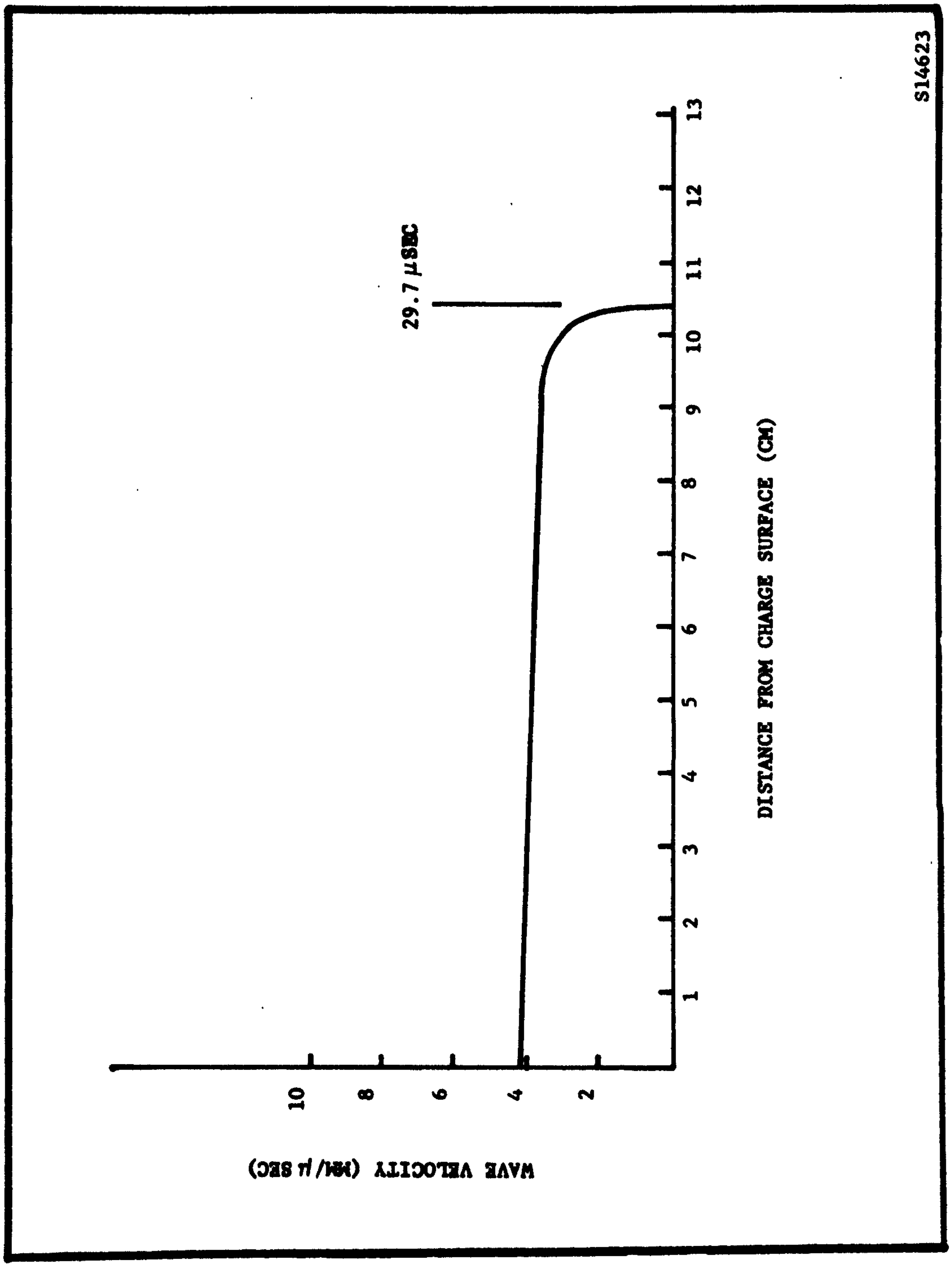

FIGURE 7. PROPAGATION OF A DETONATION IN PROPELLANT MATERIAL

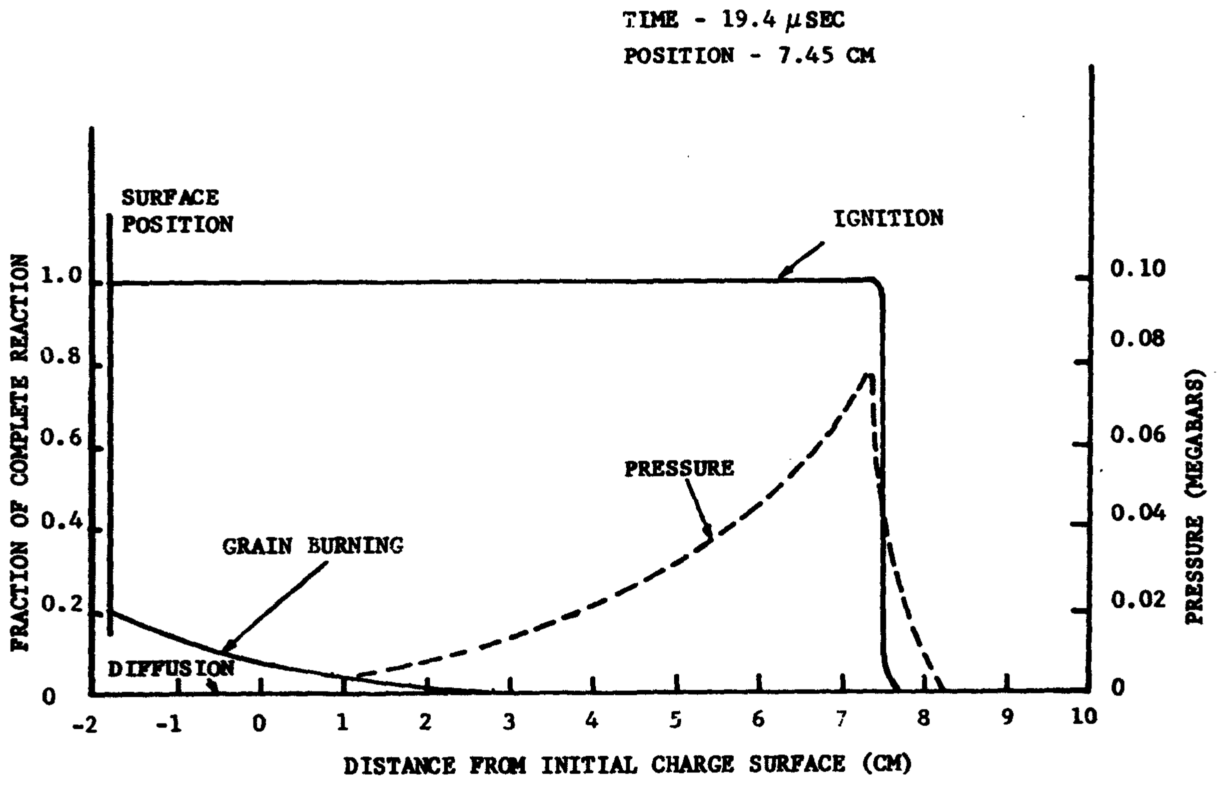

S14624

FIGURE 8. REACTION ZONE PROFILES FOR DETONATION WAVE IN PROPELLANT MATERIAL

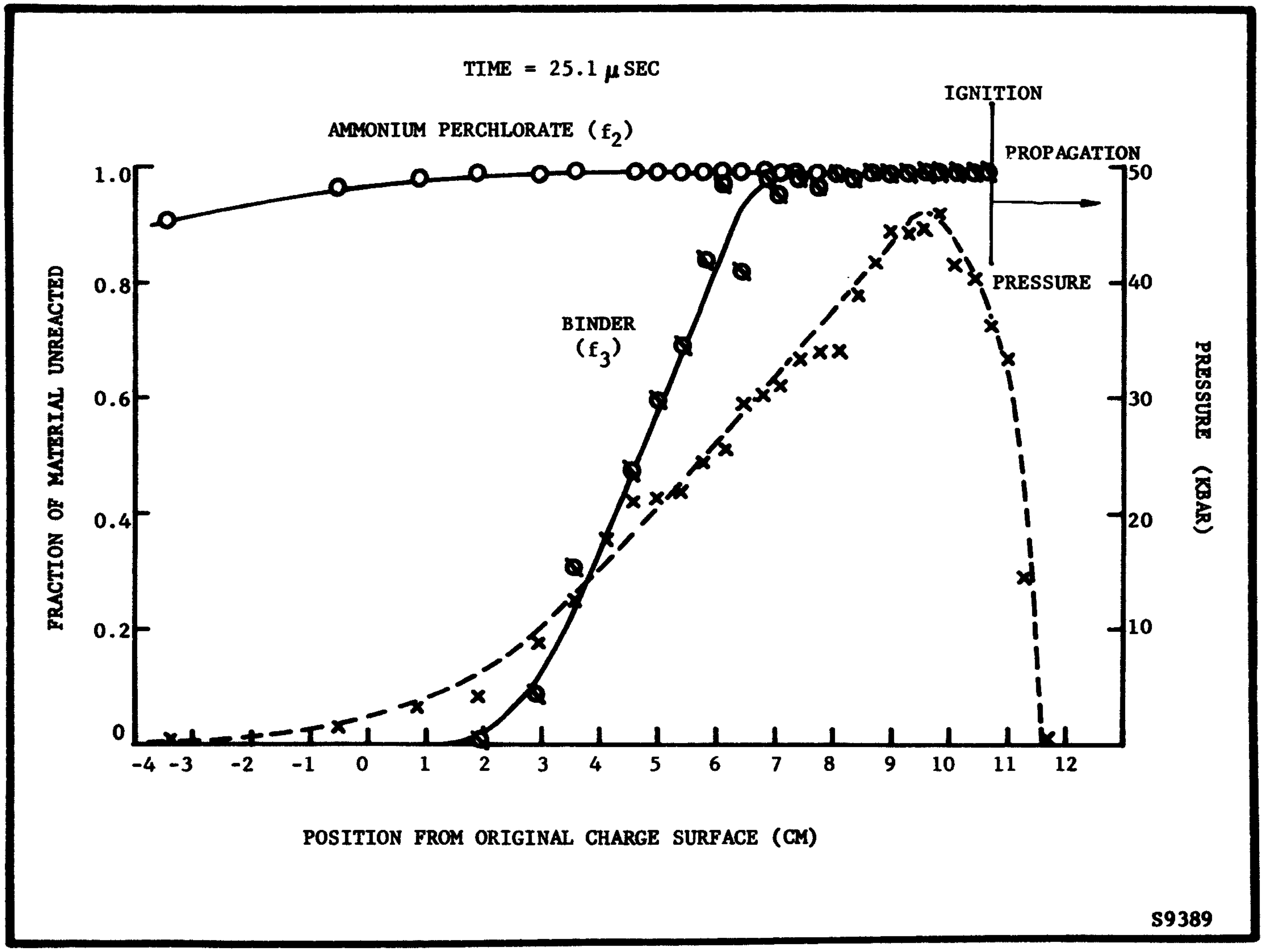

FIGURE 9. REACTION PROFILES FOR BINDER AND OXIDIZER AND PRESSURE PROFILE THROUGH A DETONATION WAVE IN COMPOSITE DOUBLE-BASE PROPELLANT

response to the initial transient. This reaction was not maintained, however, and after propagating about 7cm into the charge, all reaction except the ignition reactions had ceased.

The explanation for this behavior appears to reside in the high activation energy, (A_3), and thus the high temperature coefficient for the binder reaction. Reaction at the charge surface is rapid because of the high energy deposition in the material by the initial shock. However, the energy released by binder reaction is not sufficient to drive a shock of this intensity so that following release of the surface pressure the wave decays. As a consequence of the decreasing pressure in the wave, the energy in the solid drops to a value at which the binder no longer reacts at a significant rate. Similar behavior is not observed on the part of the ammonium perchlorate reaction because its lower activation energy makes it less sensitive to changes in solid energy density. Following the point at which the grain burning reactions subside, the wave is supported only by the ignition reaction, and this constitutes the observed steady state process.

5.3 EFFECT OF GRAIN SURFACE BURNING VS POINT BURNING ON WAVE BEHAVIOR

Considerable attention has been given during this program to the problem of differences in detonation behavior corresponding to the point and surface ignition models.

Figure 10 shows wave trajectories and peak pressures for a wave in material corresponding to TNT, computed with point ignition; otherwise the input data were as shown in Table 4. Results are to be compared with Figure 11, computed with the same input except with surface ignition. Whereas Figure 11 shows a propagating wave which would undoubtedly have grown to a steady state, the calculation represented by Figure 10 produced a fading wave.

Figure 12 shows the reaction profile through the wave of Figure 10, and it is of interest to compare this profile with that shown on Figure 13 corresponding to the trajectory of Figure 11. Considerable difference between them is expected due to the fact that the surface process starts at a maximum rate and deaccelerates, whereas the point process starts at a minimum rate and accelerates. The actual difference is substantial, as is shown in the two figures.

In order to study the character of both types of process over the entire growth period from initiation to steady state, the calculations were repeated with a smaller grain size to produce a stable wave and more

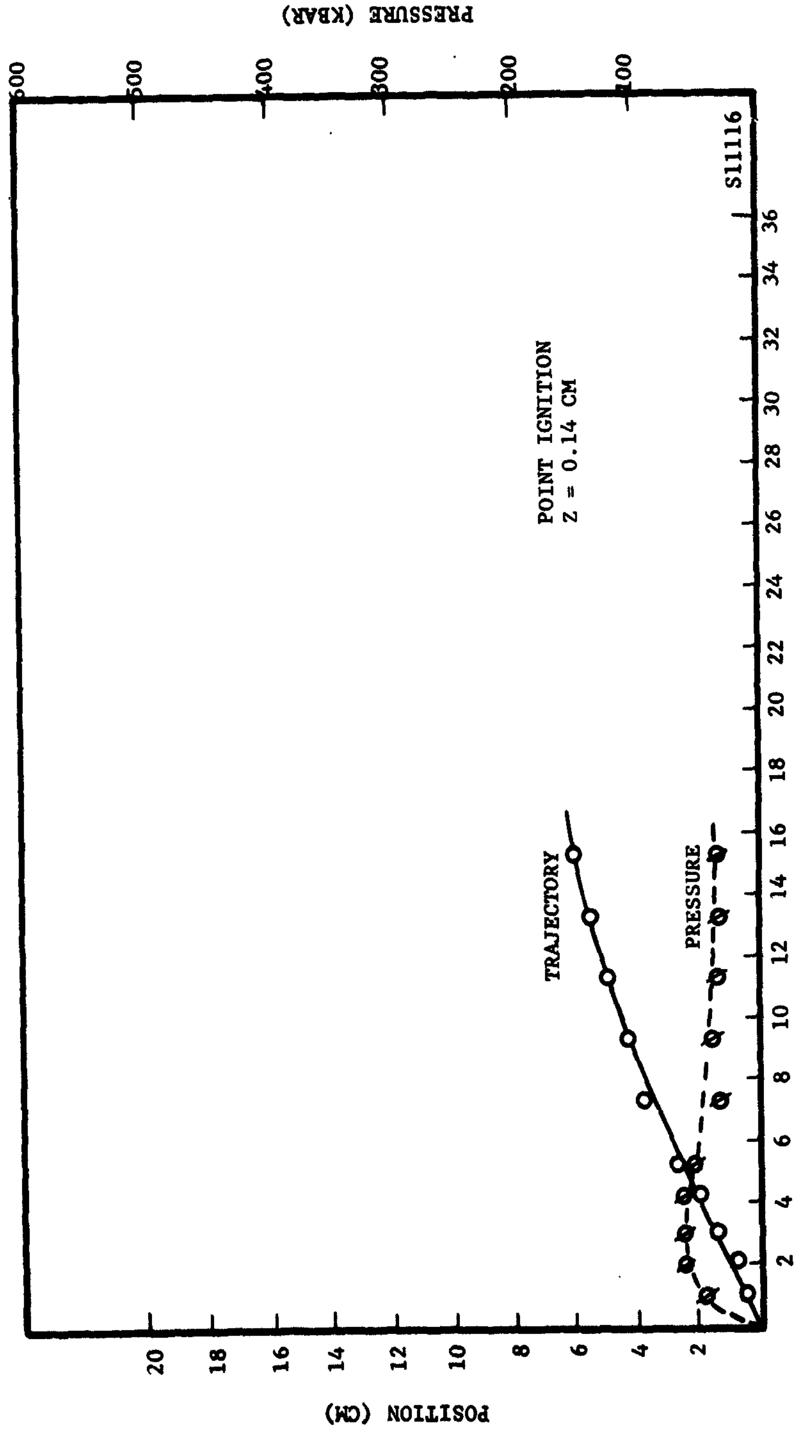

FIGURE 10. PROPAGATION OF COMPUTED DETONATION WAVE IN TNT.

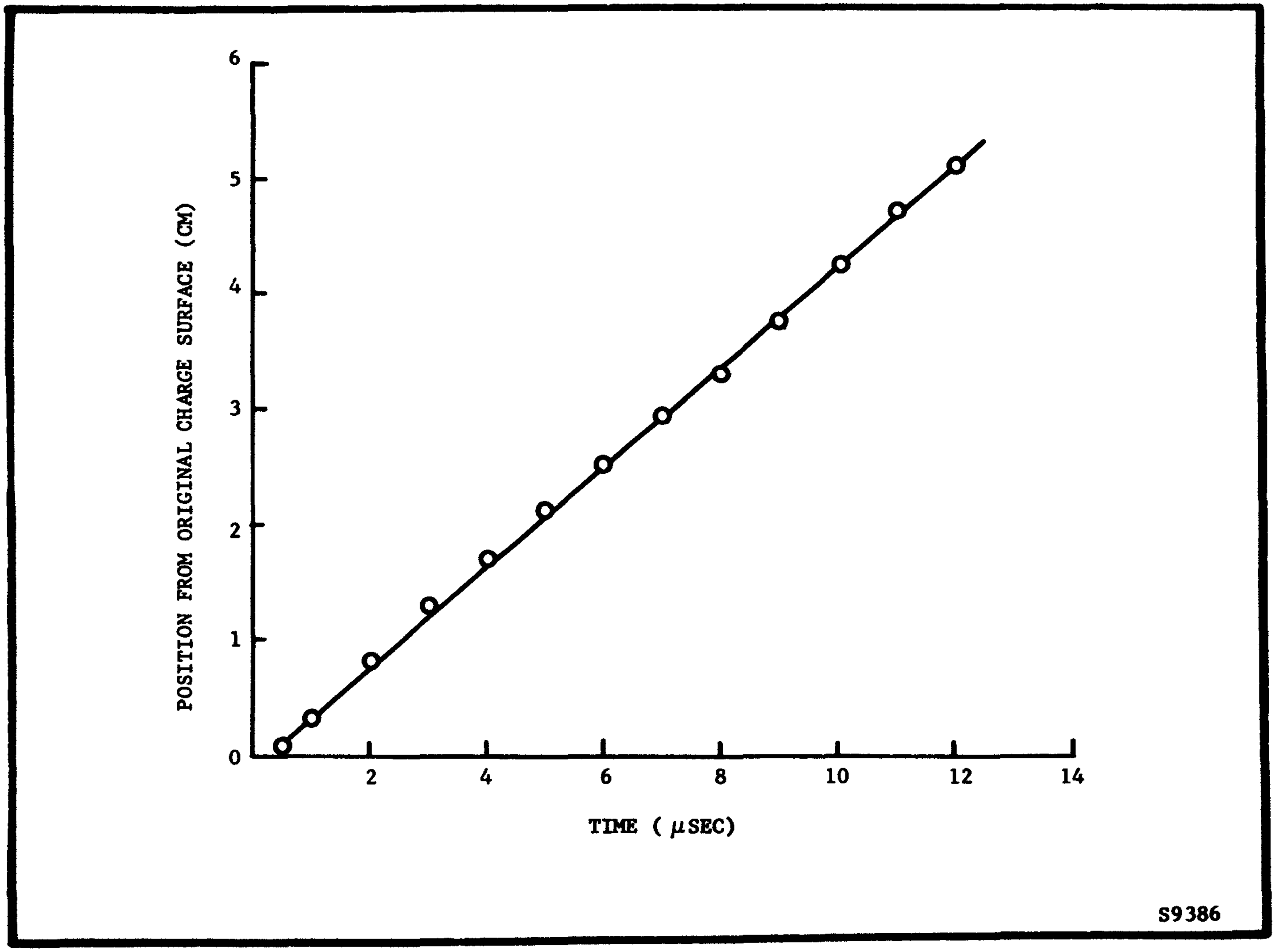

FIGURE 11. INITIAL TRAJECTORY OF DETONATION WAVE IN TNT

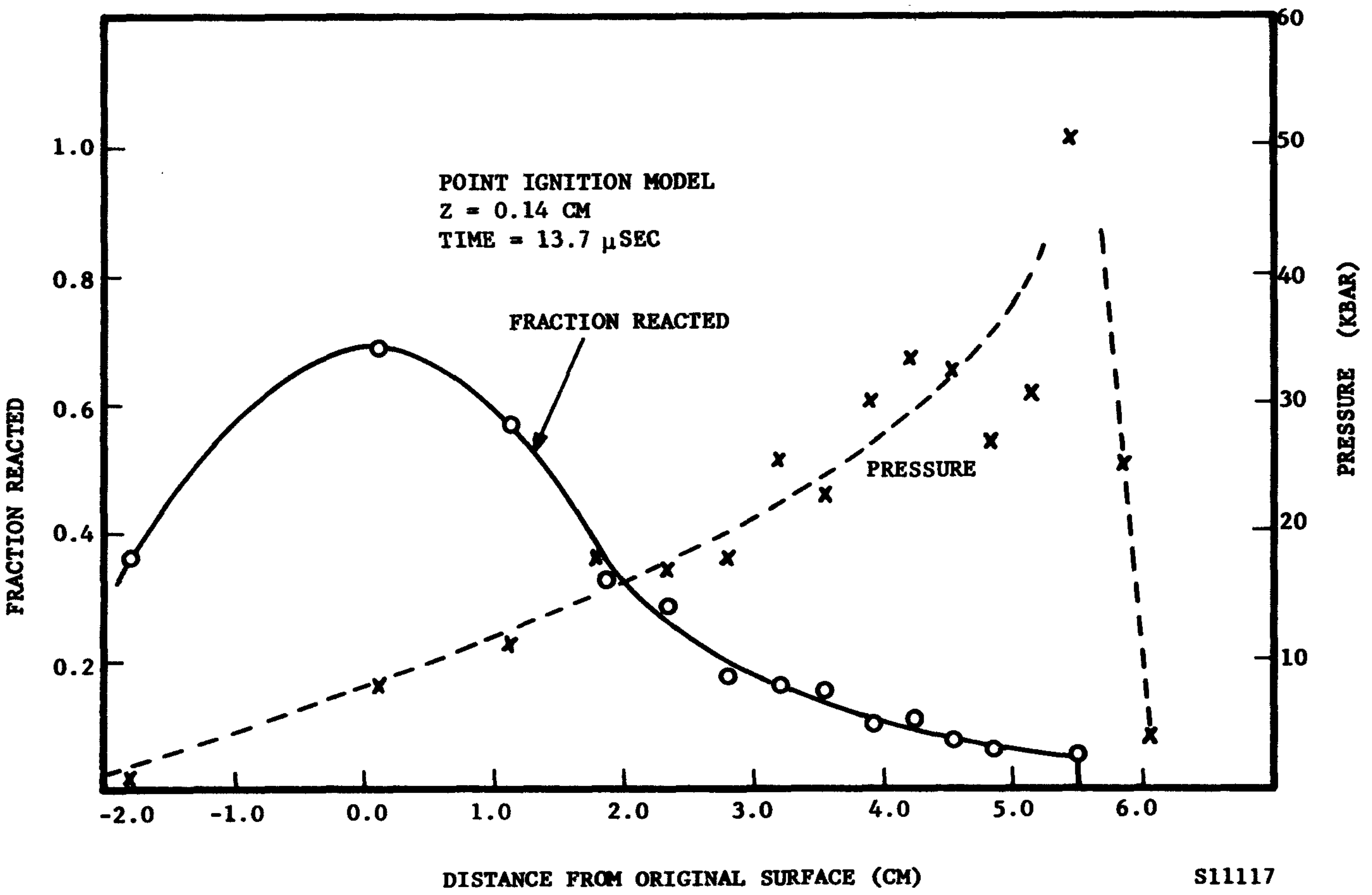

FIGURE 12. REACTION AND PRESSURE PROFILES THROUGH COMPUTED DETONATION WAVE IN TNT.

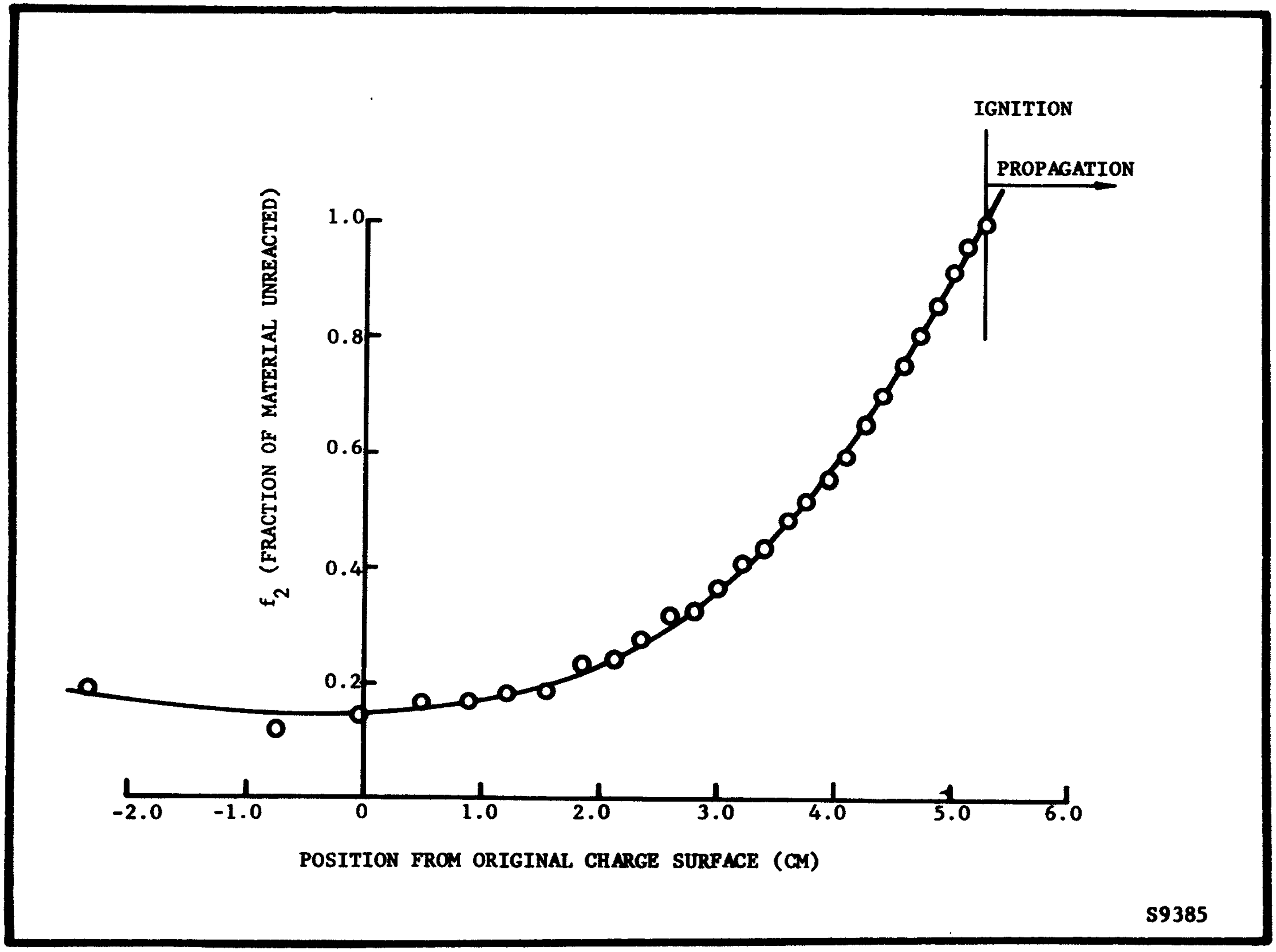

FIGURE 13. REACTION ZONE PROFILE THROUGH DETONATION WAVE IN TNT

rapid acceleration in both cases. Using a value of $Z = 0.035$ cm, the trajectories shown in Figures 14 and 15 were obtained. Also shown are wave peak pressures. The scatter in the points indicating the latter is due to oscillation in the numerical integration which is especially severe in the region of peak pressure. Since the period of oscillation is a few time cycles (0.02 μsec) which is short relative to the time required for changes to occur, it is proper to represent the pressure in this region by the appropriate average value.

The curves show pronounced difference in the growth behavior for the two ignition models. Point ignition produces a wave which, except for the period during which it is overdriven by the initial pulse, propagates for about 15 seconds at a relatively low velocity of 4.0 mm/μsec before accelerating to its final value of 11.6 mm/μsec at 23 μsec. Surface ignition leads to a wave which accelerates rapidly from initiation, attaining final velocity in about 8 μsec.

Figure 16 shows reaction zone profiles through the two waves at three points in their history. These generally conform to expectations. The decrease in reaction zone widths with time is due to the increase in energy deposition by the lead shock with increasing propagation velocities, which results in increased values of e_s.

The foregoing results on wave growth behavior are believed to indicate that the point ignition process produces a wave conforming more closely to experimental behavior, since much experimental data on wave trajectories follow the general pattern of a slow initial period followed by a relatively fast transition to a high velocity, essentially as shown by Figure 14. However, the trajectory shown on Figure 11 for a wave computed with surface ignition but with a larger value of Z also shows a low velocity regime, which is seen to extend for more than fourteen microseconds. Therefore, the comparison of experimental and computed wave trajectories cannot reliably serve to distinguish between the two types of ignition unless independent information as to the appropriate value of Z is available. It is worthy of note here that if loss terms, such as might result from lateral expansion in the case of finite charge geometry, were included in the formulation of the problem, it is entirely possible that with either type of ignition the low velocity period could be indefinitely stabilized. It would then be equivalent to the phenomena commonly known as low order detonation.

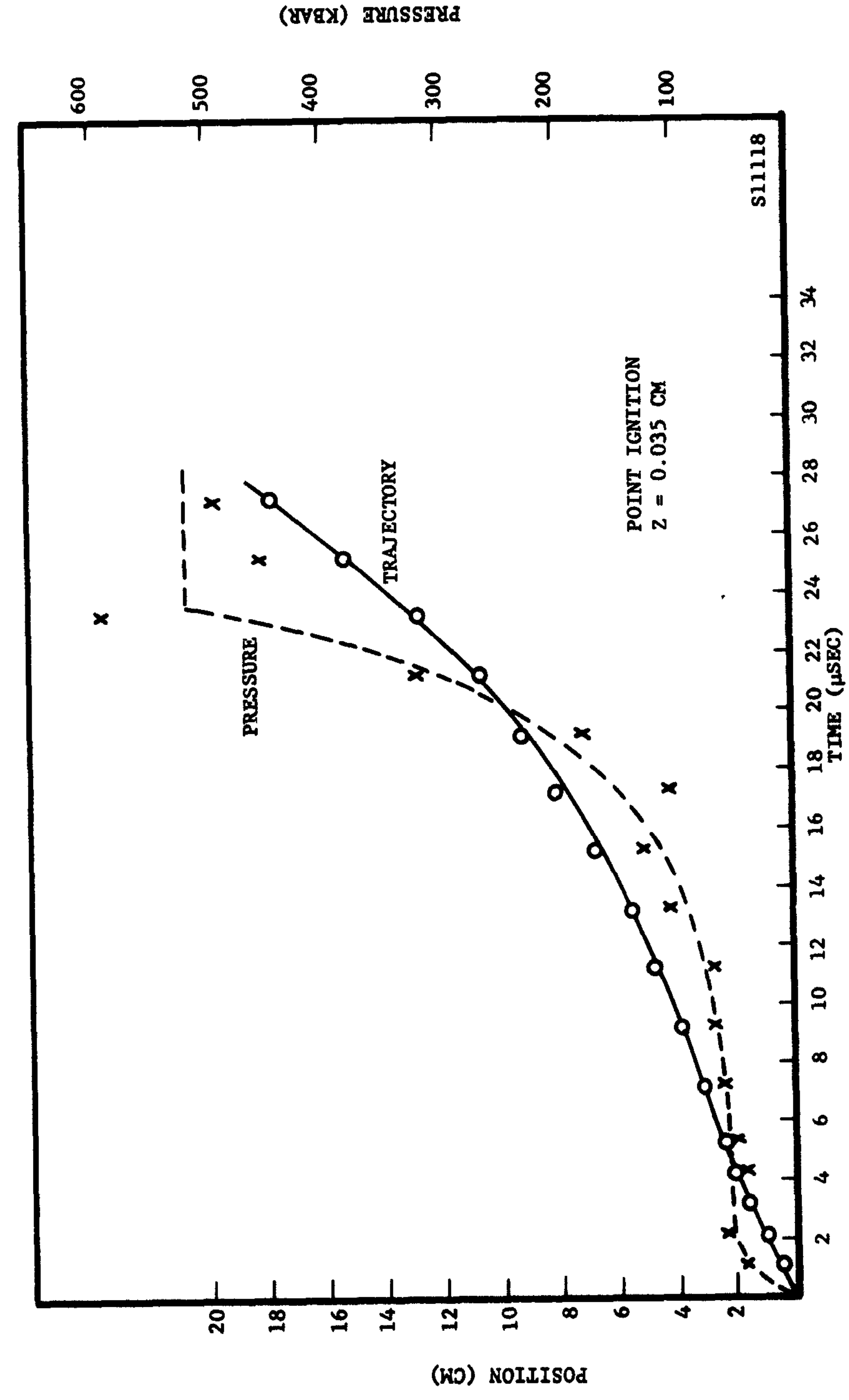

FIGURE 14. PROPAGATION OF COMPUTED DETONATION WAVE IN TNT.

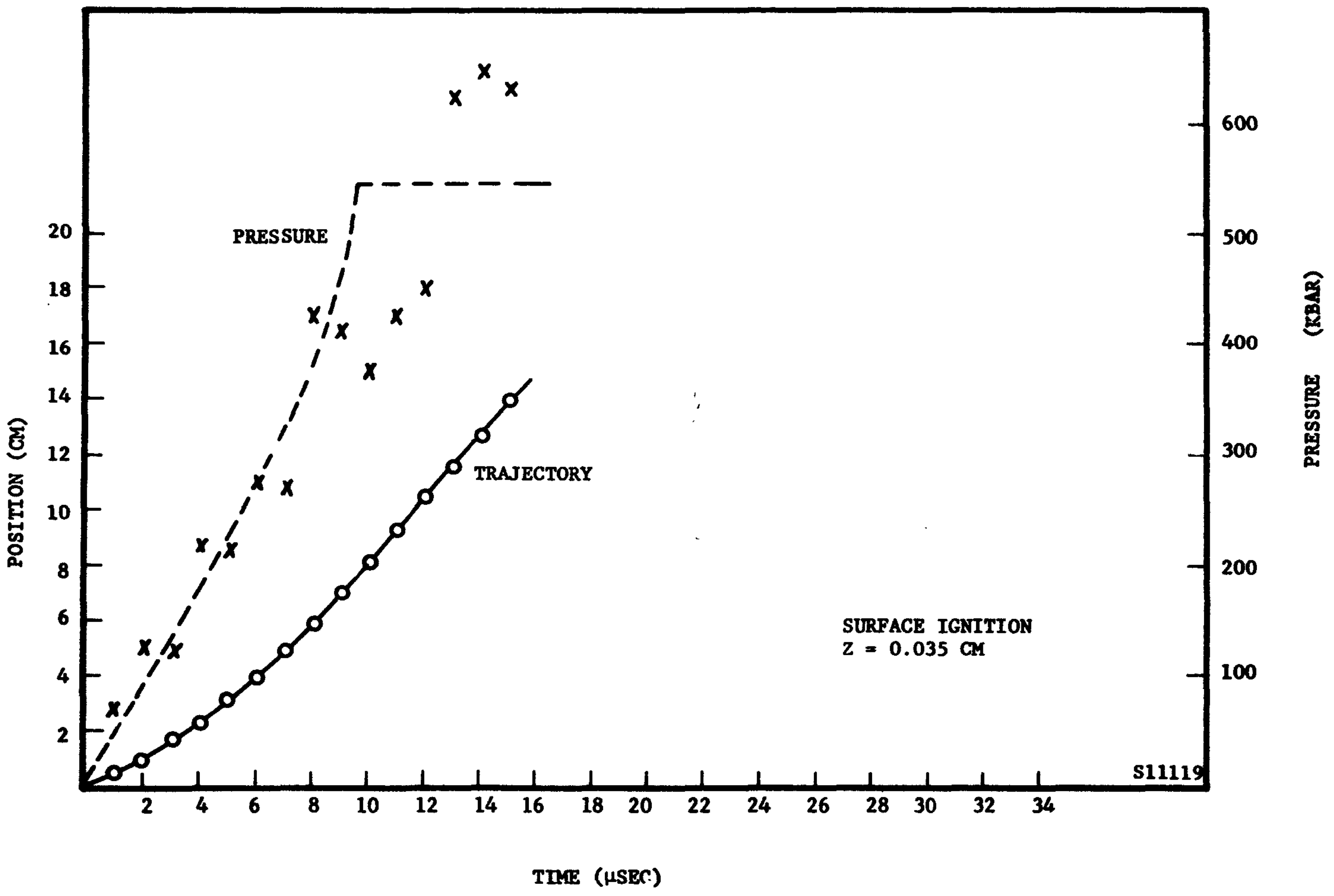

FIGURE 15. PROPAGATION OF COMPUTED DETONATION WAVE IN TNT

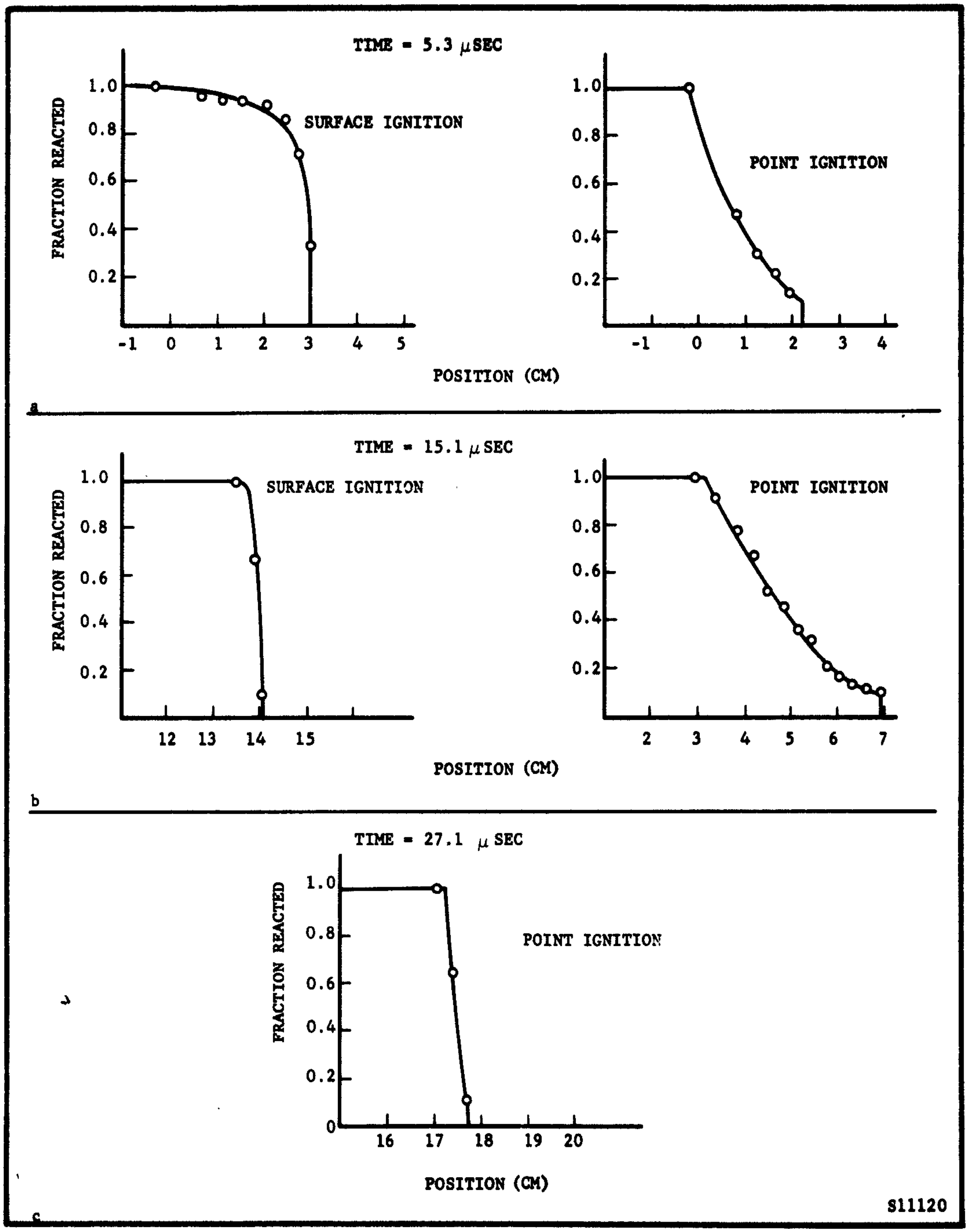

FIGURE 16. PROFILES THROUGH COMPUTED DETONATION WAVES IN TNT FOR POINT AND SURFACE IGNITION, Z = 0.035 CM.

5.4 CALCULATIONS OF MINIMUM PRESSURE FOR INITIATION

As discussed in Section 4, a factor of particular importance in calculating the detonation behavior of real materials is the selection of proper values for the rate parameters A_1, A_2, B_1 and B_2. A particularly interesting source of such data for TNT is in some experimental work carried out at the Naval Ordnance Laboratory on the shock pressures necessary for initiation of detonation in TNT.[20] Such pressures are strongly dependent upon the values used for B_1 and A_1 and the data can therefore be used to evaluate these parameters if the other needed information about the material is available. As has been discussed in Section 2, the assumption that the ignition zone is a high-temperature region in the vicinity of a bubble or void which has been passed over by a shock, leads to the postulate

$$A_1 = A_2/2$$

$$B_1 = B_2$$

The procedure for obtaining values of the rate parameters is to compare computed values of the minimum pressure for initiation of detonation obtained with different values of A_1 and B_1, with the experimental value. The computed values are obtained by setting B_2 and B_3 equal to zero so that the grain burning reactions are suppressed, and by using a low value of F_1 so that the ignition reaction alone is not capable of supporting a detonation wave. The calculation is initiated by an imposed shock of ~ 100 kbars having a duration of 1.5 μsec, which is heavy enough to cause ignition. The disturbance then propagates into the material as a fading wave, and the maximum wave pressure at the last zone which ignites is the minimum pressure for initiation.

Figure 17 shows the trajectory of such a fading wave obtained with values of A_1 and B_1 derived from the data of Cook[19] which leads to the values

$$A_2 = 43{,}400 \text{ cal/mol}$$

$$B_2 = 1.08 \times 10^{13}$$

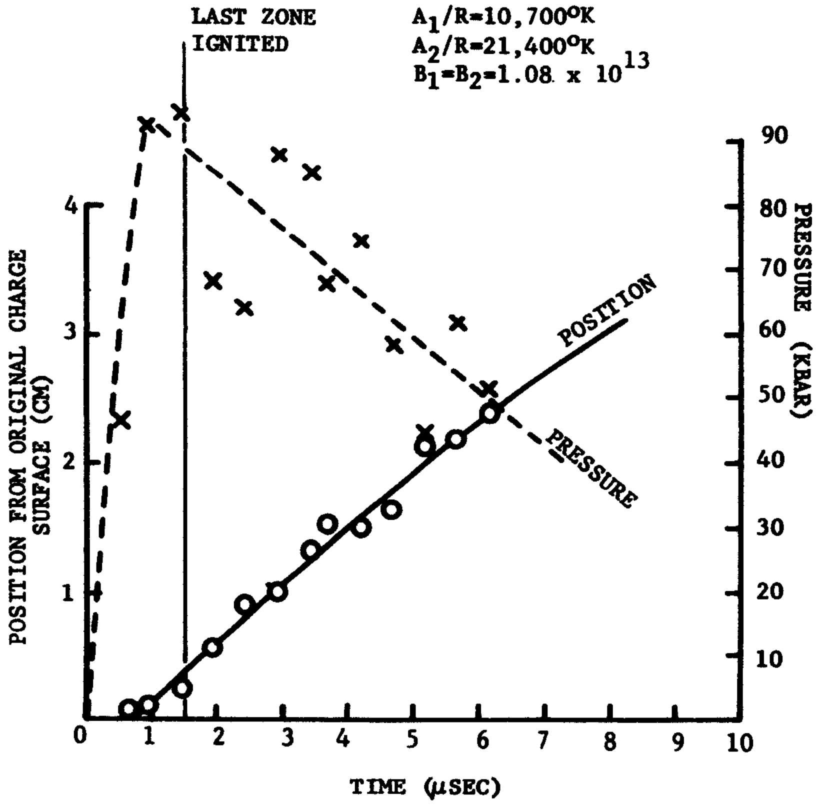

S9383

FIGURE 17. POSITION AND MAGNITUDE OF PEAK PRESSURE IN FADING

whereupon

$$A_1 = 21,700 \text{ cal/mol}$$

$$B_1 = 1.08 \times 10^{13}$$

For purposes of the calculation B_2 and B_3 were set equal to zero. Data on the heat of explosion, density, and specific heat of TNT were also obtained from Cook.[19] Values of the other input parameters were obtained as discussed in Section 4.

Comparison of the fade point with the curve of wave pressure shows that fading occurs at a pressure of ~90 kbars. This value is somewhat uncertain because of the rather wide fluctuations which occur in the computed maximum pressure. Accuracy could be increased to any desired value by increasing the stability conditions imposed on the integration and decreasing the mesh size. This would, however, increase the running time, and was not deemed to be of importance to these calculations. The experimental value reported by NOL is about 30 kbar.

It is deduced that either the rate parameters obtained from thermal decomposition data predict reaction rates much lower than are actually obtained in a detonation process, or that the assumed equation of state parameters lead to a value of energy density behind the lead shock much lower than that actually obtained. At the present time it is not possible to choose between these two explanations. However, if the value taken for A_1 is 9500, then the results are as shown in Figure 18. The minimum shock pressure for initiation here agrees very well with the experimental value. This A_1 corresponds to an A_2 for TNT of ~ 20 kcal/mol which is not regarded as unreasonable.

Calculation has also been carried out on the propagation of a detonation wave through a representative composite double-base propellant using the input data indicated in Table 5. In this problem, two grain burning reactions were used, one for the ammonium perchlorate oxidizer, and another for the double-base binder. The rate parameters for the binder were obtained from thermal decomposition and adiabatic self-heating data provided by the Hercules Powder Company. Those for ammonium perchlorate were obtained from data published by the Aerojet General Corporation on the regression rates of APC surfaces in their hot plate experiments.[21] The aluminum was treated as inert. Grain size taken for the ammonium perchlorate was the average size of the material used in the original mix; that for the binder was 1/2 the average distance between APC grains.

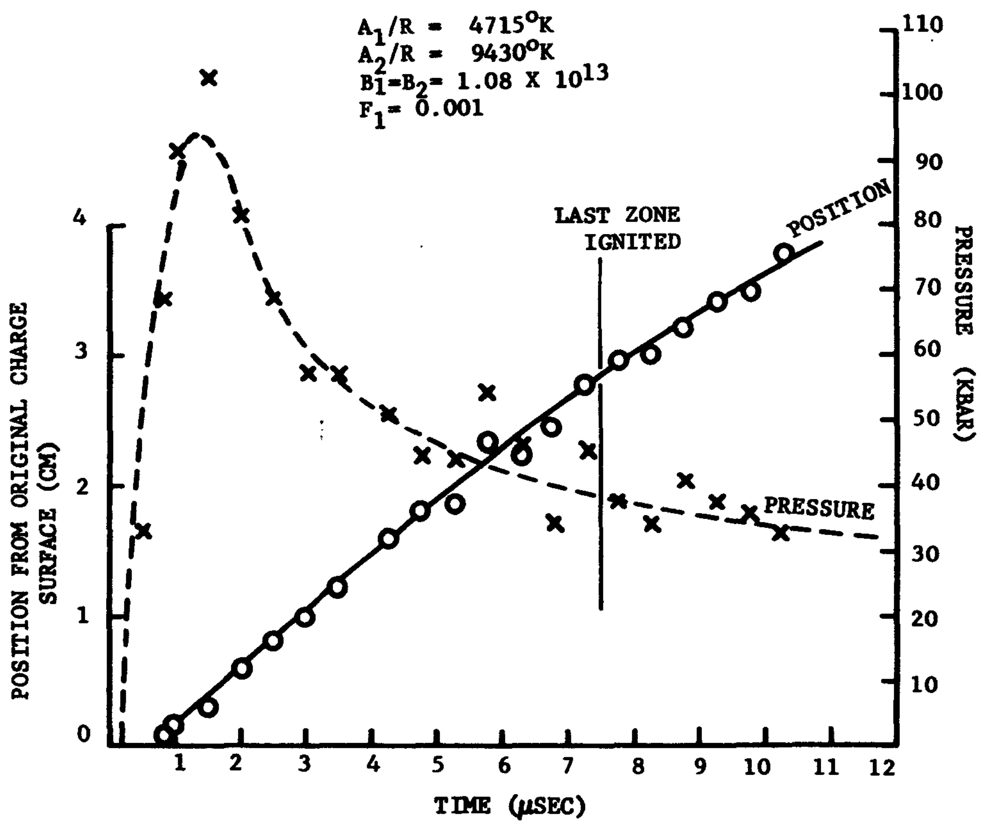

S9384

FIGURE 18. POSITION AND MAGNITUDE OF PEAK PRESSURE IN FADING WAVE IN TNT (A_1/R = 4715°K - A_2/R = 9430° K)

The rate parameters for the ignition reaction were taken as those of the ammonium perchlorate for two reasons. First, under conditions of low shock intensity the APC rate law gives a faster reaction than that for the binder. This rate would therefore be most important in the ignition process. Second, NOL data from card gap experiments 24,25,26 support this conclusion. The heat of the ignition reaction was taken as the average of the heats of reaction of the APC and binder since they are assumed to contribute equally to the ignition reaction.

Figure 19 shows the trajectory and peak pressure in a computed wave initiated with a 100 kbar shock. In this case the grain burning reactions were not suppressed as was done with TNT above. Initial wave velocity is found to be about 5 mm/μsec slowing to about 4 mm/μsec after 10μsec. Peak pressures decay rapidly from the initial imposed value of 100 kbar to about 50 kbar. Indications are that this wave approached a steady state condition. However, at the point at which the calculations were terminated, the pressure and velocity still seemed to be decreasing slightly, and it is possible that fading would ultimately have occurred. The conclusion is that the material is marginal for detonability. It is of considerable interest here that experimental data on similar propellant materials obtained at the Naval Ordnance Laboratory are consistent with the conclusions to be drawn from these calculations that a pressure of 50 kbar is somewhat above the maximum pressure required for initiation.[25,26]

An important difference between these results and those discussed previously for TNT lies in the fact that the rate data used for the ignition reaction in the present case were obtained by the hot plate technique, while those for TNT were derived from thermal decomposition data. This point may shed some light on the question of which experimental methods are most suited for obtaining kinetic information appropriate for predicting detonation behavior.

Calculation of the minimum shock pressure for initiation of a homogeneous double-base propellant was carried out using the same technique. Chemical and physical properties were taken to be in accord with data provided by the Hercules Powder Company and in this case, as with TNT, the grain burning reactions were suppressed. Since this material contains no ammonium perchlorate, the data for the binder was used in the ignition rate equation, in contrast to the procedures for composite double-base propellant. Complete input data for the calculations are shown in Table 6.

Results of the calculation are shown in Figure 20, as plots of wave position and maximum pressure in the wave, as a function of time. The last zone ignited, and the pressure in the wave upon passing over this zone, is shown by the vertical line A-A. According to the previous discussion, this is the fade point of the wave which thus occurs at a pressure of 85 kbar.

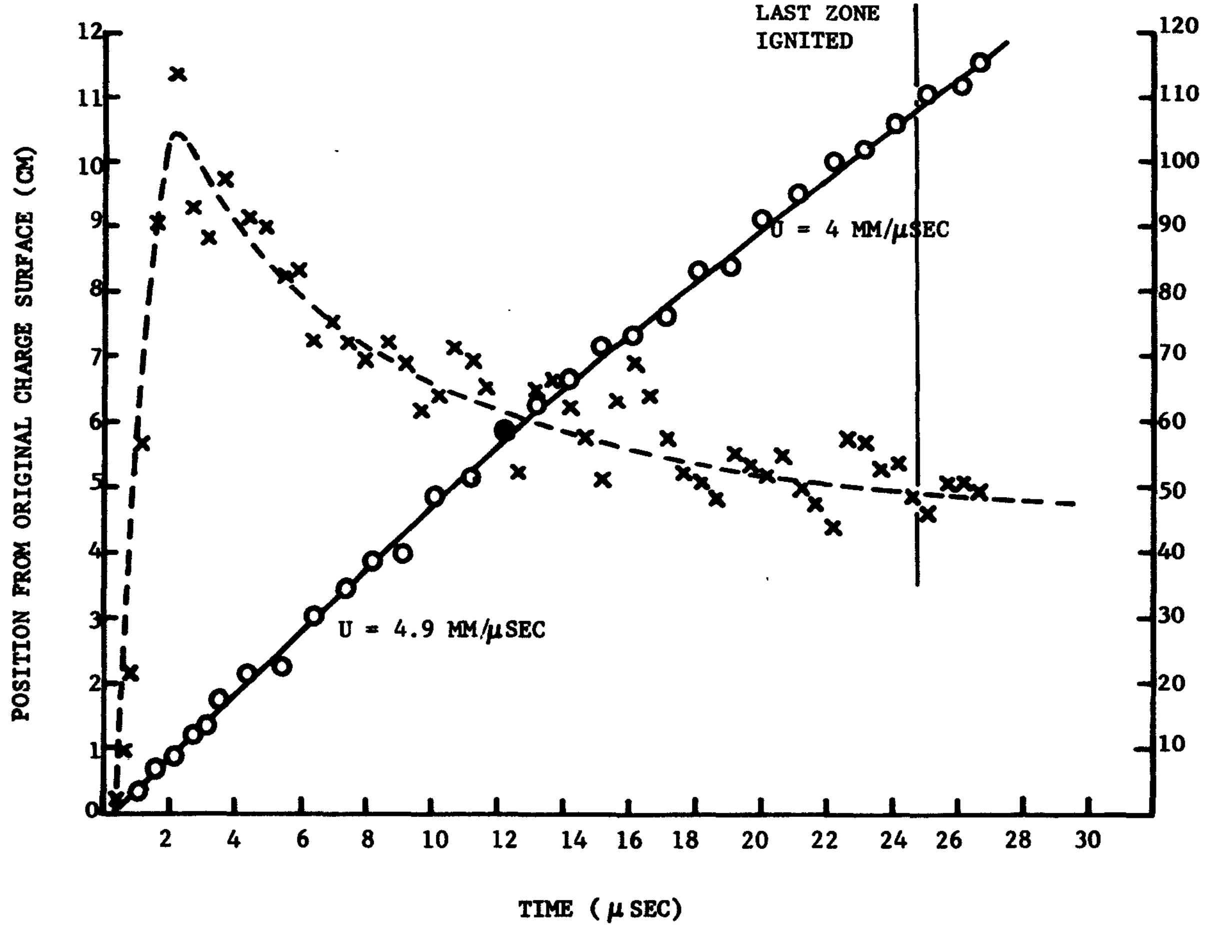

S9388

FIGURE 19. TRAJECTORY AND PEAK PRESSURES OF DETONATION WAVE IN COMPOSITE DOUBLE-BASE PROPELLANT

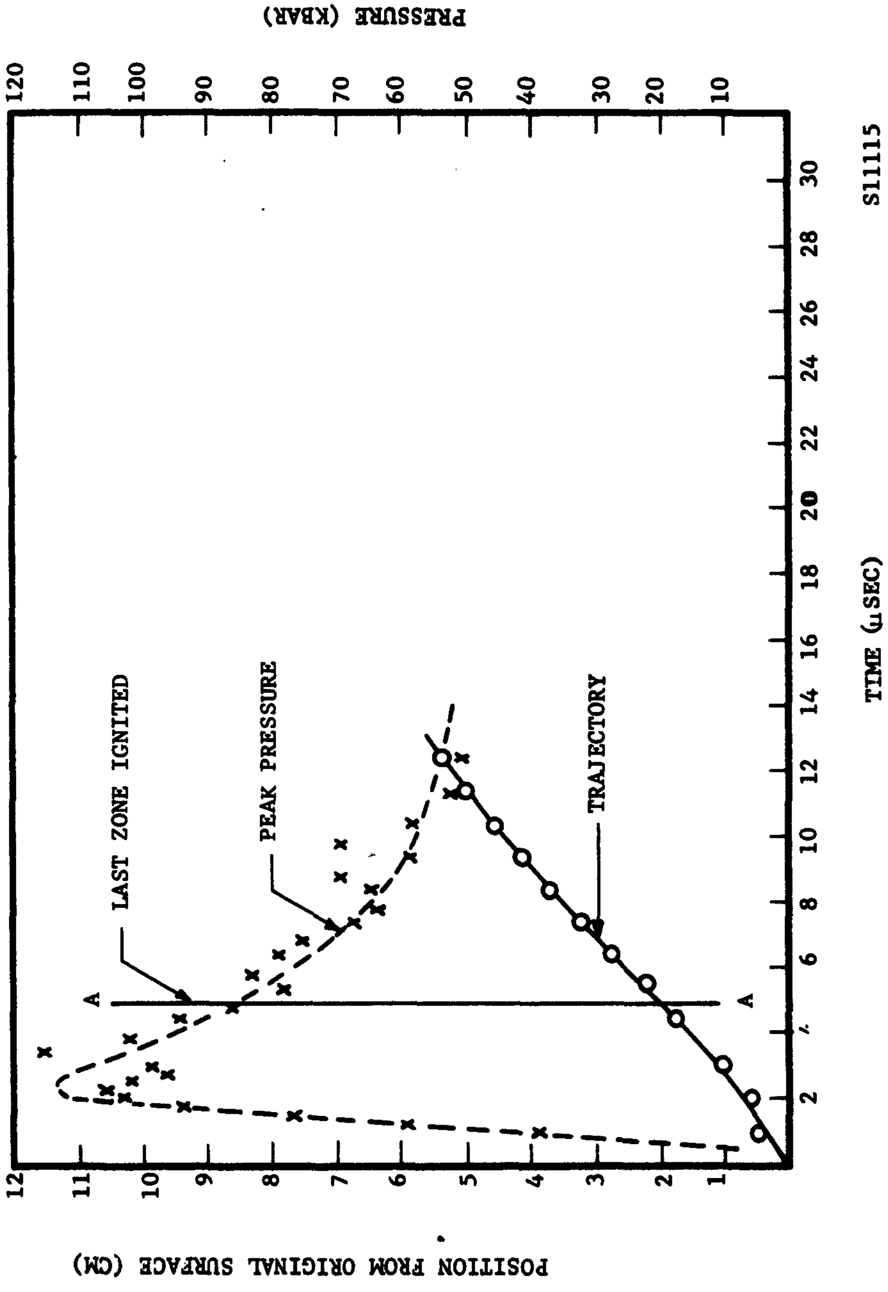

FIGURE 20 TRAJECTORY AND PEAK PRESSURE OF FADING DETONATION WAVE IN TNT

This calculation is comparable with experimental determinations of the minimum initiation pressure for such propellants as carried out by the Naval Ordnance Laboratory.[27] The agreement between experimental and computed values is good, and lends considerable support to the physical model and mathematical techniques which have been used in this program. However, some reservations are necessary because of discrepancies, described below, which have appeared in the properties of the computed steady state wave.

5.5 CALCULATION OF STEADY STATE CHARACTERISTICS

When the basic equations of a detonation process are expressed in time independent form, they are amenable to analytic solution through the use of the Chapman-Jouguet condition. The solution provides a theoretical steady state value for the propagation velocity and for a set of values of the pressure, and temperature in the burnt gas at the so-called Chapman-Jouguet point, which is a point in the detonation wave defined by the condition that reaction is complete and the particle velocity relative to the wave shock front equals the sound speed at that point. An important test of the validity of the mathematical procedures developed under this program for computing nonsteady detonation waves is in whether or not the computed waves ultimately attain the characteristics predicted by the steady state theory.

This question has been discussed to some extent in Section 3 and at other places in this report. It has been pointed out that the computed waves have persistently reached steady state values in which the propagation velocities are much higher than predicted from steady state theory. Such behavior is shown, for example, in Figures 4 (curve a), 14, and 15, in which final velocities in the range of 11 mm/μsec are indicated. This value compares to a predicted Chapman-Jouguet velocity for TNT of about 7 mm/μsec. Pressures at the Chapman-Jouguet point in these waves was in the vicinity of 300-400 kilobars compared to theoretical value of about 100 kbars.[15]

The most recent work on this program has been extensively concerned with attempts to ascertain the cause of this discrepancy. Two possibilities exist. First, it may be due to an error in the input data which is being used. Such error would most likely be in the values of the equation of state parameters used either for the solid or burnt gas phases. In an attempt to ascertain the sensitivity of the steady state velocity to these parameters, one calculation was run using a value of 0.66 for b, which defines both γ_s and γ_g according to Equations 14 and 31. Results are shown in the two curves of Figure 4 which were obtained with identical input except for the indicated difference in b. They show that use of b = 0.66 gave final propagation velocities much closer to that predicted from steady state theory than were obtained with the previous value of b = 1.03.

The considerations presented in Section 2 which led to the assignment of b = 1.03 are not sufficiently unequivocal to justify discarding this explanation of the discrepancy in steady state wave behavior. However, together with additional evidence found in the agreement between computed and experimental values of the minimum pressures for initiation, discussed previously, they constitute a persuasive argument in favor of the value, 1.03. For this reason, as well as in the interest of confidence, a re-examination of the mathematical procedures was undertaken with particular attention to the possibility that small consistent errors could accumulate in the integration of the basic equations and result in the observed discrepancy in the steady state behavior. A consequence was the finding that under some conditions the von Neuman q could lead to error as discussed in Section 3. This led to the change in procedure to provide for a delay in the ignition until the material had passed completely through the shock.

The effect of this change is shown by the two curves of Figure 21. Curve 1 is the trajectory shown on Figure 15, Curve 2 was computed with identical input, but with the delayed ignition. The pronounced difference in the two curves is an indication of the importance of this effect.

An additional consequence of the delayed ignition routine was the discovery that the computational procedure was depositing shock energy in the unreacted solid in substantially lower amount than required by the Hugoniot relation:

$$e = p \frac{v_x - v_a}{2}$$

Some additional alterations have been made as a consequence of this discovery primarily in the ignition routine and in the handling of the hydrodynamics in the region of the shock. The most recent modification has been the insertion of the fine zone routine as discussed in Section 3. It is believed that this provides a substantial improvement in the accuracy of the treatment. However, as of the present date, success has not been achieved in providing for the correct deposition of shock energy.

A wave trajectory run with the computational program incorporating all of the foregoing modifications, and with the same input as Figure 21 (Table 4, except Z = 0.035 cm)is shown on Figure 22. It is believed to represent the most accurate treatment presently possible. It was, however, not continued to steady state, so that the question of computation of the correct Chapman-Jouguet velocity remains unresolved.

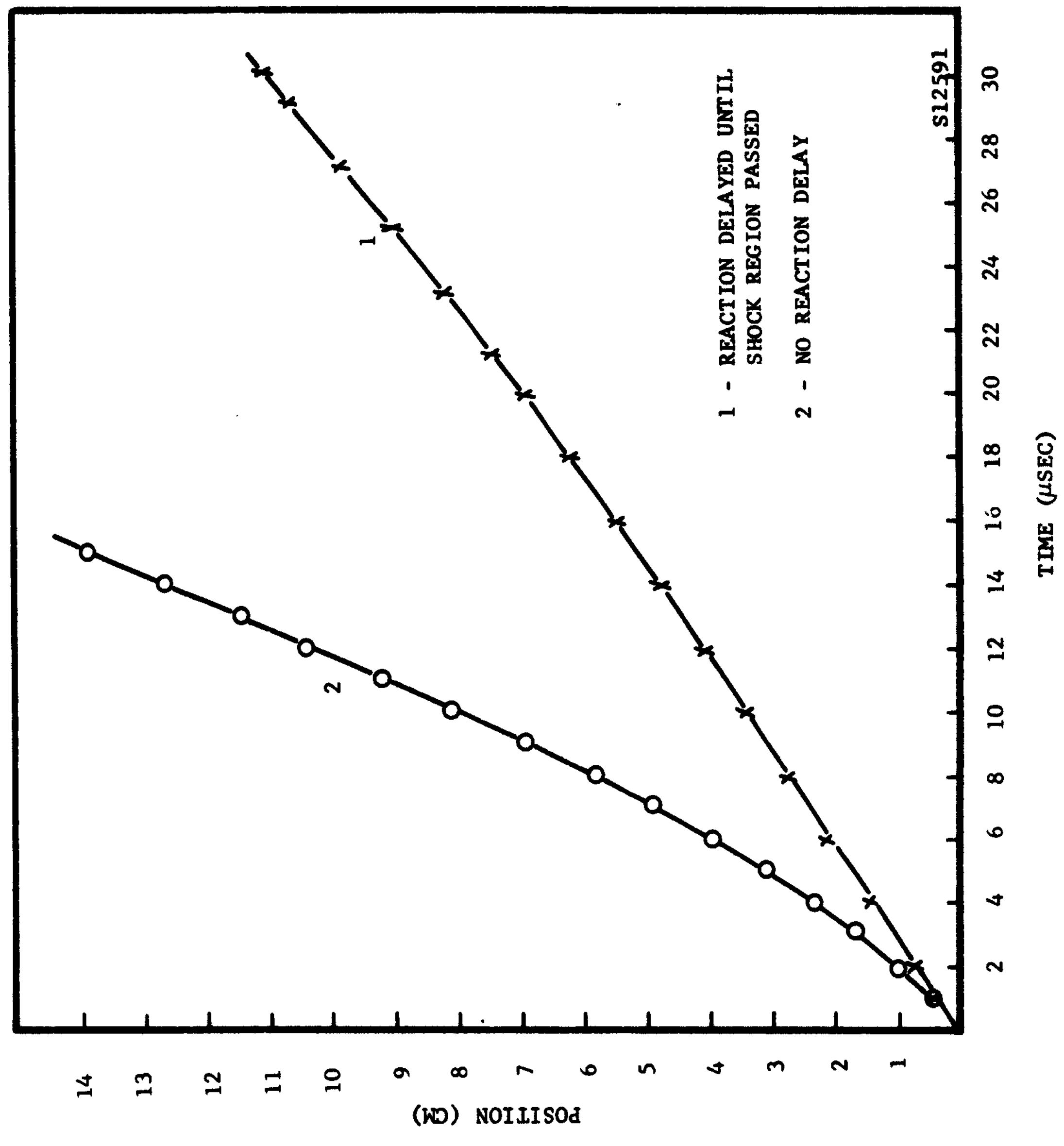

FIGURE 21. WAVE TRAJECTORIES SHOWING EFFECT OF PROGRAMMED REACTION DELAY

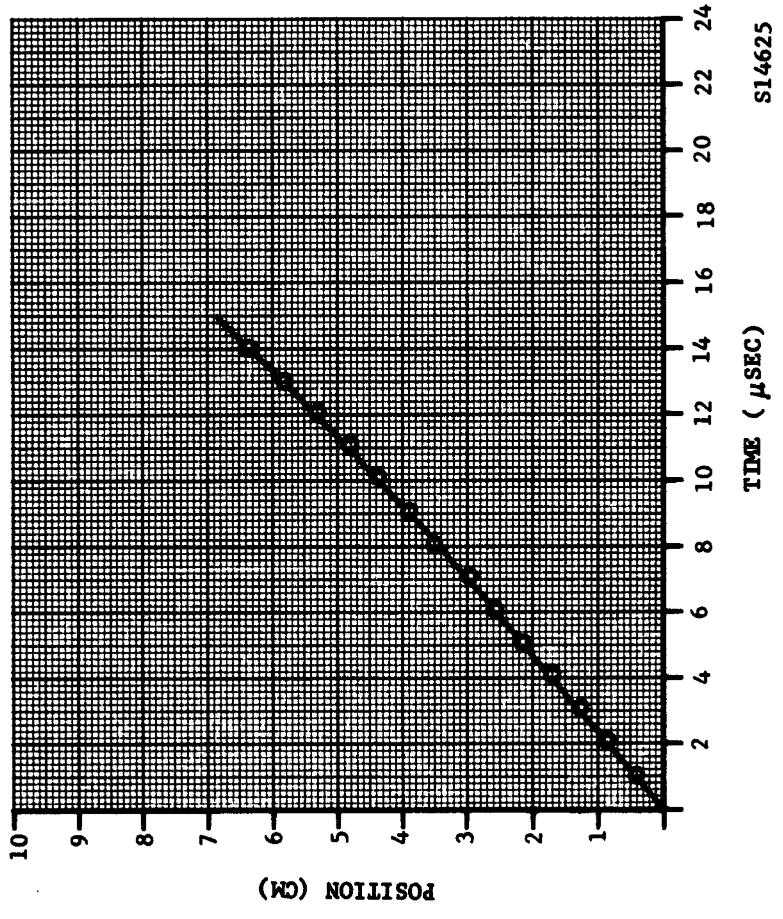

FIGURE 22. TRAJECTORY OF COMPUTED WAVE IN TNT WITH DELAYED IGNITION AND FINE ZONING

SECTION 6

TWO DIMENSIONAL TREATMENT

A number of important questions presently exist concerning the relationship between propellant grain geometry and detonation behavior, and the effect of the propellant properties upon this relationship.

First, there is the dependence of detonability upon overall lateral charge dimensions. For the case of a cylindrical charge, this is the effect of charge diameter. One aspect of this dependence, namely, the relation between charge diameter and steady state detonation velocity, has been the subject of much of the classical work on detonation theory, and the ability to correctly predict the observed relation constitutes an important test of the validity of the theoretical methods devised under this program. Other important aspects of this problem exist, however, which have been subjected to little or no experimental study. Examples are (1) the effect of point initiation vs. initiation by a plane wave, and (2) the effective charge diameter in the case of a cylindrical charge initiated at a point half-way between the two ends. In all of such cases the most important item of information, particularly in the case of large propellant charges, where experimental data are lacking, is the critical diameter or dimension at which a stable detonation wave can no longer be supported.

A second problem relates to charges which have cylindrical symmetry, but are not solid cylinders. Included here are such configurations as cylinders with axial cavities of cylindrical or other shape. Some experimental data have been reported[31] to the effect that such cavities have little or no effect and that only the outside diameter affects detonation behavior, at least until some critical web thickness is reached. Another configuration of considerable practical interest is that of a grouping of solid propellant charges arranged in various symmetrical patterns around a common axis. In all of the foregoing, the intensity and form of the initiation event required to cause detonation, and the effect of location or other geometrical factors thereon is of great importance, and would be especially amenable to investigation by the techniques developed during past work on this program.

In order to provide for the treatment of geometry dependent problems of this type, a two dimensional computer program has been written which incorporates the procedures described in the foregoing sections. This program is based upon a two-dimensional hydrodynamic program (with cylindrical symmetry), employing a Lagrangean, triangular mesh and incorporating the variable-time-step features introduced in HOP, the one-dimensional code. This program was prepared for Picatinny Arsenal under contract DA-04-495-ORD-3095.[28] The original code associates two (triangular) zones with each point of the mesh. The triangular zones give somewhat improved accuracy and stability than the more typical quadrilateral zones.

The extra data required for each zone in order to include chemical kinetics severely restricts the number of mesh points which can be internally stored in a 32000 word computer. Accordingly, the triangular code, called ROC-VTS, was rewritten using a quadrilateral mesh but retaining the variable time step feature. It is possible to store about 1200 mesh points internally. Basic concepts used in this code are the following.

Introduce Eulerian coordinates R, the distance from the axis of symmetry, and Z, distance measured along the axis. Mesh points are characterized by Lagrange coordinates K, L and the temporal mesh is characterized by the superscript n. The momentum equations to be solved for new velocities, $\dot{R}$ and $\dot{Z}$ are:

$$\dot{R}^{n+\frac{1}{2}}_{K,L} = \dot{R}^{n-\frac{1}{2}}_{K,L} + \Big[(p+q)^n_{K-\frac{1}{2},L+\frac{1}{2}}\,(Z^n_{K-1,L}-Z^n_{K,L+1}) + (p+q)^n_{K+\frac{1}{2},L+\frac{1}{2}}\,(Z^n_{K,L+1}-Z^n_{K+1,L}) + (p+q)^n_{K+\frac{1}{2},L-\frac{1}{2}}\,(Z^n_{K+1,L}-Z^n_{K,L-1}) + (p+q)^n_{K-\frac{1}{2},L-\frac{1}{2}}\,(Z^n_{K,L-1}-Z^n_{K-1,L})\Big]\left(\frac{\Delta t}{\rho A}\right)^n_{K,L} \tag{134}$$

$$\dot{Z}^{n+\frac{1}{2}}_{K,L} = \dot{Z}^{n-\frac{1}{2}}_{K,L} - \Big[(p+q)^{n}_{K-\frac{1}{2},L+\frac{1}{2}}(R^{n}_{K-1,L}-R^{n}_{K,L+1}) + (p+q)^{n}_{K+\frac{1}{2},L+\frac{1}{2}} (R^{n}_{K,L+1} - R^{n}_{K+1,L}) + (p+q)^{n}_{K+\frac{1}{2},L-\frac{1}{2}}(R^{n}_{K+1,L}-R^{n}_{K,L-1}) + (p+q)^{n}_{K-\frac{1}{2},L-\frac{1}{2}}(R^{n}_{K,L-1}-R^{n}_{K-1,L})\Big]\left(\frac{\Delta t}{\rho A}\right)^{n}_{K,L} \tag{135}$$

where $$\left(\frac{\Delta t}{\rho A}\right)^{n}_{K,L} = \frac{\Delta t^{n+\frac{1}{2}}_{K,L} + \Delta t^{n-\frac{1}{2}}_{K,L}}{(\rho A)^{n}_{K-\frac{1}{2},L+\frac{1}{2}} + (\rho A)^{n}_{K+\frac{1}{2},L+\frac{1}{2}} + (\rho A)^{n}_{K+\frac{1}{2},L-\frac{1}{2}} + (\rho A)^{n}_{K-\frac{1}{2},L-\frac{1}{2}}}. \tag{136}$$

In the above, ρ is the density and A the area (of revolution) of the quadrilateral zone in question. These momentum equations are felt to be a substantial improvement over those typically used for two-dimensional cylindrical Lagrange hydrodynamic codes.(30) The interested reader is referred to references 28, 29, or 30 for further discussions and references of two-dimensional hydrodynamic computing techniques.

This two dimensional program is presently running and has been used for short demonstrations. However, no full problems have been run.

SECTION 7

EXPERIMENTAL INVESTIGATION OF EQUATION OF STATE

The objective of this phase of the program was the determination of the quantities β and γ in Equation 18 as functions of the variables p, v, and e. The work involved the procurement of p-v-T data by static pressure techniques, making use of apparatus and experimental methods described by Kennedy for work in the ultra-high pressure region.

The experimental method involves the use of a high pressure piston-cylinder press[32] shown schematically in Figure 23. In this apparatus a tungsten carbide piston is driven by a high pressure hydraulic system into a tungsten carbide cylinder supported by a specially designed pressure plate consisting of a series of press-fitted concentric rings (see Figure 24). Pressure within the cylinder is determined from ram oil pressure as measured on a calibrated Heise gauge, and the known ratio of cylinder diameter to ram diameter. Volume within the cylinder is determined from piston position as measured either by a dial gauge, micrometer, or a linear potentiometer, the latter being used to drive one leg of an x-y recorder.

Information is obtained as an upward and downward curve of pressure versus volume change, first, by increasing the pressure, in steps, to the maximum value desired, and then similarly decreasing it stepwise back to zero, with measurements of the piston movement at each step. In all such curves, the upward and downward legs demonstrate a definite hysteresis having the general characteristics shown in the linearized diagram of Figure 25. This is due primarily to frictional forces - both of the piston on the walls of the cylinder and internal friction of the sample. Thus, for example, the pressure difference between points 3 and 4 represents the vector difference of the frictional forces for the up and down strokes. If the magnitudes of these forces

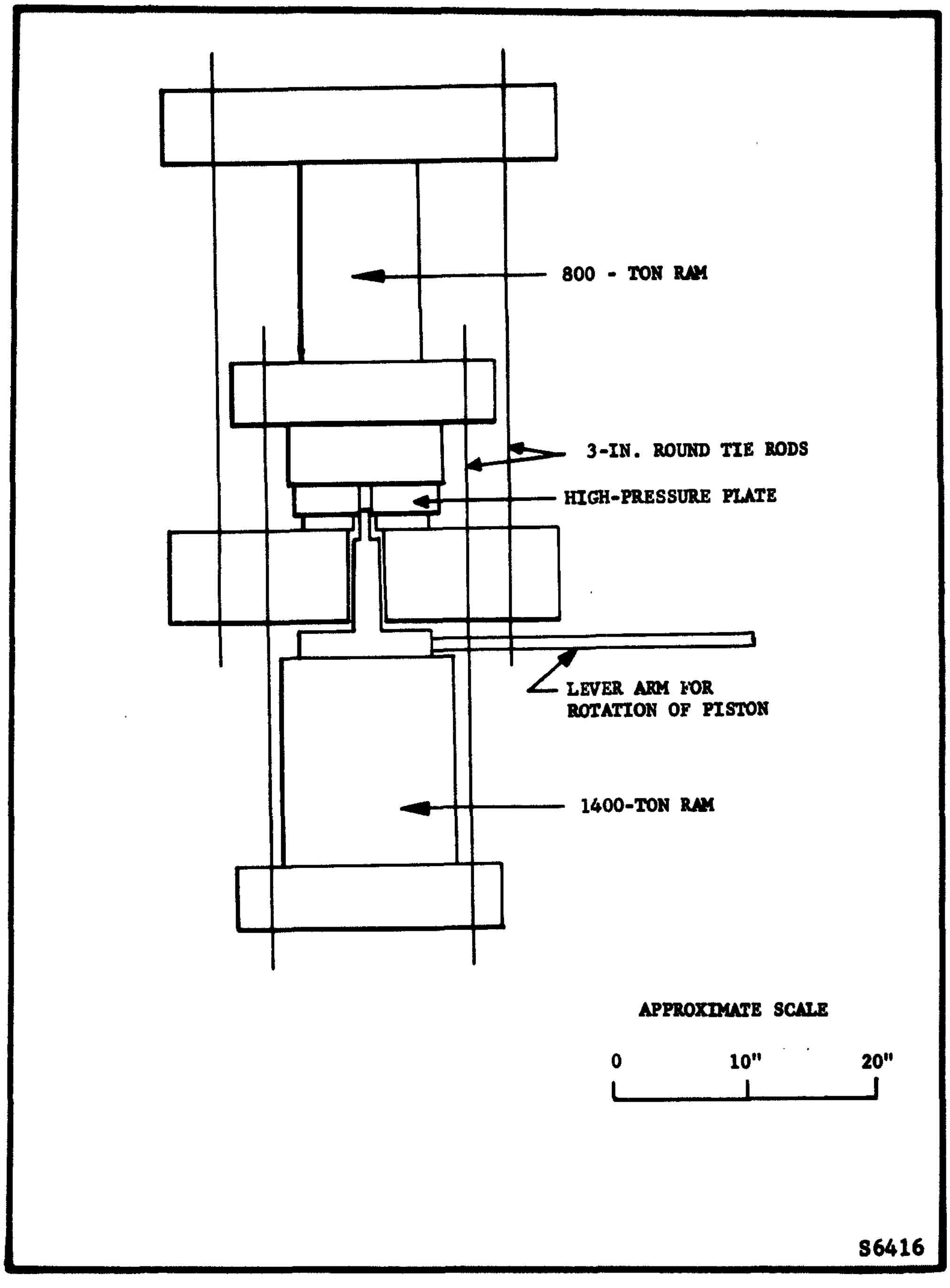
800 - TON RAM
3-IN. ROUND TIE RODS
HIGH-PRESSURE PLATE
LEVER ARM FOR
ROTATION OF PISTON
1400-TON RAM
APPROXIMATE SCALE
0
10"
20"
S6416

FIGURE 23. HIGH PRESSURE PISTON-CYLINDER PRESS

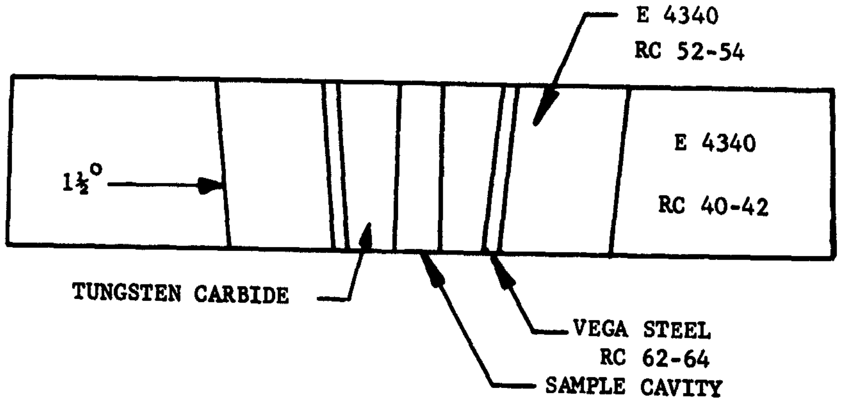
E 4340
RC 52-54
E 4340
RC 40-42
1½°
TUNGSTEN CARBIDE
VEGA STEEL
RC 62-64
SAMPLE CAVITY

S6417

FIGURE 24. HIGH-PRESSURE PLATE

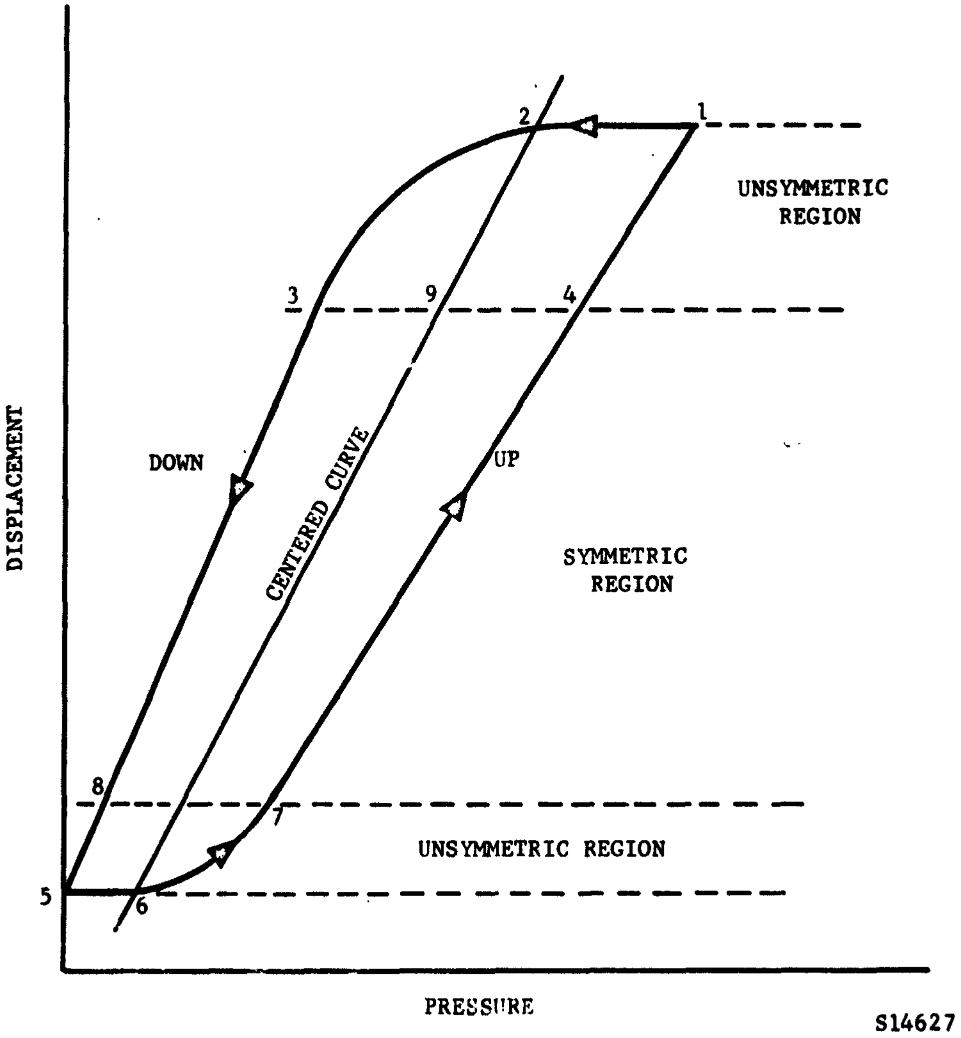
1
2
UNSYMMETRIC REGION
3
9
4
DOWN
CENTERED CURVE
UP
SYMMETRIC REGION
DISPLACEMENT
8
7
UNSYMMETRIC REGION
5
6
PRESSURE
S14627

FIGURE 25. TYPICAL FORM OF PRESSURE - DISPLACEMENT CURVE

are the same (at the same displacement) an average sample pressure at this displacement is represented by a point half-way between 3 and 4 (i.e. point 9). It follows that to a good approximation the true p-v curve for the material in the cylinder is given by the curve 2,6. Direct observation of the curve 2,6 is possible if sliding friction is relieved prior to each observation by rotating the piston, and if sufficiently long times are allowed between observations for sample internal friction to anneal out. It has been reported by Kennedy,[33] however, that use of the mid points between the ascending and descending curves will give the true p-v curve with an accuracy which is within the other experimental errors of the experiment.

It is necessary to convert the information such as shown in Figure 25 into a sample compressibility, and ultimately into a p-v curve. To do so requires the input of certain information about the press geometry and its distortion as a function of pressure. The latter is known as the press constant.

Figure 26 shows a detailed diagram of the press set-up during an experiment. Here A^s is the pressure plate shown in detail in Figure 24 and which forms the high pressure cylinder, and B^s is the piston. C^s is the end loading platon for clamping the sides of the pressure plate between the cylinder head block, D^s, which in turn rests against the press head E^s, and the spacer F^s. G^s is a force transmitting column, H^s is a pillow plate and I^s is the master ram.

The sample volume is defined at any time by the distance between the piston head and the cylinder head, i.e.

$$X_1^s = X_2^s - X_3^s$$

The change in this distance with ram motion is equal to the ram movement less the press constant. If the distances X_2^s and X_3^s are known at any reference ram position, then the distance X_1^s at any other ram position is given by

$$X_1^s = X_{10}^s + X_{20}^s - X_{30}^s + \Delta X^s + C^s \qquad (137)$$

where the subscript zero refers to the reference position.

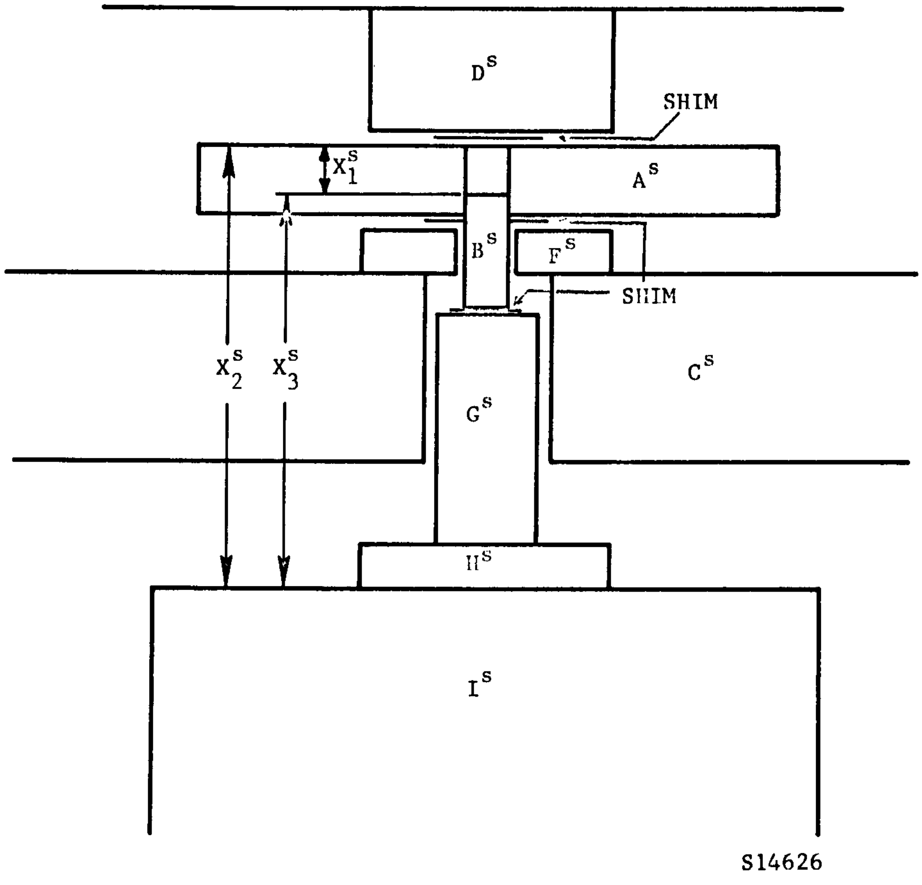
D^s
SHIM
X^s_1
A^s
B^s
F^s
SHIM
X^s_2
X^s_3
C^s
G^s
H^s
I^s
S14626

FIGURE 26 DETAIL OF PRESS SET-UP

With a given piston diameter, it is assumed that the press constant is dependent only upon cylinder pressure rather than ram position, i.e. sample volume. This is true only if the radial distortion of the cylinder wall is independent of the volume or other factors related to the sample. Evidence obtained by Kennedy has indicated that radial expansion of the cylinder is negligible under the pressures considered here. Consequently if the sample volume, X_1^s, is zero:

$$X_1^s = X_{10}^s = 0$$

$$X_{20}^s = X_{30}^s$$

and the press constant is readily determined as

$$C^s = \Delta X^s \tag{138}$$

The reference point for measurement of the ram motion, ΔX^s, is generally chosen in such a way as to provide the smallest value of the press constant.

The foregoing considerations lead to the following procedure for a press run. First, with no sample in the cylinder the ram is set at a position corresponding to zero simple chamber volume. This is readily recognized as a point at which hydraulic pressure rises steeply with ram motion. A plot of ram displacement vs pressure beyond this point is, according to Equation 138 also a plot of press constant vs pressure. Little or no hysteresis is found in the up and down legs of this curve.

A sample is then inserted in the pressure chamber and a press cycle run as described in the foregoing. It frequently happens that sliding friction does not disappear completely at zero pressure, so that the curves of the up and down legs show unsymmetric regions at both ends as indicated in Figure 25. In such cases the points in these regions cannot be used for centering. They are normally excluded by restricting the centering procedure to that region where the up and down legs are relatively parallel.

The centered curve is corrected for the press constant and for extrusion of the sample into champfered spaces at the piston and cylinder heads. Additional corrections relate to the presence in the cylinder of items other than the material of interest. These include a thermocouple and thermocouple retainer made of stainless steel, and sometimes a wafer of inert material between the piston head and the sample. The latter was used in working with combustible materials which conceivably could become ignited by viscous heating if they were forced into the space between piston and cylinder wall. Corrections to be made for these substances must be derived from data on their compressibility obtained in separate experiments.

Pressure-volume curves at elevated temperatures were obtained by clamping ring heaters to the sides of the pressure plate A^s. Maximum temperatures investigated were about 100°C. Sample temperatures were monitored in all cases by means of a chromel-alumel thermocouple inserted through the cylinder head block and into a hole in the sample. Temperature variation over a cycle was not found to be more than 1-2°C.

The p-v-T data obtained are presented in Figures 27 to 40, inclusive. Curves are included for a number of pure or homogeneous materials, and on their various mixtures. Tables 8 and 9 give pertinent data on the composition of the salt-polyurethane speciman and on the polyurethane-APC propellant speciman. Table 10 gives p-v-T data on the propellant in tabulated form.

A number of the figures showing data on mixtures also include curves labeled "calculated". These were deduced by assuming that the specific volumes of the constituents of the mixture were additive at all pressures. Interest in this point derives from two considerations. In the first place, some mixtures pertinent to this program are combustible and susceptible to ignition at elevated temperatures, whereas their major constituents are much less so in the pure state. This would be true, for example, of a polyurethane ammonium perchlorate propellant, such as the one for which data is presented in Figure 39. In the second place, many mixtures of interest are composed of a relatively small number of the same basic constituents, and a considerable saving in time would be possible if their p-v-T relationships could be derived directly from the corresponding curves for the components.

Agreement between the experimental and calculated curves are fairly good in some cases, and less so in others. No general conclusions have been drawn as to the feasibility of this technique. However, it was used to obtain the p-v curve for a polyurethane propellant at about 100°C. The result is shown on Figure 40.

The information presented in the figures can be used to evaluate the parameters β and γ in Equation 18, Section 2, in a straightforward way. However, this had not been done as of the date of this report.

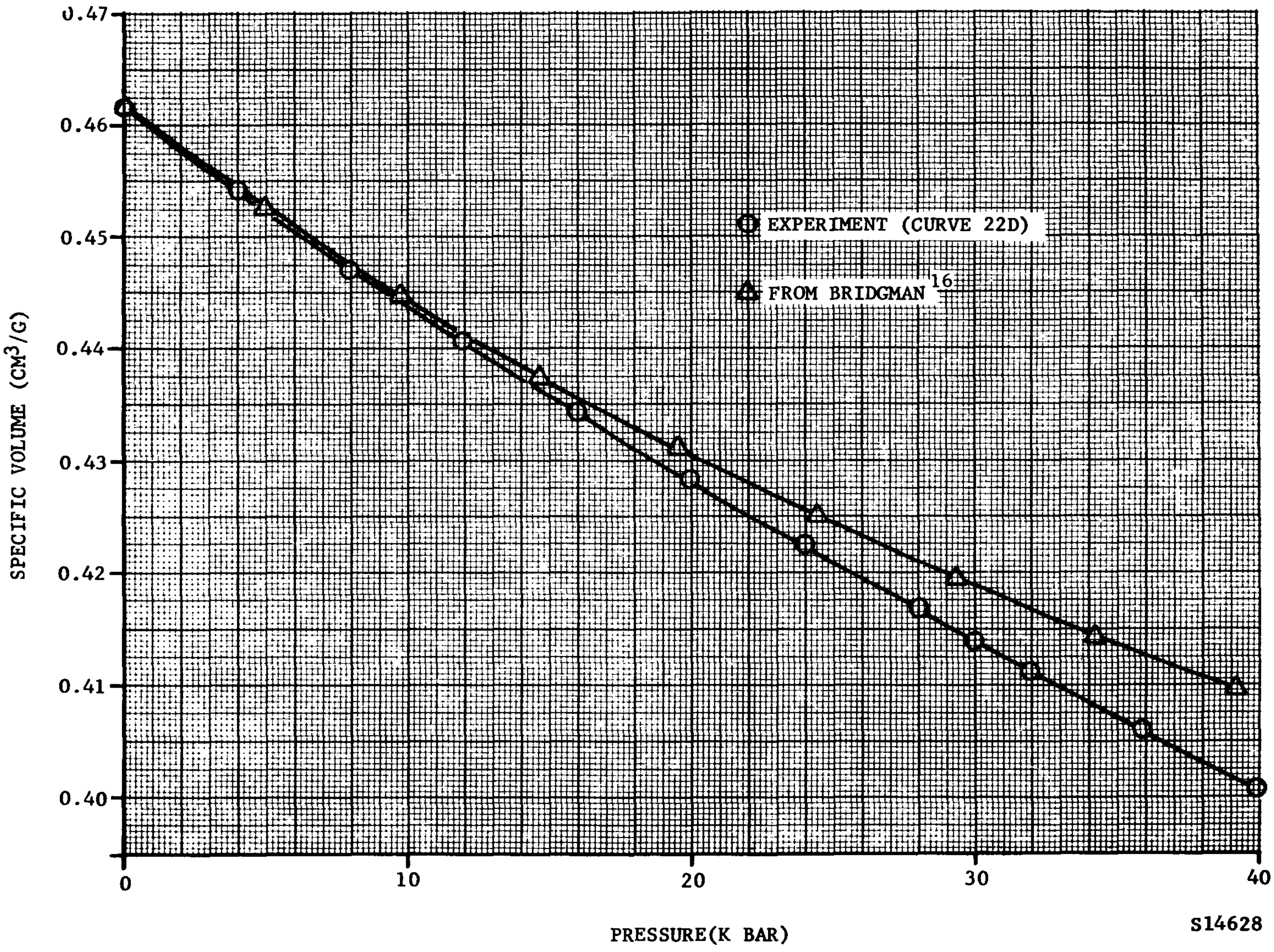

S14628

FIGURE 27. PRESSURE-VOLUME CURVES FOR SODIUM CHLORIDE AT 24°C

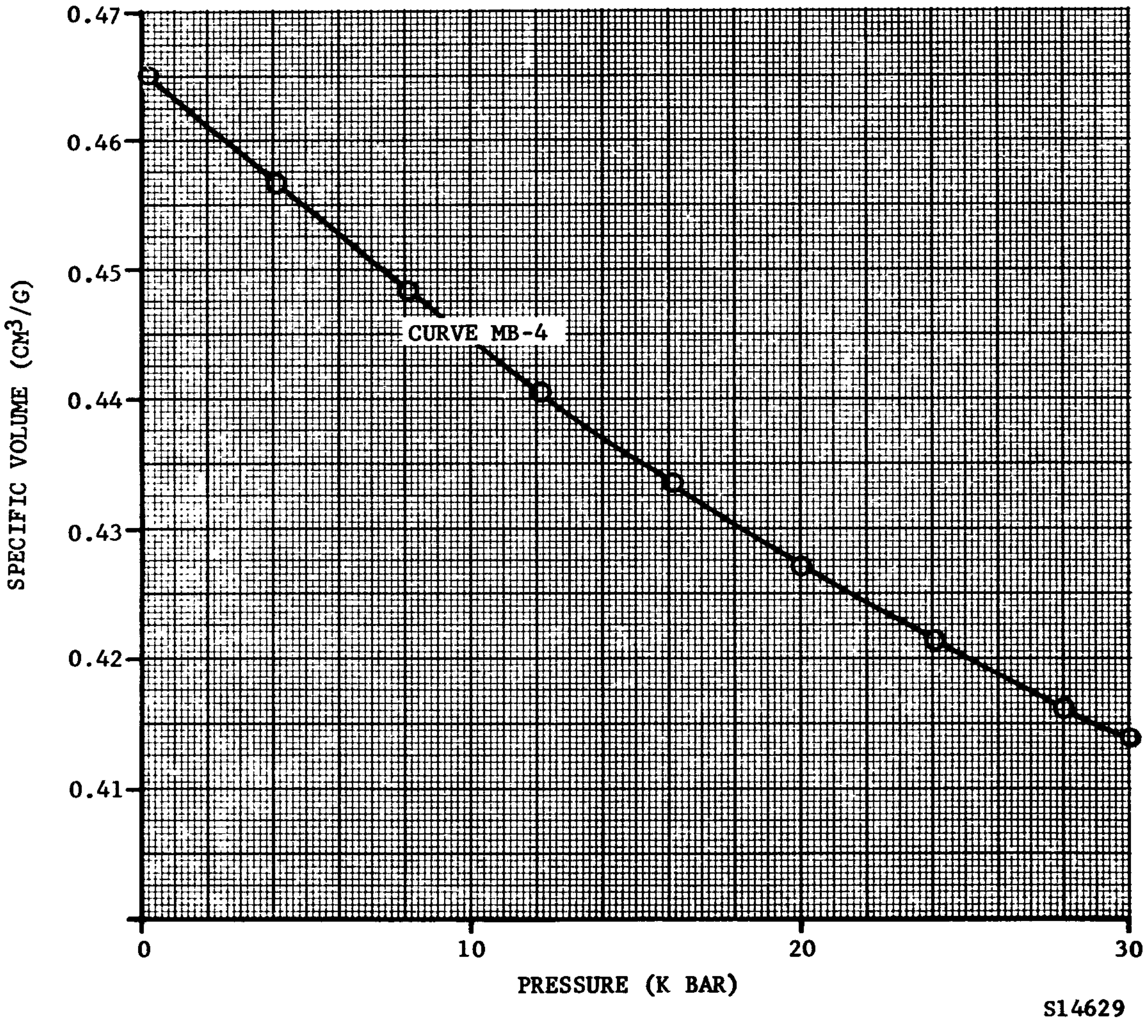

FIGURE 28. PRESSURE-VOLUME CURVE FOR SODIUM CHLORIDE AT 100°C

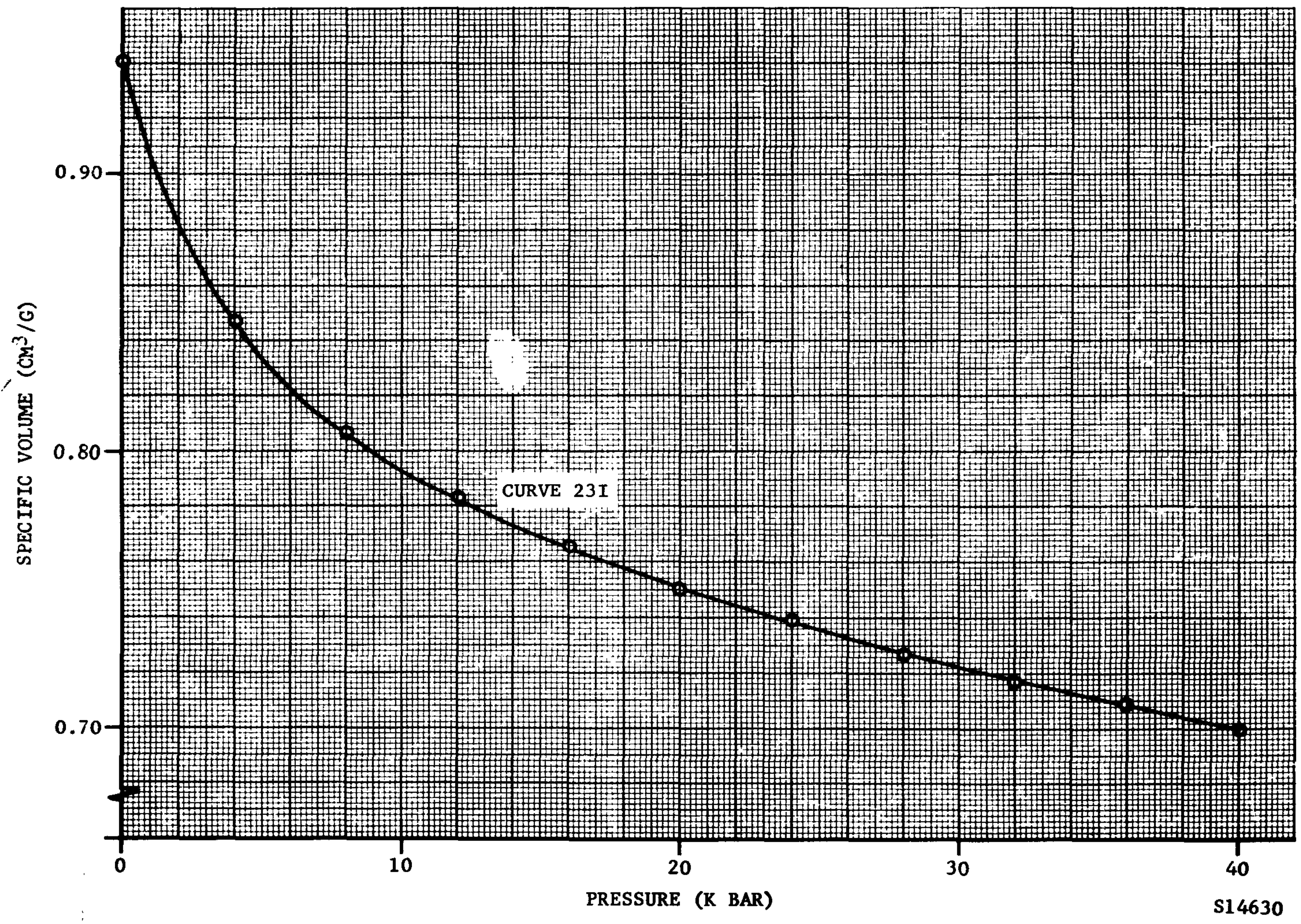

FIGURE 29. PRESSURE-VOLUME CURVE FOR POLYURETHANE AT 23°C

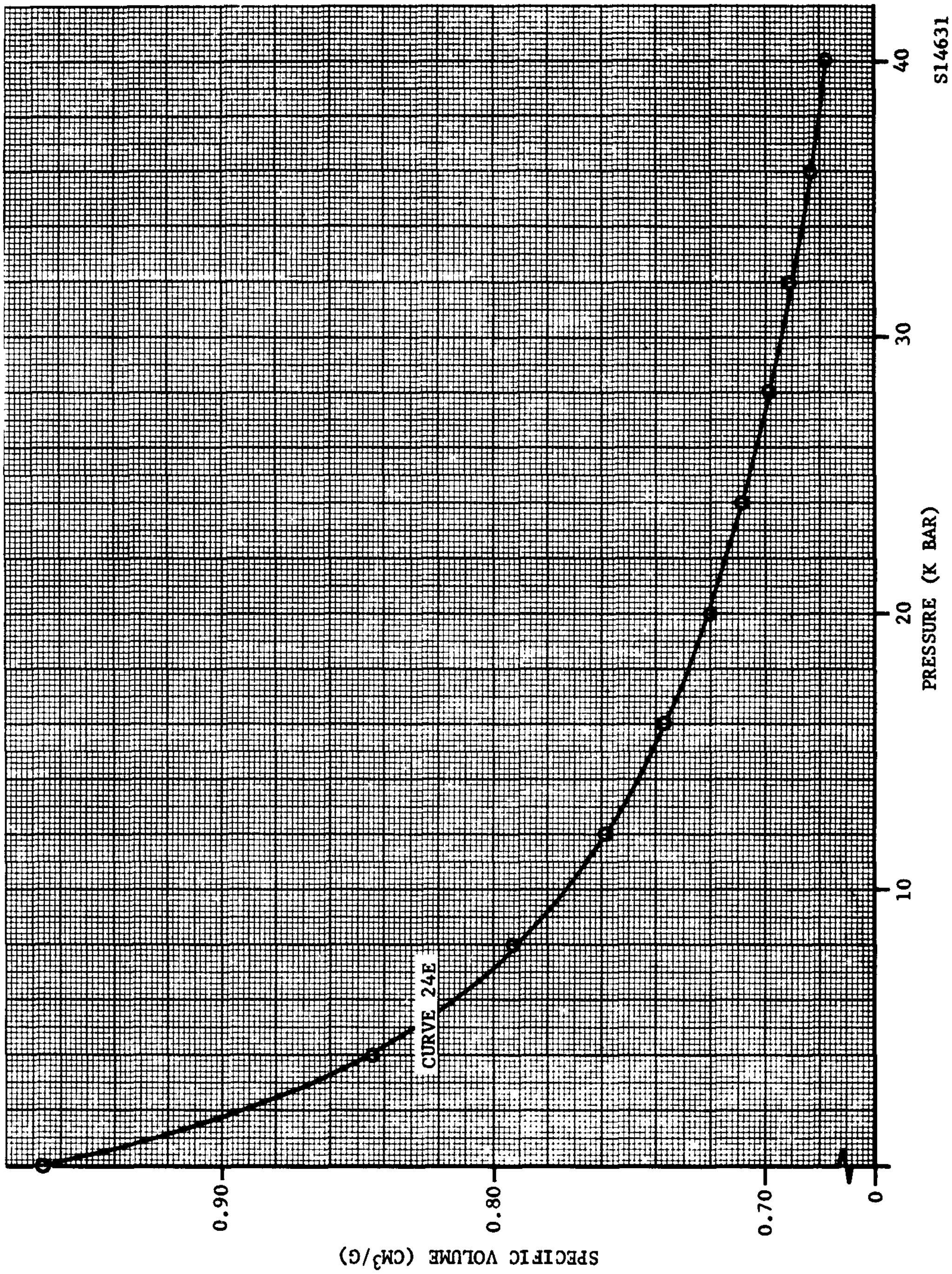

FIGURE 30. PRESSURE-VOLUME CURVE FOR POLYURETHANE AT 99.5 - 101°C

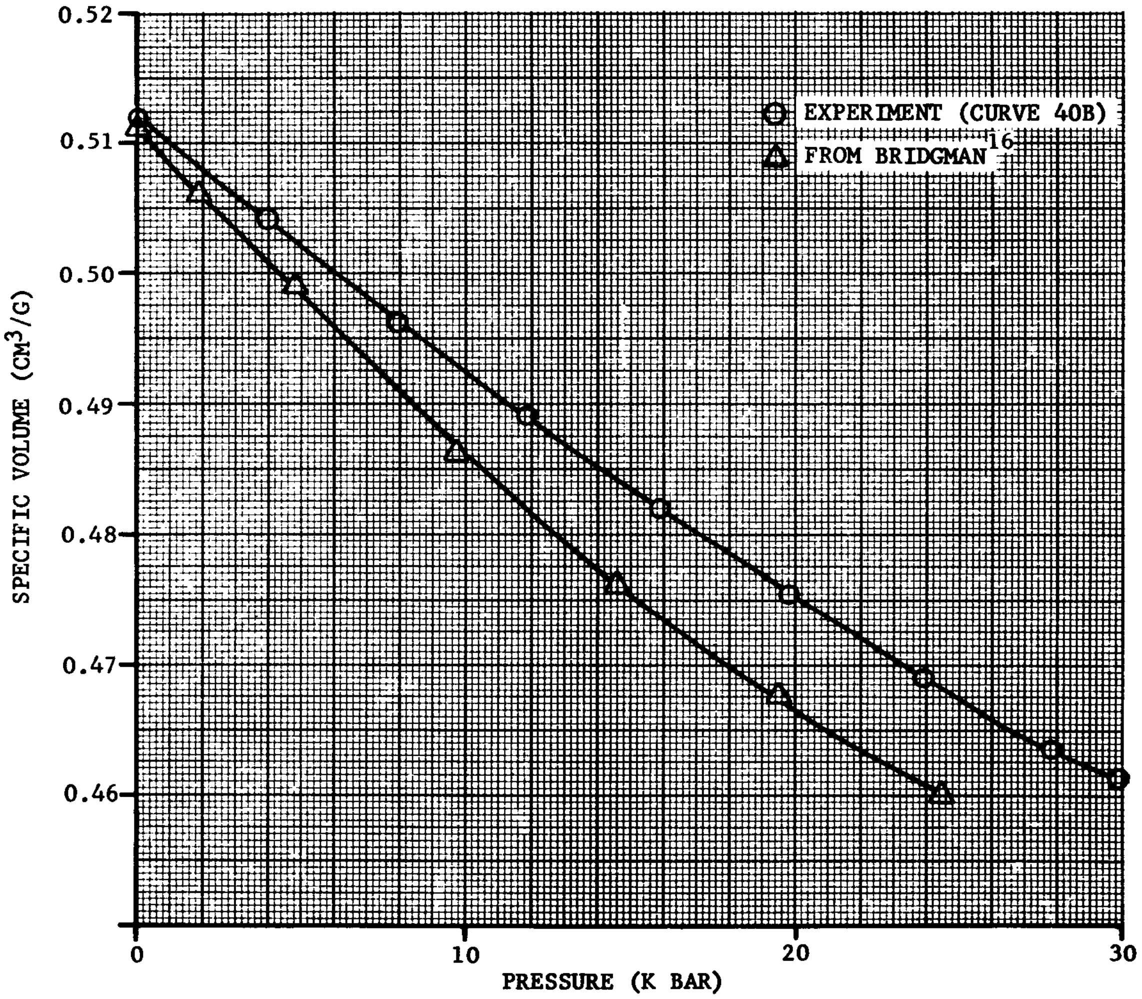

S14632

FIGURE 31. PRESSURE-VOLUME CURVES FOR AMMONIUM PERCHLORATE AT 21.5 - 22.06°C

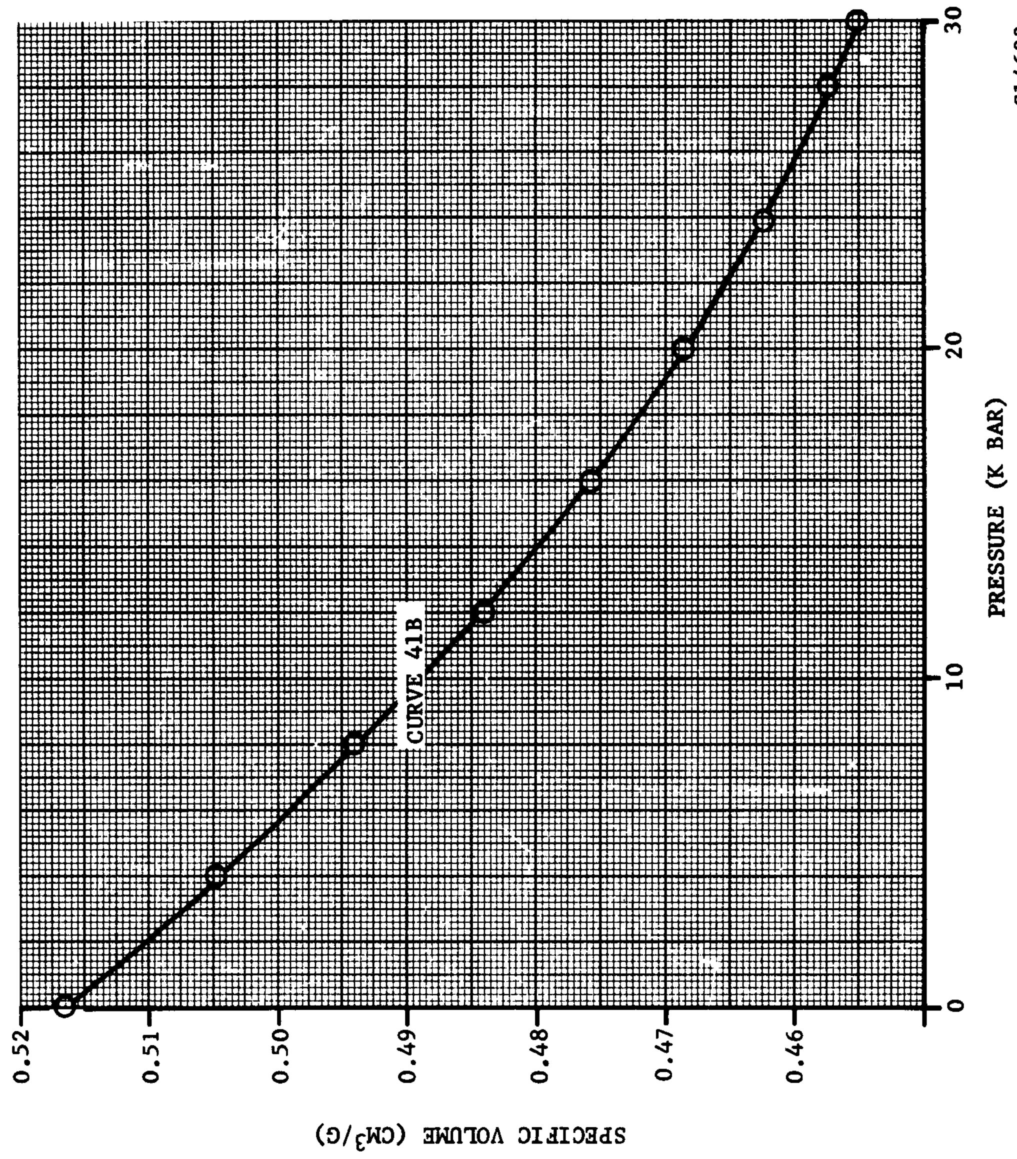

S14633

FIGURE 32. PRESSURE-VOLUME CURVE FOR AMMONIUM PERCHLORATE AT 100 - 102°C

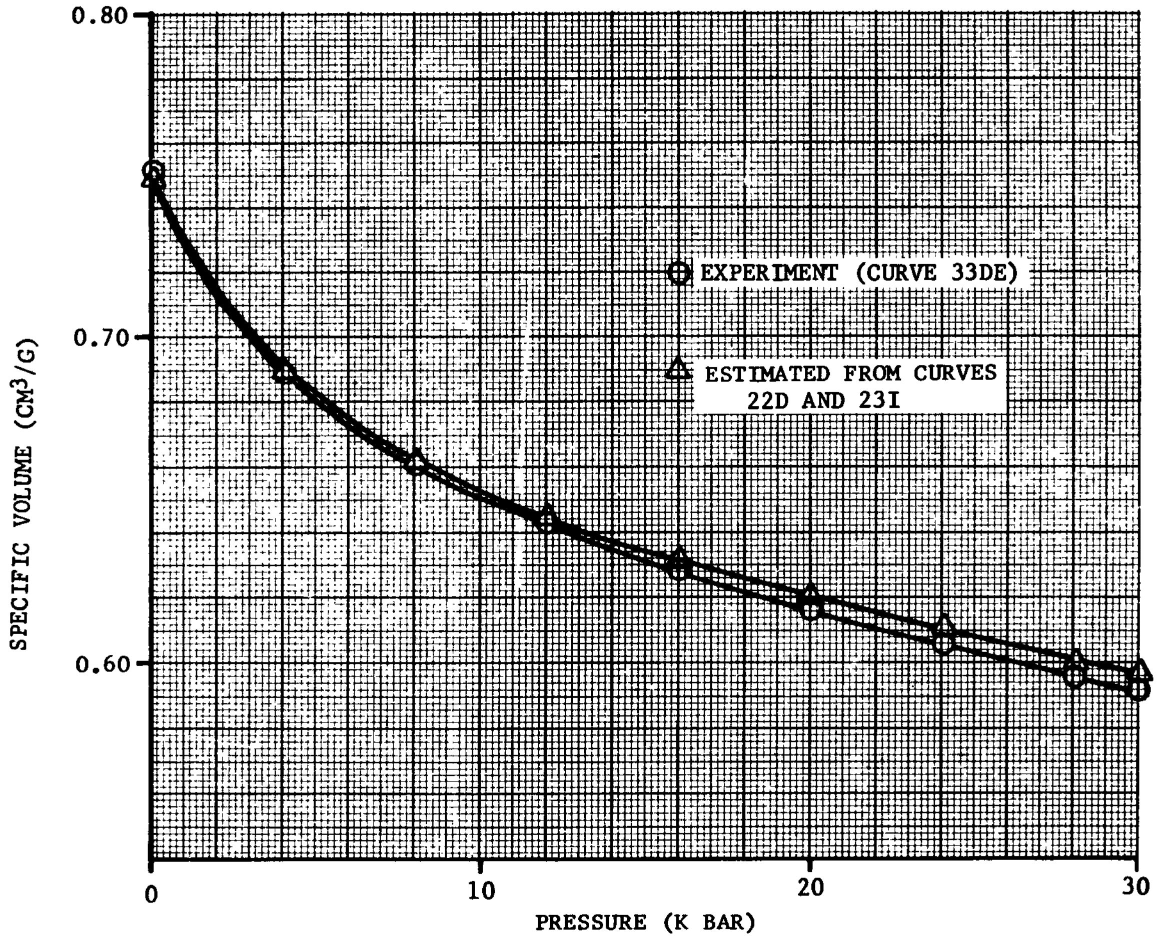

S14634

FIGURE 33. PRESSURE-VOLUME CURVES FOR SODIUM CHLORIDE-POLYURETHANE MIXTURE (40 - 60% BY WT) AT 22 - 23°C

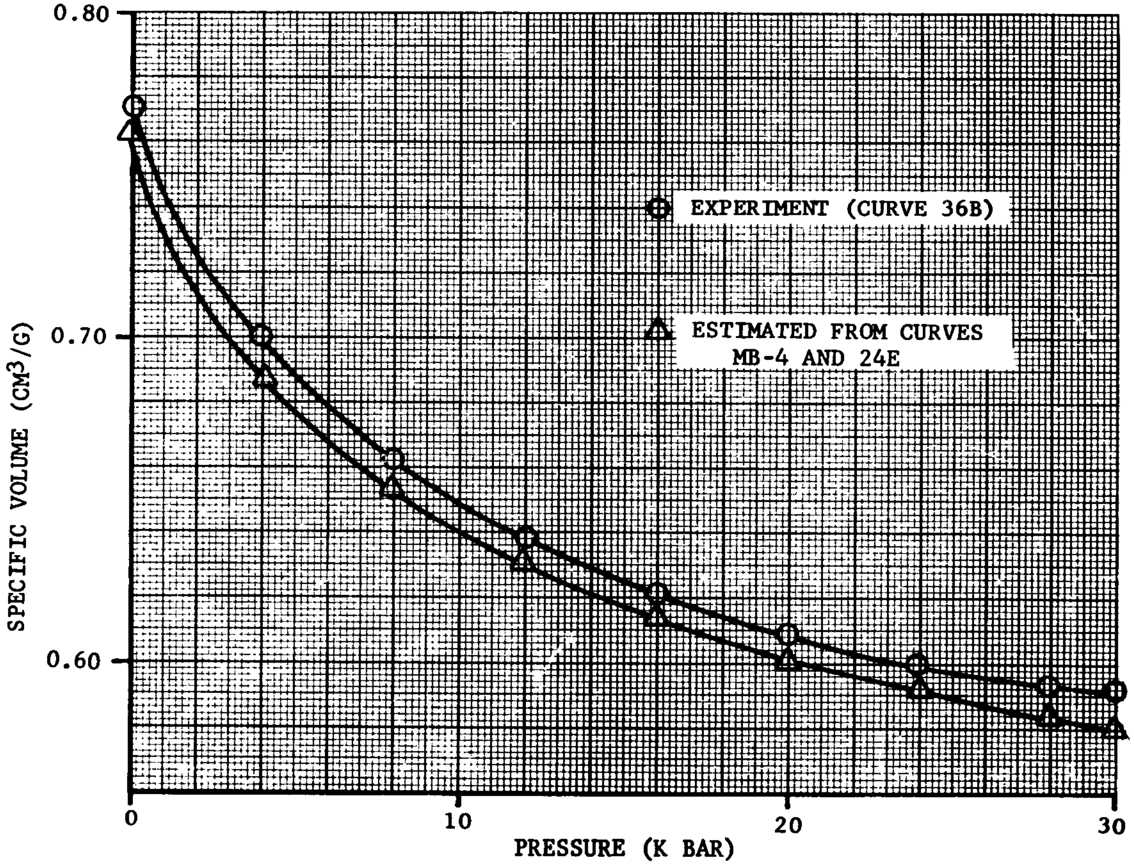

S14635

FIGURE 34. PRESSURE-VOLUME CURVES FOR SODIUM CHLORIDE-POLYURETHANE MIXTURE (40 - 60% BY WT) AT 91 - 94°C

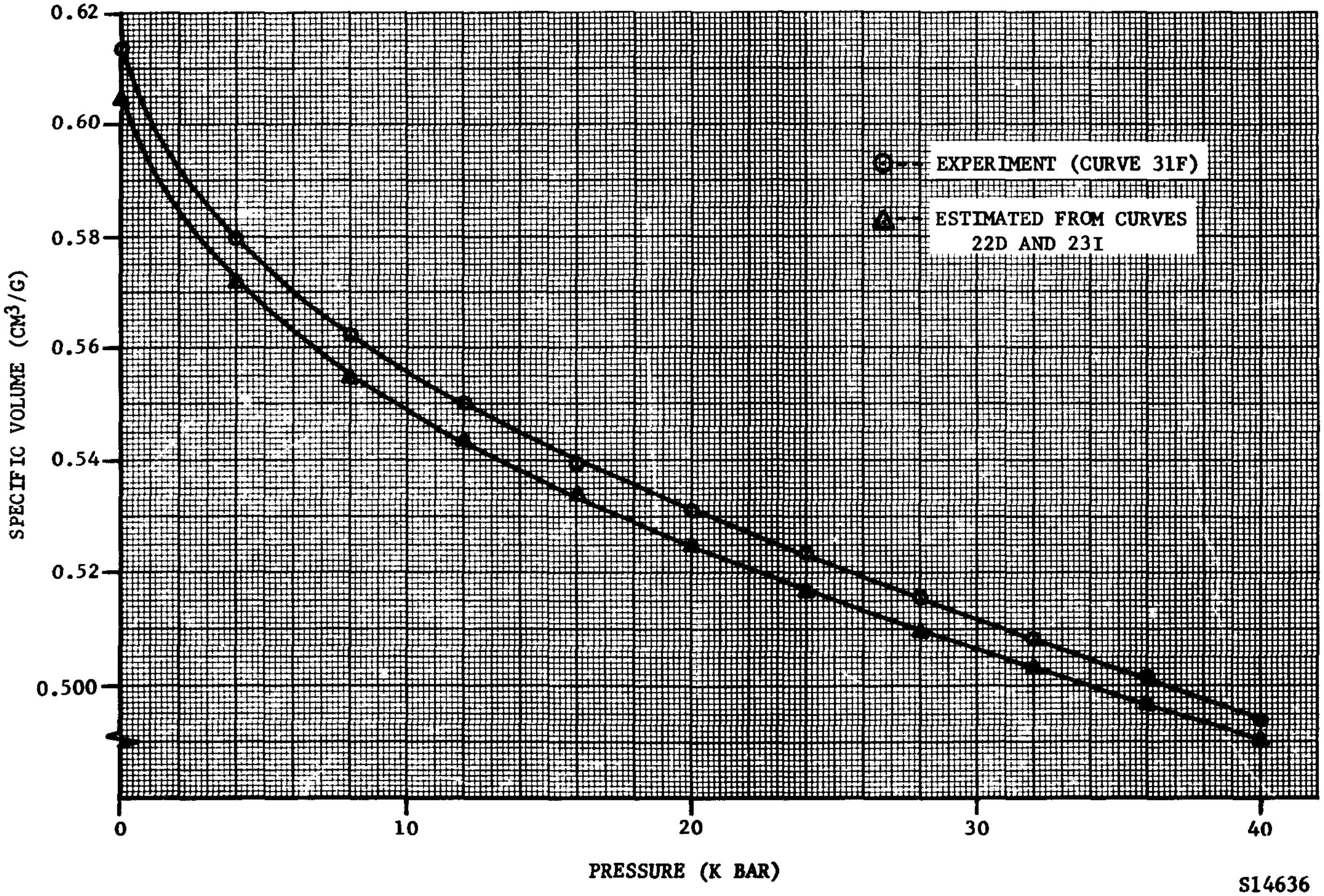

S14636

FIGURE 35. PRESSURE-VOLUME CURVES FOR SODIUM CHLORIDE-POLYURETHANE MIXTURE (70 - 30% BY WT) AT 23°C

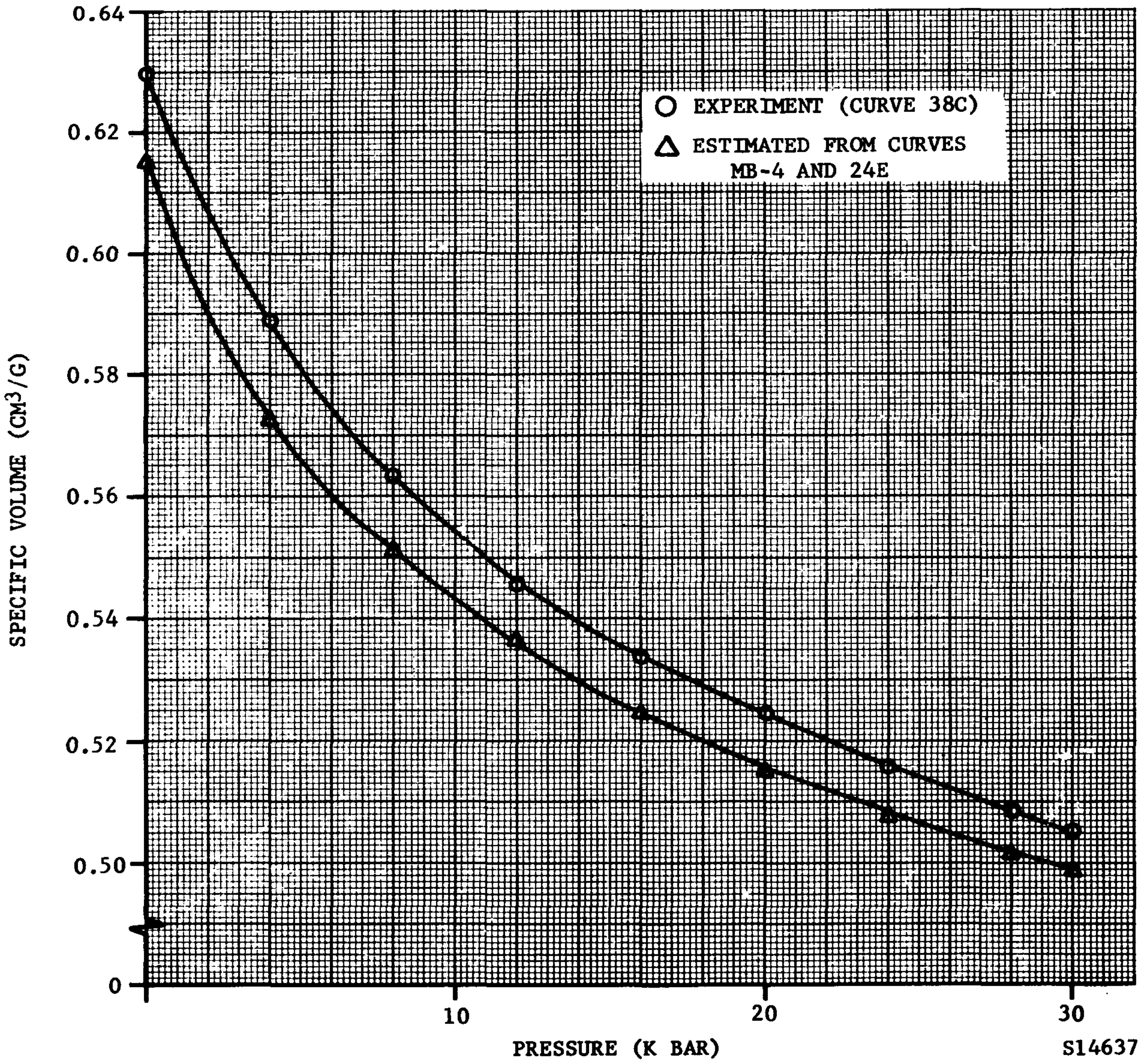

FIGURE 36. PRESSURE-VOLUME CURVES FOR SODIUM CHLORIDE-POLYURETHANE MIXTURE (70 - 30% BY WT) AT 99 - 102°C

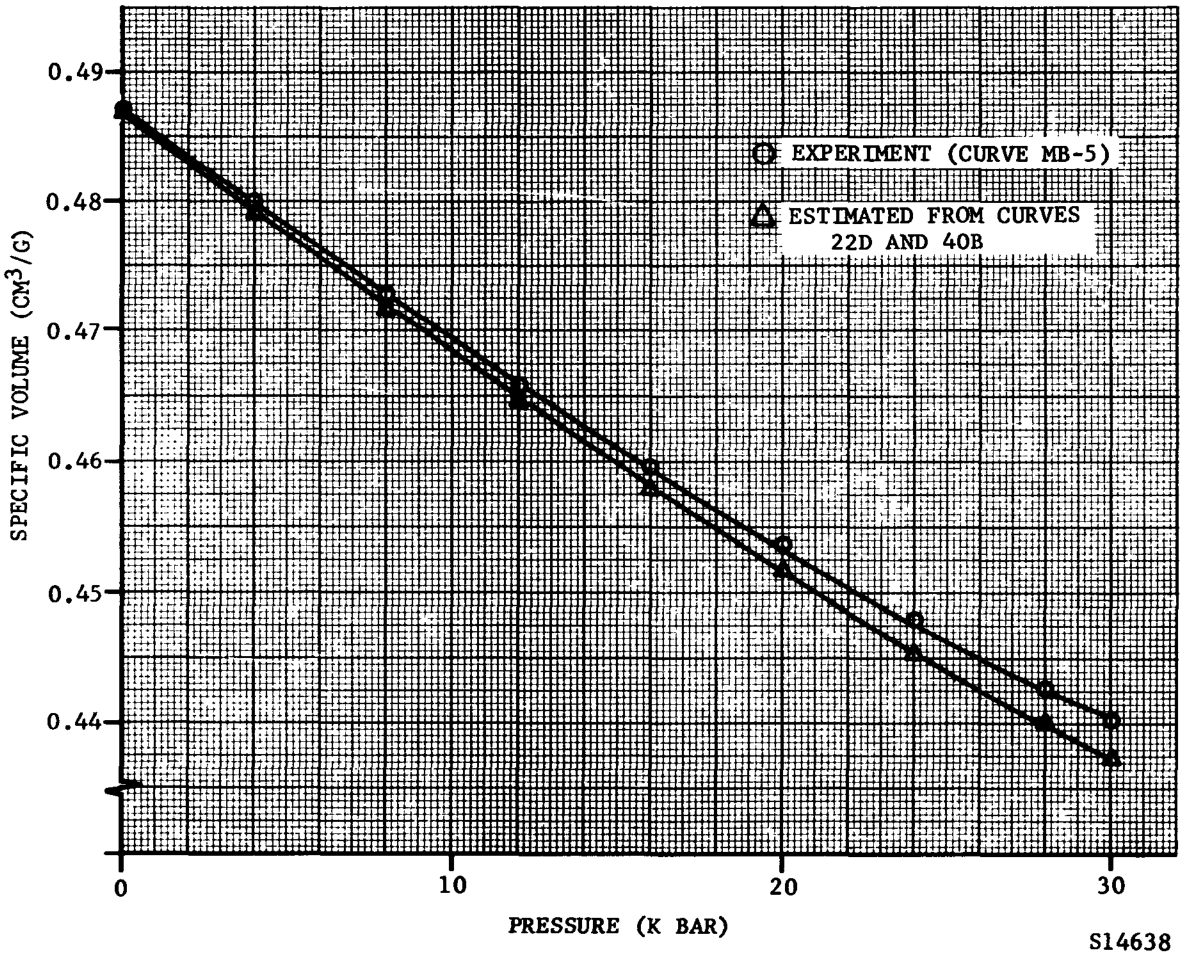

S14638

FIGURE 37. PRESSURE-VOLUME CURVES FOR SODIUM CHLORIDE-AMMONIUM PERCHLORATE MIXTURE (50 - 50% BY WT) AT 21°C

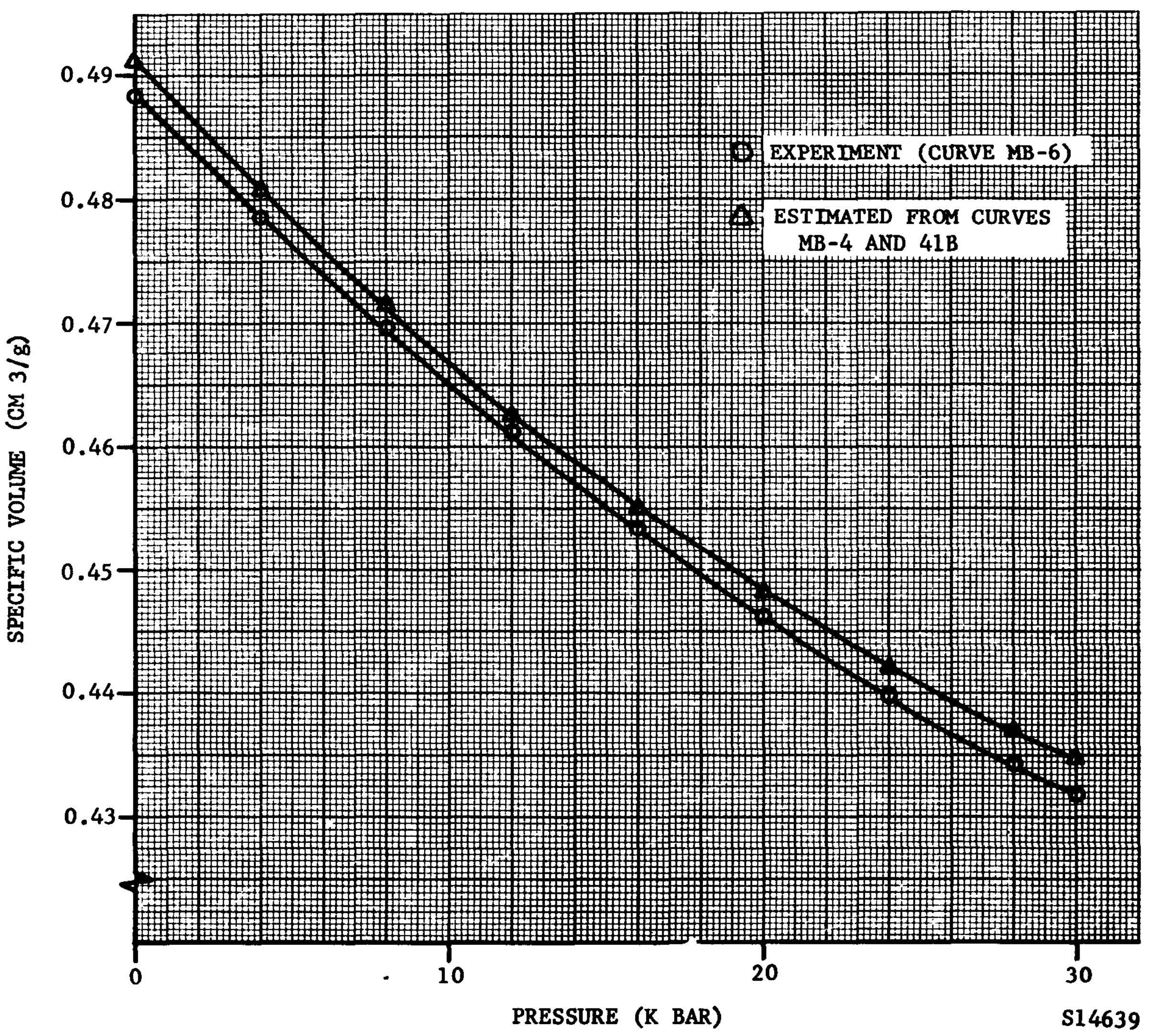

FIGURE 38. PRESSURE-VOLUME CURVES FOR SODIUM CHLORIDE-AMMONIUM PERCHLORATE MIXTURE (50 - 50% BY WT) AT 99 - 101°C

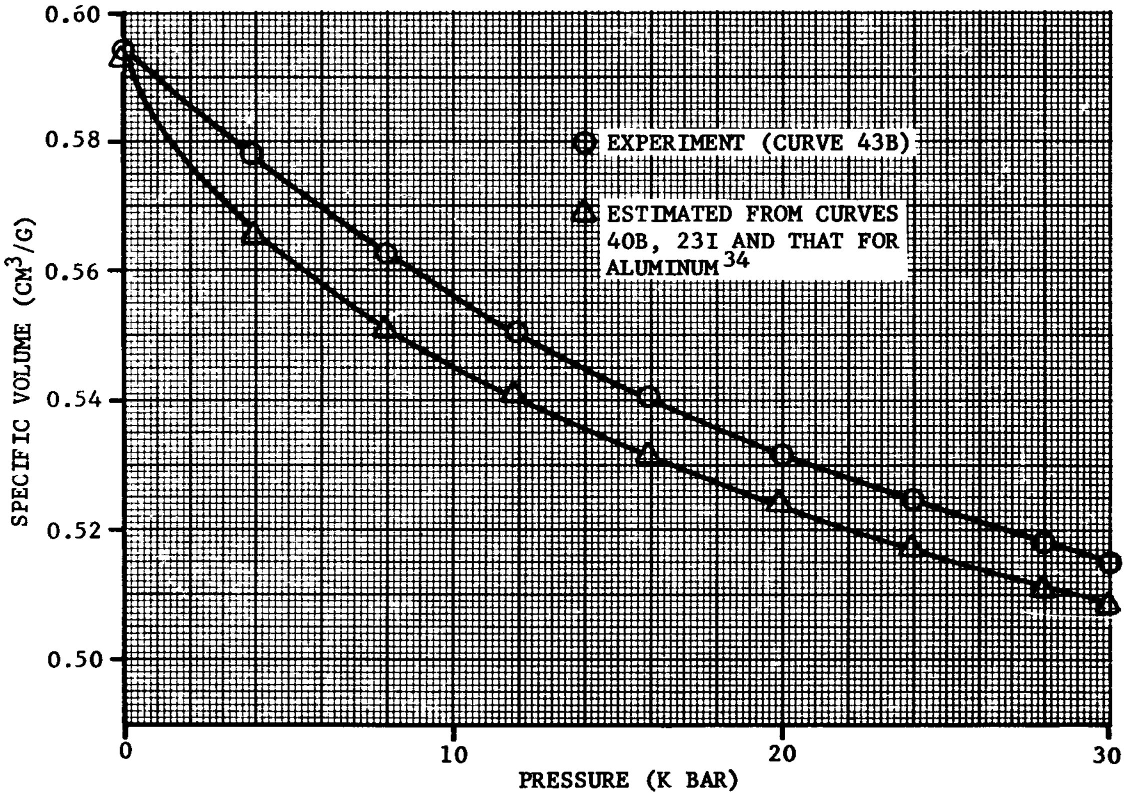

S14640

FIGURE 39. PRESSURE-VOLUME CURVES FOR ALUMINIZED SOLID PROPELLANT (B. F. GOODRICH DESIGNATION E107M) AT 23°C

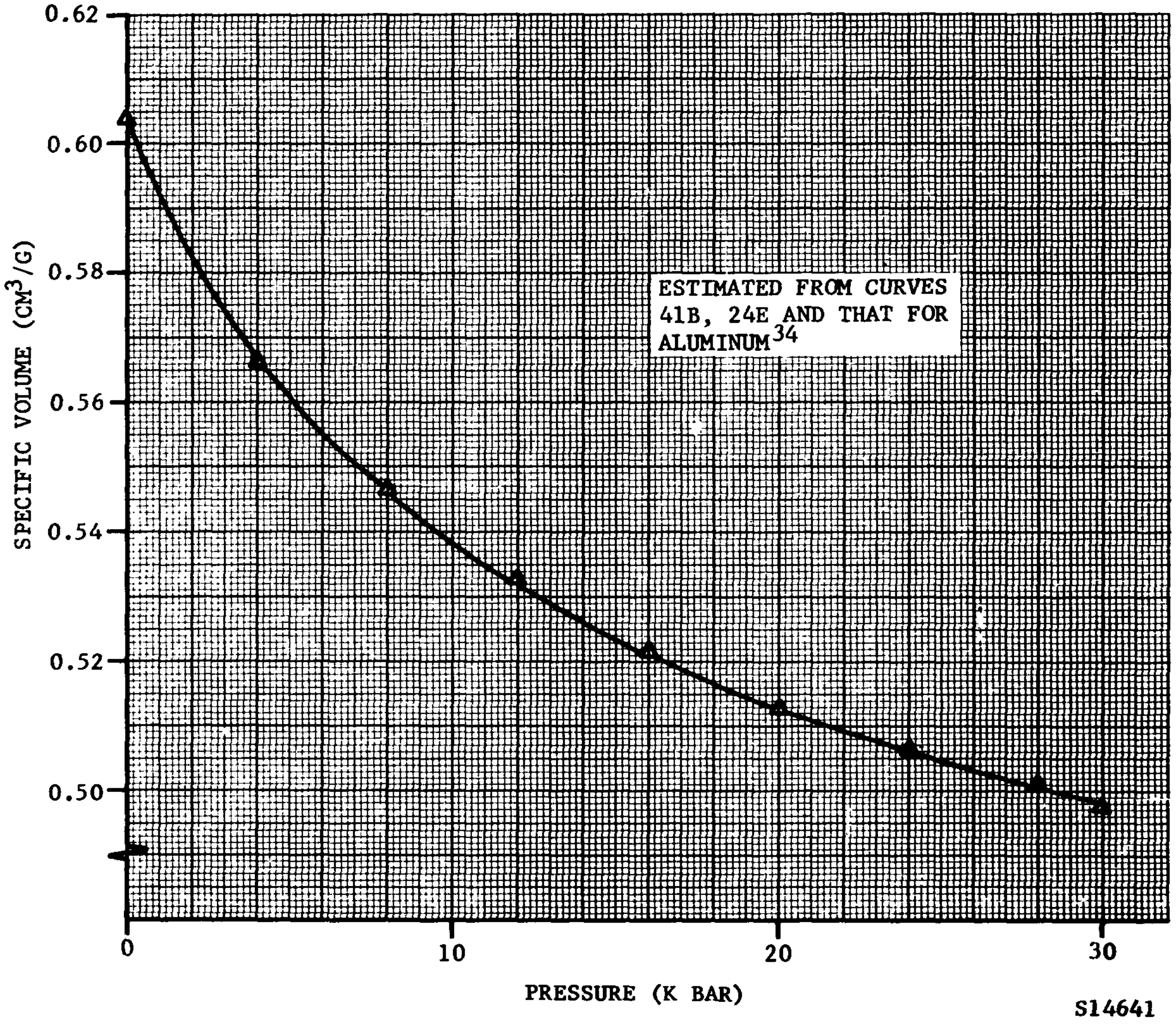

FIGURE 40. PRESSURE-VOLUME CURVE FOR ALUMINIZED SOLID PROPELLANT (B. F. GOODRICH DESIGNATION E107M) AT 100°C

TABLE 7

INPUT COMMON TO ALL PROBLEMS

$a = 4.0 \times 10^{-8}$ cm

$\gamma_o = 1.3$

$b = 1.03$

$D_s = 10^{-4}$ cm^2/sec

$D_o = 10^{-1}$ cm^2-bar/sec

$w = 20$ kbar

$m = 1$

$C_v = 0.3$ cal/gm-deg

TABLE 8

PREPARATION OF SALT-POLYURETHANE SPECIMENS

Composition	Weight % of Salt-Polyurethane 70-30%	 40-60%
Polyproylene glycol 2025	24.980	50.02
Trimethylol propane	0.956	1.91
Ferric acetylacetonate	0.04	0.07
Toluene-2, 4-diisocyanate	4.042	8.00
Sodium Chloride	70.000	40.000
Cure	24 hrs @ 160°F	24 hrs @ 160°F

TABLE 9

DATA FOR SOLID PROPELLANT (E107M)*

Type: high energy polyurethane base, castable and case-bondable, slow-burning, composite solid propellant

Theoretical Performance: I_{sp} (1000) = 255 sec.

Density (77°F): 0.0608 lbs/in^3

Composition:

	Components	Weight %
1.	polyurethane	25.0
2.	ammonium perchlorate	57.3
3.	aluminum	17.7

---

* "High Energy Composite Solid Rocket Propellants - Polyurethane Base and "c" - Rubber Base" B. F. Goodrich Aviation Products, Division of B. F. Goodrich Co., Rocket Motors, Rialto, California.

TABLE 10

COMPARISON OF EXPERIMENTAL AND CALCULATED SPECIFIC VOLUMES FOR SOLID PROPELLANT (E107M B. F. GOODRICH) AT AMBIENT TEMPERATURES

Pressure, k bar	Specific Volumes, cm^3/g	
	Calculated	Experimental (Curve #43B)
0	.5939	.5944
4	.5656	.5781
8	.5509	.5628
12	.5403	.5502
16	.5315	.5403
20	.5329	.5316
24	.5166	.5243
28	.5106	.5178
30	.5076	.5146

Notes:

1. Specific Volume at 77°F is given as 0.5945 cm^3/g by the manufacturer and compares closely with the figures shown in Table
2. The experimental and calculated curves are different by 2% in regions of maximum difference.

REFERENCES

1. J. von Neuman and R. D. Richtmeyer, Journ. Appl. Phys. 21, 232-237, (1950).

2. Henry Eyring, Richard E. Powell, George H. Duffy and Ransom B. Parlin Chem. Rev. 45, 69-181 (1949).

3. M. A. Cook, J. Chem. Phys., 15, 518 (1947).

4. H. Jones, Third Symposium on Combustion, Flame and Explosion Phenomenon, p. 590, Williams and Wilkins Co., Baltimore (1949).

5. Robert H. Cole "Underwater Explosions",Princeton University Press(1948).

6. a. John M. Walsh and Melvin H. Rice, Journ. Chem. Phys., 26, 815-823, 1957.

   b. Melvin H. Rice, Journ. Chem. Phys., 26, 824-830, (1957).

7. M. H. Rice, R. G. McQueen and J. M. Walsh, Solid State Physics, 6, 1-63, Academic Press (1958).

8. J. C. Slater "Introduction to Chemical Physics", Chapter XIII, McGraw-Hill, 1939.

9. F. P. Bowden and A. D. Yoffe, "Initiation and Growth of Explosions in Liquids and Solids", Cambridge Press (1952).

10. F. P. Bowden and A. D. Yoffe, "Fast Reactions in Solids", Academic Press (1958).

11. C. H. Johansson, Proc. Roy. Soc.,A246, 160-167 (1958).

12. J. Crank, "The Mathematics of Diffusion", Oxford Press (1956).

13. R. D. Richtmeyer, "Difference Methods for Initial Value Problems", Interscience (1957).

14. I. B. Zeldovitch, "Theory of Detonation", Academic Press, (1960).

15. J. Taylor, "Detonation in Condensed Explosives", Clarendon Press (1952).

16. P. W. Bridgman, Proc. Amer. Acad. Arts and Sci., 74, #3, 21-51 (1940).

17. Charles E. Weir, Journ. Res. National Bureau of Standards, 46, 207 (1951).

18. Melvin A. Cook, G. Smoot Horsley, W. S. Partridge and W. O. Ursenbach, Journ. Chem. Phys., 24, 60 (1956).

19. Melvin A. Cook, "The Science of High Explosives", Reinhold (1958).

20. I. Jaffee, R. Beauregard and A. Amster, ARS Journal, 32, 22 (1962).

21. W. H. Anderson and R. F. Chaiken, "On the Detonability of Solid Composite Propellants", Presented at the Solid Propellant Rocket Conference, Salt Lake City, Utah, February 1-3, 1961.

22. P. D. Drechsel, Private Communication.

23. M. H. Boyer and Ray Grandey, "Detonation and Two-Phase Flow", Ed. S. S. Penner and F. A. Williams, p. 75, Academic Press (1962).

24. Informal Technical Progress Report on Task NOL-323 of 2 December 1959, Naval Ordnance Laboratory, White Oak, Maryland.

25. Information Technical Progress Report on Task NOL-323 of 2 February 1962, Naval Ordnance Laboratory, White Oak, Maryland.

26. Informal Technical Progress Report on Task NOL-323 of 22 December 1961, Naval Ordnance Laboratory, White Oak, Maryland.

27. Informal Technical Progress Report on Task NOL-323 of 1 July to 31 August 1959, Naval Ordnance Laboratory, White Oak, Maryland

28. R. A. Grandey, Application of Finite Difference Methods to Problems in Two-Dimensional Hydrodynamics, Aeronutronic Publication U-1130, 26 January 1961.

29. T. Orlow, D. Piacesi and H. M. Sternberg, A Computer Program for the Analysis of Transient, Axially Symmetric, Explosion and Shock Dynamics Problems, NAVWEPS 7265, December 1960.

30. R. A. Grandey, The ROC-VTS Computer Program, AFSWC-TDR-62-114, September 1962.

31. Henry M. Shuey, Rohm and Haas Company, Redstone Arsenal Research Division, Private Communication.

32. George C. Kennedy and P. N. LaMori, J. Geophysical Research, 67, 851, (1962).

33. George C. Kennedy, UCLA Institute for Geophysics and Planetary Physics, Private Communication.

34. P. W. Bridgman, "The Physics of High Pressure", G. Bell and Sons Ltd., London, pp. 417, 160 (1958).

JANAF/SPIA DISTRIBUTION LIST

March 1963

Director
Advanced Research Projects Agency
The Pentagon, Room 3D165
Washington 25, D. C.

Attn: Advanced Propellant Chemistry Office D-1
4 Copies

U. S. Dept of the Interior
Bureau of Mines
4800 Forbes Street
Pittsburgh 13, Pennsylvania

Attn: M. M. Dolinar, Rpts Librarian
Explosives Research Lab
D-2
1 Copy

Scientific and Tech Info Facility
P. O. Box 5700
Bethesda, Maryland

Attn: NASA Representative
(S-AK/DL) D-7
2 Copies

National Aeronautics and Space Administration
Lewis Research Center
21000 Brookpark Road
Cleveland 35, Ohio

Attn: Library D-8
1 Copy

National Aeronautics and Space Administration
Langley Research Center
Langley Air Force Base, Virginia

Attn: Library D-9
1 Copy

National Aeronautics and Space Administration
Goddard Space Flight Center
Greenbelt, Maryland

Attn: Library D-10
1 Copy

National Aeronautics and Space Administration
George C. Marshall Space Flight Center
Huntsville, Alabama

Attn: Library D-11
1 Copy

JANAF/SPIA DISTRIBUTION LIST (Continued)

National Aeronautics and
Space Administration
Manned Spacecraft Center
P. O. Box 1537
Houston 1, Texas

Attn: Library D-12
1 Copy

Rocket Research Laboratories
Air Force Systems Command
Edwards, California

Attn: DGS AF-4
1 Copy

Space Systems Division
Air Force Systems Command
P. O. Box 262
Air Force Unit Post Office
Los Angeles 45, California

Attn: TDC AF-11
1 Copy

Armed Services Tech Information
Agency
Arlington Hall Station
Arlington 12, Virginia

AF-12
10 Copies

Rocket Research Laboratories
Air Force Systems Command
Edwards, California

Attn: DGPS AF-14
1 Copy

Aeronautical Systems Division
Wright-Patterson Air Force Base
Ohio

Attn: ASRCEM-1 AF-15
1 Copy

Commanding General
Aberdeen Proving Ground
Maryland

Attn: Ballistic Research Lab
ORDBG-BLI A-1
1 Copy

Commanding General
U. S. Army Ordnance Missile Command
Redstone Arsenal
Alabama

Attn: Technical Library A-11
5 Copies

Bureau of Naval Weapons
Department of the Navy
Washington 25, D. C.

Attn: DLI-3 N-2
2 Copies

Bureau of Naval Weapons
Department of the Navy
Washington 25, D. C.

Attn: RMMP-2 N-3
2 Copies

JANAF/SPIA DISTRIBUTION LIST (Continued)

Bureau of Naval Weapons
Department of the Navy
Washington 25, D. C.

Attn: RMMP-3 N-4
1 Copy

Commanding Officer
U. S. Naval Propellant Plant
Indian Head, Maryland

Attn: Technical Library N-7
2 Copies

Commander
U. S. Naval Ordnance Laboratory
White Oak
Silver Spring, Maryland

Attn: Library N-9
1 Copy

Commander
U. S. Naval Ordnance Test Station
China Lake, California

Attn: Tech Library Branch N-10
1 Copy

Department of the Navy
Office of Naval Research
Washington 25, D. C.

Attn: Code 429 N-12
1 Copy

Director
Special Projects Office
Department of the Navy
Washington 25, D. C.
N-18
1 Copy

U. S. Naval Ordnance Laboratory
Corona
California

Attn: P. J. Slota, Jr N-22
1 Copy

Bureau of Naval Weapons
Department of the Navy
Washington 25, D. C.

Attn: RRRE-6 N-23
1 Copy

Aerojet-General Corp
P. O. Box 296
Azusa, California

Attn: Librarian C-1
3 Copies

Hercules Powder Company
Allegany Ballistics Laboratory
P. O. Box 210
Cumberland, Maryland

Attn: Library C-2
3 Copies

JANAF/SPIA DISTRIBUTION LIST (Continued)

Atlantic Research Corp
Shirley Highway and Edsall Road
Alexandria, Virginia
C-5
1 Copy

Jet Propulsion Laboratory
4800 Oak Grove Drive
Pasadena 3, California

Attn: I. E. Newlan, Chief Reports Group — C-20
1 Copy

Rohm and Haas Company
Redstone Arsenal Research Division
Huntsville, Alabama

Attn: Librarian — C-36
2 Copies

Solid Propellant Information Agency
Applied Physics Laboratory
The Johns Hopkins University
Silver Spring, Maryland
C-37
3 Copies

Solid Propellant Information Agency
The Johns Hopkins University
Silver Spring, Maryland

Attn: Technical Rpts Group — C-37
2 Copies

Thiokol Chemical Corporation
Redstone Division
Huntsville, Alabama

Attn: Technical Director — C-39
2 Copies

Thiokol Chemical Corporation
Elkton Division
Elkton, Maryland

Attn: Librarian — C-41
1 Copy

Olin Mathieson Chemical Corporation
Marion, Illinois

Attn: Research Library Box 508 — C-43
1 Copy

Reaction Motors Division
Thiokol Chemical Corporation
Denville, New Jersey

Attn: Librarian — C-44
1 Copy

Rocketdyne, A Division of North American Aviation Inc.
Solid Propulsion Operations
P. O. Box 548
McGregor, Texas

Attn: Library — C-49
1 Copy

New York University
233 Fordham Landing Road and Cedar Avenue
University Heights 68, New York

Attn: Document Control - CJM
C-57
1 Copy

JANAF/SPIA DISTRIBUTION LIST (Continued)

Rocketdyne
6633 Canoga Avenue
Canoga Park, California

Attn: Library C-61
Dept 596-306 3 Copies

Lockheed Propulsion Company
P. O. Box 111
Redlands, California

Attn: Miss Belle Berlad C-65
Librarian 3 Copies

Aerojet-General Corporation
P. O. Box 1947
Sacramento, California

Attn: Tech Info Office C-72
3 Copies

Thiokol Chemical Corporation
Wasatch Division
P. O. Box 524
Brigham City, Utah

Attn: Library Section C-73
2 Copies

Olin Mathieson Chemical Corporation
Research Library 1-K-3
275 Winchester Avenue
New Haven, Connecticut

Attn: Mail Control Room C-76
Miss Laura M. Kajuti 3 Copies

Wright Aeronautical Division
Curtiss-Wright Corporation
Wood-Ridge, New Jersey C-78
1 Copy

Ethyl Corporation
Research Laboratories
1600 West Eight Mile Road
Ferndale, Michigan

Attn: E. B. Rifkin, Asst Dir
Chemical Research C-90
1 Copy

The Dow Chemical Company
Security Section
Box 31
Midland, Michigan

Attn: Dr. R. S. Karpiuk
1710 Building C-91
1 Copy

Minnesota Mining and Manufacturing Co
900 Bush Avenue
St. Paul 6, Minnesota

Attn: J. D. Ross C-94
2 Copies

VIA: Mr. H. C. Zeman
Security Administrator

American Cyanamid Company
1937 W. Main Street
Stamford, Connecticut

Attn: Dr. A. L. Peiker C-96
1 Copy

JANAF/SPIA DISTRIBUTION LIST (Continued)

Hercules Powder Company
Bacchus Works
Magna, Utah

Attn: Librarian C-98
2 Copies

Allied Chemical Corporation
General Chemical Division
Research Laboratory
P. O. Box 405
Morristown, New Jersey

Attn: L. J. Wiltrakis C-106
Security Officer 1 Copy

General Electric Company
Cincinnati 15, Ohio

Attn: Tech Info Center C-107
1 Copy

Callery Chemical Company
Research and Development
Callery, Pennsylvania

Attn: Document Control C-112
1 Copy

Pennsalt Chemicals Corporation
Box 4388
Philadelphia 18, Pennsylvania

Attn: Dr. G. Barth-Wehrenalp
C-114
1 Copy

Space Technology Laboratory, Inc.
5730 Arbor-Vitae Street
Los Angeles 45, California

Attn: Mr. Robert C. Anderson
C-116
1 Copy

Union Carbide Corporation
270 Park Avenue
New York 17, New York

Attn: B. J. Miller C-121
1 Copy

United Technology Corporation
P. O. Box 358
Sunnyvale, California

Attn: Librarian C-124
1 Copy

Aerospace Corporation
P. O. Box 95085
Los Angeles 45, California

Attn: Library - Documents C-129
2 Copies

JANAF/SPIA DISTRIBUTION LIST (Continued)

Thiokol Chemical Corporation
Rocket Operations Center
P. O. Box 1640
Ogden, Utah

Attn: Librarian C-133
1 Copy

Institute for Defense Analyses
Research and Engineering
Support Division
1825 Connecticut Ave, N.W.
Washington 9, D. C.

Attn: Technical Information Office C-134
1 Copy

British Defense Staff
British Embassy
3100 Massachusetts Avenue
Washington, D. C.

Attn: Scientific Information Officer F-1
4 Copies

VIA: Chief, Bureau of Naval Weapons
Department of the Navy
Washington 25, D. C.

Attn: DSC-3

Defense Research Member
Canadian Joint Staff (W)
2450 Massachusetts Avenue, N. W.
Washington, D. C. F-2
4 Copies

VIA: Chief, Bureau of Naval Weapons
Department of the Navy
Washington 25, D. C.

Attn: DSC-3

J. I. Thompson and Company
1118 22nd Street, N.W.
Washington 25, D. C.

Attn: Mr. K. Dahl-Hansen 1 Copy

VIA: U. S. Bureau of Naval Weapons
Resident Representative
Applied Physics Laboratory
Silver Spring, Maryland

Thompson Ramo Wooldridge
23555 Euclid Avenue
Cleveland 17, Ohio

Attn: Librarian C-135
2 Copies

AMCEL Propulsion Co
Box 3049
Asheville, N. C.
C-136
1 Copy

Aerojet-General Corporation
11711 South Woodruff Avenue
Downey, California

Attn: Florence Walsh, Librarian C-125
1 Copy